NONLINEAR FINITE ELEMENT ANALYSIS OF REINFORCED CONCRETE STRUCTURES SUBJECTED TO IMPACT LOADS

A Thesis Submitted to

the Graduate School of Engineering and Sciences of

İzmir Institute of Technology

in Partial Fulfillment of the Requirements for the Degree of

MASTER OF SCIENCE

in Civil Engineering

by

Neriman Çare CAĞALOĞLU

October 2010

İZMİR

We approve the thesis of **Neriman Çare CAĞALOĞLU**

Assist. Prof. Selçuk SAATCI
Supervisor

Assist. Prof. Gürsoy TURAN
Committee Member

Assoc. Prof. Alper TAŞDEMİRCİ
Committee Member

04 October 2010

Prof. Gökmen TAYFUR
Head of the Department of
Civil Engineering

Assoc. Prof. Talat YALÇIN
Dean of the Graduate School of
Engineering and Sciences

ACKNOWLEDGEMENTS

First of all I would like to thank to my supervisor Assistant Professor Selçuk Saatci who gave me the opportunity to do this research, guided with his valuable experiences and knowledge. He never let me down, when I went him with my questions and my problems about my research. Without his support and helps, it would be impossible for me to complete this research.

Moreover, I am so thankful for two people (who are not with us right now) in my life; one is my father who encouraged me to begin this project and second is my grandmother that supported me by her prayers and love all the time. And of course to my mother, brother and my best friends Gülbinay Can and İnci Bağdaş Tok for their sympathy and concern.

Finally, my thanks are to Mayor of Urla Municipality Mr.Selçuk Karaosmanoğlu, all staff of Urla Municipality and the whole people I cannot remember now for their support at my hard times during researches.

ABSTRACT

NONLINEAR FINITE ELEMENT ANALYSIS OF REINFORCED CONCRETE STRUCTURES SUBJECTED TO IMPACT LOADS

Design of reinforced concrete structures against extreme loads, such as impact and blast loads, is increasingly gaining importance. However, due to the problem's complicated nature, there exists no commonly accepted methodology or a design code for the analysis and design of such structures under impact loads. Therefore, engineers and researchers commonly resort to the numerical methods, such as the finite element method, and utilize different methods and techniques for the analysis and design. Although each method has its advantages and disadvantages, usually engineers and researchers persist on their method of choice, without evaluating the performance of other methods available. In addition, there is no significant study in the literature comparing the methods available that can guide the engineers and researchers working in the area. This study compares the performance of some numerical methods for the impact analysis and design with the help from actual impact test results in the literature. Computer programs VecTor2 and VecTor3 were selected for nonlinear finite element methodology, which were based on the Modified Compression Field Theory. Impact tests conducted on reinforced concrete beams were modeled and analyzed using these programs. Moreover, same beams were modeled also using a single degree of freedom spring system method. The results obtained from both approaches were compared with each other and the test results, considering their accuracy, computation time, and ease of use.

ÖZET

DARBE YÜKLERİNE MARUZ KALAN BETONARME YAPILARIN DOĞRUSAL OLMAYAN SONLU ELEMANLAR YÖNTEMİ İLE ANALİZİ

Betonarme yapıların darbe ve patlama yükleri gibi ani ve yüksek şiddetli yüklere karşı tasarımı günümüzde gittikçe daha önem kazanan bir konu haline gelmiştir. Ancak problemin karmaşıklığından ötürü betonarme yapıların bu tür yüklere karşı tasarımı için genel kabul görmüş bir yöntem veya detaylı bir teknik yönetmelik bulunmamaktadır. Dolayısıyla, darbe yüklerine maruz kalan betonarme yapıların tasarım ve analizi için yaygın olarak sonlu elemanlar yöntemi gibi sayısal yöntemlere başvurulmakta ve birbirinden çok farklı sonlu eleman metotları ve betonarme modelleme teknikleri kullanılmaktadır. Kullanılan her değişik yöntemin avantajları ve dezavantajları bulunmakla birlikte, bu konu üzerinde çalışan araştırmacı ve mühendisler genellikle analizlerini kendi seçtikleri belli bir yöntem ile yapmakta, farklı yöntemleri denemeye gerek duymamaktadır. Literatürde yaygın kullanılan farklı yöntemlerin karşılaştırılması ve değerlendirilmesi ile ilgili bir çalışma yoktur. Bu tezde, darbe yüklerine karşı betonarme yapıların analizi için yaygın olarak kullanılan bazı sayısal yöntemler literatürde yer alan darbe testleri ışığında karşılaştırılarak birbirlerine karşı avantaj ve dezavantajları ortaya konulmuştur. Doğrusal olmayan sonlu elemanlar yöntemi olarak Değiştirilmiş Basınç Alanı Teorisi tabanlı VecTor2 ve VecTor3 programları seçilmiş ve betonarme kirişler üzerinde yapılan darbe testleri bu programlarla modellenmiştir. Aynı kirişler başka bir yöntem olarak tek serbestlik dereceli yaylar olarak modellenmiş ve analizleri yapılmıştır. Elde edilen sonuçlar birbirleriyle ve test sonuçlarıyla karşılaştırılmış, kullanılan yöntemler sonuçların doğruluğu, çözüm süresi ve kullanım kolaylıkları bakımından değerlendirilmişlerdir.

TABLE OF CONTENTS

LIST OF FIGURES

Figure **Page**

LIST OF TABLES

LIST OF SYMBOLS

a	Maximum aggregate size
c_d	Compression softening, strain softening factor
c_t	Compression softening coefficient
$[D]$	Material stiffness matrix
$[D_c]$	Concrete material matrix
$[D_c]'$	Concrete material stiffness matrix relative to principal axes
$[D_s]$	Reinforcement component material stiffness matrices
$[D_s]'$	Reinforcement material stiffness matrix relative to principal axes
E_c	Elastic modulus of concrete
E_s	Elastic modulus of reinforcement
$\bar{E}_{c1}$	Secant modulus of concrete in the principal tensile direction
$\bar{E}_{c2}$	Secant modulus of concrete in the principal compressive direction
$\bar{E}_s$	Secant modulus of reinforcement
F	A function (to be discussed) of the principal stress state (σ_{xp}, σ_{yp}, σ_{zp})
f_c	Ultimate uniaxial compressive strength
f_c'	Peak compressive stress obtained from a standard cylinder test
f_{cb}	Ultimate biaxial compressive strength
f_{cx}	Stress in concrete in *x* -directions
f_{cy}	Stress in concrete in *y*-directions
f_{c1}	*S*tress in concrete in principal 1-directions
f_{c2}	*S*tress in concrete in principal 2-directions
f_p	Peak concrete compressive stress
f_{scrx}	Local stress at a crack of reinforcement parallel to the x-direction
f_{scry}	Local stress at a crack of reinforcement parallel to the y-direction
f_{sx}	Average stress of axial stress in the x-direction
f_{sy}	Average stress of axial stress in the y-direction
f_{yx}	Yield strength of reinforcement in the x-direction
f_{yy}	Yield strength of reinforcement in the y-direction
f_t	Ultimate uniaxial tensile strength
f'_t	Concrete cracking strength
f_y	Yield stress

f_1	Ultimate compressive strength for a state of biaxial compression superimposed on hydrostatic stress state σ_h^a
f_2	Ultimate compressive strength for a state of uniaxial compression superimposed on hydrostatic stress state σ_h^a
$\bar{G}_c$	Secant shear modulus of concrete
m_1, m_2	Collision of two masses
R_1, R_2	A contact spring
S	Failure surface (to be discussed) expressed in terms of principal stresses and five input parameters f_t, f_c, f_{cb}, f_1 and f_2
s_θ	Average crack spacing perpendicular to the crack
s_{mx}	Average crack spacing in the x-direction
s_{mx}	Average crack spacing in the y-direction
$[T]$	Coordinate transformation matrix
u_1, u_2	Displacement of two masses (m_1, m_2)
$\ddot{u}_2, \ddot{u}_1$	Acceleration vector
w	Average crack width
β_d	Compression softening reduction factor
Δu	Differential displacement
ε_{cr}	Concrete cracking strain
$\varepsilon_x, \varepsilon_y$	Total strains in the membrane element
$\varepsilon_{cx}, \varepsilon_{cy}$	Average strains in concrete
ε_{c1}	Principle compressive strain
ε_{c2}	Tensile strain
ε_p	Concrete compressive strain corresponding to f_p
$\varepsilon_{sx}, \varepsilon_{sy}$	Average strains in reinforcement
ε_0	Strain at the peak stress obtained from the standard cylinder test
$\varepsilon_1, \varepsilon_2$	Average strains in principal directions
γ_{xy}	Total shear strain
σ_h	Hydrostatic stress
σ_h^a	Ambient hydrostatic stress state
σ_{xp}	Principal stresses in principal x-directions
σ_{yp}	Principal stresses in principal y-directions
σ_{zp}	Principal stresses in principal z-directions

σ_1	Principal stresses in principal 1-directions
σ_2	Principal stresses in principal 2-directions
σ_3	Principal stresses in principal 3-directions
ρ	Reinforcement ratio
θ_c	Principal strain direction
θ_{nx}	Angles between the normal to the crack and the reinforcement in the x-direction
θ_{ny}	Angles between the normal to the crack and the reinforcement in the y-direction
θ_σ	Orientation of principal stress field, measured counter-clockwise from x-direction
τ_{xy}	Applied shear stress
υ_{ci}	Local concrete shear at a crack
υ_{cxy}	Shear stress
ψ	Transformation angle between principal direction and positive x-direction

CHAPTER 1

INTRODUCTION

Extreme loading conditions, like impact loads, are loads that occur at a high rate of speed and can transfer a large amount of energy into a structure over a short period of time, causing extreme local deformations and damage to a structure. Structures can be exposed to extreme loads in their lifetimes. For example, military, offshore, and nuclear power structures are susceptible to extreme loads. Numerous studies on reinforced concrete (RC) structures subjected to impact loads have been carried out by many researchers.

The analysis of RC structures subjected to impact loads can be made in several ways. However, it is difficult to name one commonly accepted method. The choice of method is dependent on the type, geometry or the required information about the structure's behavior. Generally, in common buildings, linear analysis is used in modeling of structure. For taking into nonlinear behavior of materials, principles of solid mechanics are adapted to the analysis of RC structures. Mostly nonlinear analysis is used for: 1) Performance assessment of previously built structures due to situations that was not accounted for in design and construction, 2) evaluating the effects of changes in design codes, 3) Design of unique new structures, 4) Analysis of structures showing distress or deterioration, 5) Determining response at service load levels, ultimate capacity and failure mode.

In this study, an advanced method of reinforced concrete analysis is applied to the case of impact loads. The Modified Compression Field Theory (MCFT) (Vecchio and Collins 1986) was chosen as the main methodology, since this method was proven to perform well in cases of shear dominant behavior, which is the main mechanism developed in RC structures under impact loads. The plasticity based five-parameter Willam-Warnke (Willam and Warnke 1975) is also explored for possible use. Both methods have been applied to static analysis of reinforced concrete beams as well. The main purpose of this study is to apply these methods of static analysis to the analysis of dynamic loads and to demonstrate an efficient and reliable tool for impact analysis of reinforced concrete. A two-dimensional nonlinear finite element reinforced concrete

analysis program called VecTor2, a three-dimensional nonlinear finite element reinforced concrete analysis program called VecTor3 and a three-dimensional finite element program called ANSYS is used for analysis. In addition, simple mass-spring models were also established and explored. Tests reported in the literature carried on shear-critical beams were modeled using these methods, since modeling shear behavior is a challenging issue in reinforced concrete.

Chapter 2 documents the methodologies are used by the selected computer programs. The models used for the analysis of selected impact tests and calculated behavior of RC structures subjected to impact loads are described in Chapter 3. Chapter 4 presents the models using mass-spring models.

CHAPTER 2

NONLINEAR FINITE ELEMENT MODELING OF REINFORCED CONCRETE

2.1. Introduction

Structures can be idealized as being composed of finite elements. The force-displacement relation of an individual element can be derived from the constitutive modeling of materials in the element concerned, and the overall structural behavior can be computed by solving equilibrium and deformational compatibility among elements. Therefore, the accuracy of structural analysis mainly depends on the constitutive modeling defined in each finite element domain. In general, the finite element discretization and the selection of constitutive modeling are performed so that the sizes of elements and the control volume for the model meet consistency requirements (Belytschko et al. 2000).

The main purpose of this study was evaluating the numerical methods available for predicting the behavior of reinforced concrete (RC) structures subjected to impact loads. In this section, the methods chosen for this evaluation are described and the software used are introduced. Additionally, static analysis of RC beams are performed using these software, results of which are used both to test the performances of the methods and to use later in the spring models as described in Chapter 4.

ANSYS was one of the finite element software used in this study (ANSYS 2009). It is commercial software with three-dimensional analysis capabilities, delivering innovative, dramatic simulation technology advances in every major physics discipline, along with improvements in computing speed and enhancements to enabling technologies such as geometry handling, meshing and post-processing. ANSYS was chosen in this study because of its popularity and capabilities in the plasticity analysis of concrete. The method used in ANSYS for RC analysis was a five-parameter plasticity based model developed by Willam-Warnke (Willam and Warnke 1975).

VecTor2 (VT2) is another finite element program utilized in this study (Vecchio and Wong 2002). It is a two-dimensional finite element program, used to analyze RC structures in plane stress conditions under various types of loads including static, cyclic,

dynamic and thermal loads. The program is based on the Modified Compression Field Theory (MCFT) formulations (Vecchio and Collins 1986), which was developed as a rational method for determining the shear behavior of RC structures. Over the years, MCFT proved its performance through numerous studies, and it was chosen in this study to compare its capabilities under impact loads with the alternative plasticity formulations. VecTor3 (VT3) is the three-dimensional counterpart of VT2, similarly based on MCFT formulations. VT3 is also used in this study to observe if the same methodology (e.g. MCFT) formulated for two- and three-dimensional finite element models show any significant difference on the performance under impact loads.

This chapter documents the methodologies used by the selected computer programs. Static analyses of RC beams using these programs are also included in this chapter. Section 2.2 gives the details of the five-parameter RC model Willam-Warnke, used by ANSYS. Section 2.3 gives the details of the Modified Compression Field Theory (MCFT) employed by VT2 and VT3. Section 2.4 describes the finite element models used for the static analysis of RC beams and presents results as compared with the actual test results.

2.2. Plasticity Method

The plasticity based five-parameter Willam-Warnke (Willam and Warnke 1975) model is explained in this section as used for the concrete element (SOLID65) in ANSYS (ANSYS 2009).

Failure criteria typically assume concrete to be isotropic (Chen 1982). Both cracking and crushing failure modes are accounted for. The criterion for failure of concrete due to a multiaxial stress state can be expressed in the form,

$$\frac{F}{f_c} - S \geq 0 \tag{2.1}$$

where;

F : a function (to be discussed) of the principal stress state (σ_{xp}, σ_{yp}, σ_{zp})

S : failure surface (to be discussed) expressed in terms of principal stresses and five input parameters f_t, f_c, f_{cb}, f_1 and f_2 defined in Table 2.1.

f_c : uniaxial crushing strength

σ_{xp}, σ_{yp}, σ_{zp} : principal stresses in principal directions

If Equation 2.1 is satisfied, the material will crack or crush. A total of five input strength parameters are needed to define the failure surface as well as an ambient hydrostatic stress state. These are presented in Table 2.1.

Table 2.1. Concrete material table

Label	**Description**
f_t	Ultimate uniaxial tensile strength
f_c	Ultimate uniaxial compressive strength
f_{cb}	Ultimate biaxial compressive strength
σ_h^a	Ambient hydrostatic stress state
f_1	Ultimate compressive strength for a state of biaxial compression superimposed on hydrostatic stress state σ_h^a
f_2	Ultimate compressive strength for a state of uniaxial compression superimposed on hydrostatic stress state σ_h^a

The failure surface can be specified with a minimum of two constants, f_t and f_c. The other three constants are calculated in the Willam-Warnke model by default as follows;

$$f_{cb} = 1.2 f_c \tag{2.2}$$

$$f_1 = 1.45 f_c \tag{2.3}$$

$$f_2 = 1.725 f_c \tag{2.4}$$

However, these default values are valid only for stress states where the following condition is satisfied;

$$\left|\sigma_h\right| \leq \sqrt{3} f_c \tag{2.5}$$

where;

σ_h is the hydrostatic stress expressed as,

$$\sigma_h = \frac{1}{3}\left(\sigma_{xp} + \sigma_{yp} + \sigma_{zp}\right) \tag{2.6}$$

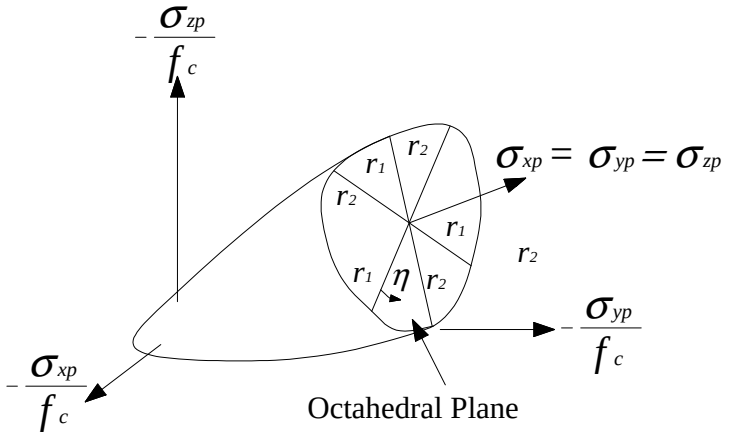

Figure 2.1. 3-D failure surface in principal stress space
(Source: ANSYS 2009)

Thus, the condition in Equation 2.5 applies to stress situations with a low hydrostatic stress component. All five failure parameters should be specified when a large hydrostatic stress component is expected. If condition Equation 2.5 is not satisfied and the default values shown in Equation 2.2 thru Equation 2.4 are assumed, the strength of the concrete material may be incorrectly evaluated.

When the crushing capability is suppressed with f_c = -1.0, the material cracks whenever a principal stress component exceeds f_t.

Both the function *F* and the failure surface *S* are expressed in terms of principal stresses denoted as σ_1, σ_2, and σ_3 where;

$$\sigma_1 = max\left(\sigma_{xp}, \sigma_{yp}, \sigma_{zp}\right) \tag{2.7}$$

$$\sigma_3 = min\left(\sigma_{xp}, \sigma_{yp}, \sigma_{zp}\right) \tag{2.8}$$

and $\sigma_1 \geq \sigma_2 \geq \sigma_3$ .The failure of concrete is categorized into four domains:

1. $0 \geq \sigma_1 \geq \sigma_2 \geq \sigma_3$ (compression - compression - compression)
2. $\sigma_1 \geq 0 \geq \sigma_2 \geq \sigma_3$ (tensile - compression - compression)
3. $\sigma_1 \geq \sigma_2 \geq 0 \geq \sigma_3$ (tensile - tensile - compression)
4. $\sigma_1 \geq \sigma_2 \geq \sigma_3 \geq 0$ (tensile - tensile - tensile)

In each domain, independent functions describe *F* and the failure surface *S*, which is shown in Figure 2.1 andFigure 2.2, for three-dimensional and biaxial stress states, respectively. These functions are discussed in detail in Willam and Warnke (1975).

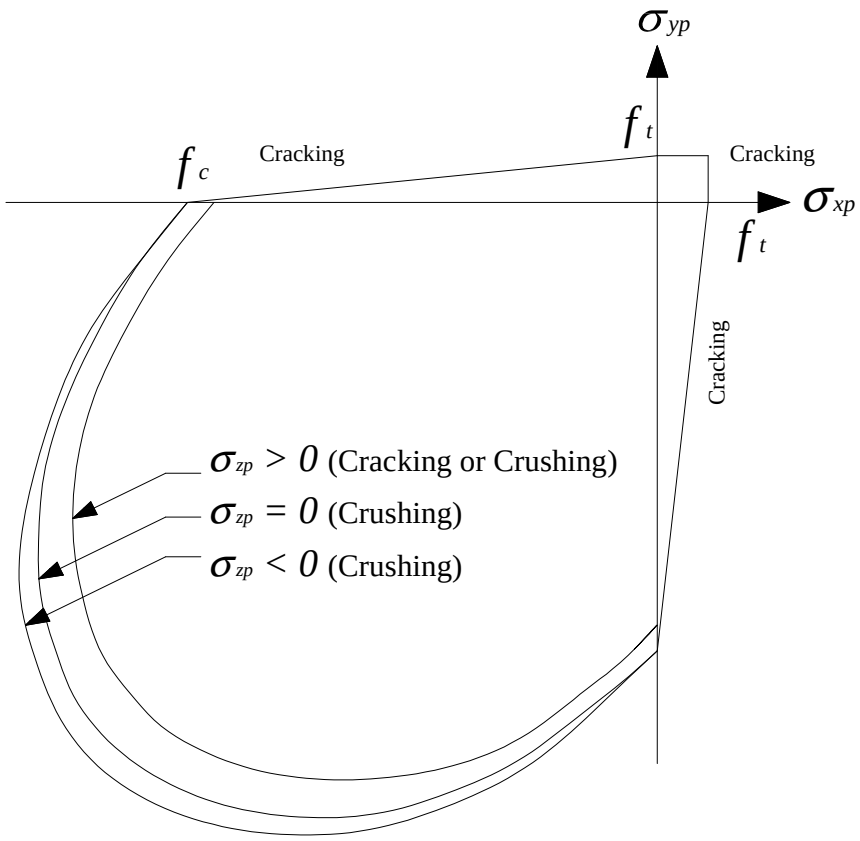

Figure 2.2. Failure surface in principal stress space with nearly biaxial stress (Source: ANSYS 2009)

2.3. Modified Compression Field Theory

VecTor2 (VT2) is a two-dimensional finite element program, based on the Modified Compression Field Theory (MCFT) formulations (Vecchio and Collins 1986), whereas VecTor3 (VT3) is the three-dimensional counterpart of VT2. In this section, MCFT is explained in two-dimensional form. Details for the three-dimensional version can be found in Selby (1993).

MCFT follows a rotating smeared-crack approach for modeling reinforced concrete. The membrane element shown in Figure 2.3, symbolizes a small part of the reinforced concrete structure considered as a plane stress problem that has uniform

thickness. The element contains reinforcement in both longitudinal (x) and transverse (y) axes. Uniform axial (σ_i) and shear (τ_i) stresses are applied on the element, where ρ_i is the reinforcement ratio, f_y is yield stress, and E_s is elastic modulus of reinforcement.

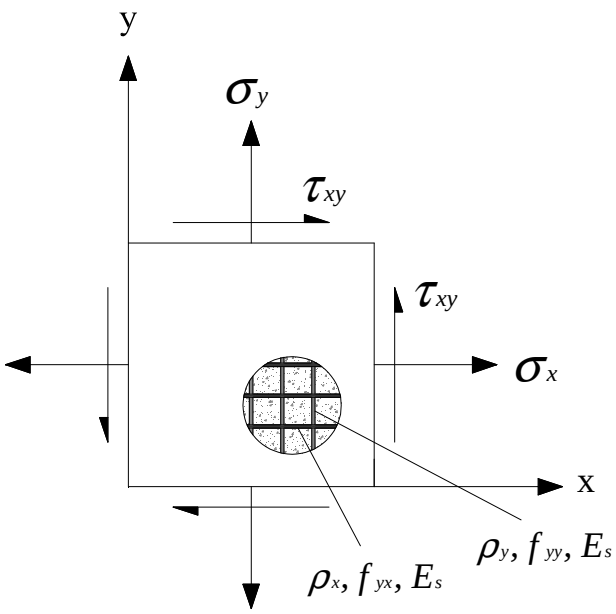

Figure 2.3. Reinforced concrete membrane element subject to in-plane stresses

2.3.1. Assumptions

The MCFT accepts the following assumptions for the derivation of the formulations for a single membrane element;

1. Reinforcement is uniformly distributed within element.
2. Cracking is uniformly distributed within element (smeared crack).
3. Stresses are uniformly applied.
4. Perfect bond exists between the reinforcement and the concrete.
5. Cracks rotate (rotating crack approach).
6. Stress-strain history has no effect.

2.3.2. Compatibility Conditions

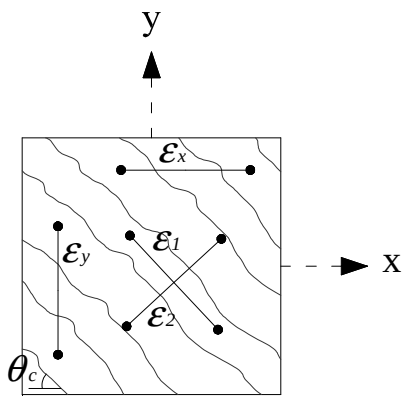

Figure 2.4. Avarage strains in cracked element

In line with the assumptions listed in the previous section, the deformation of the reinforcement must be compatible with the deformation of concrete as represented in Figure 2.4 . In this case,

$$\varepsilon_{sx} = \varepsilon_{cx} = \varepsilon_x \text{ and } \quad \varepsilon_{sy} = \varepsilon_{cy} = \varepsilon_y \tag{2.9}$$

where;

ε_x, ε_y: total strains in the membrane element, measured with a gauge length passing several cracks

ε_{cx}, ε_{cy},: average strains in concrete

ε_{sx}, ε_{sy},: average strains in reinforcement

Note that in Figure 2.4, ε_1 and ε_2 represent the average strains in principal directions, taken as perpendicular and parallel to the cracks, respectively.

If the three strain components ε_x, ε_y, and γ_{xy} are known, the strains in any direction can be found from geometry (Figure 2.5). After the deformation of the membrane element shown in Figure 2.5 the relations between principal strains ε_1 and ε_2 , strains ε_x and ε_y and principal strain direction θ_c can be found from Mohr's circle of strain as shown in Figure 2.6;

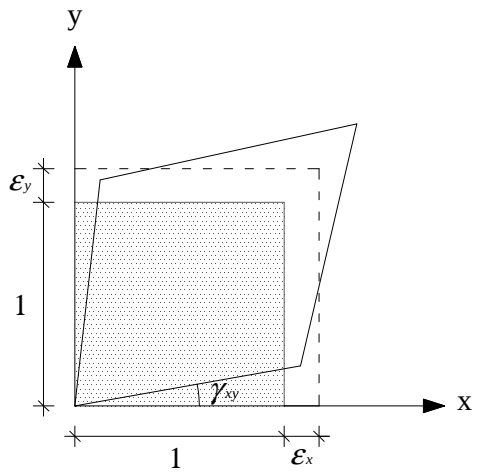

Figure 2.5. Deformation of membrane element

$$\varepsilon_{1,2} = \frac{(\varepsilon_x + \varepsilon_y)}{2} \pm \frac{1}{2}\left[(\varepsilon_y - \varepsilon_x)^2 + \gamma_{xy}^2\right]^{1/2} \tag{2.10}$$

$$\theta_c = \frac{1}{2}\tan^{-1}\left[\frac{\gamma_{xy}}{(\varepsilon_x - \varepsilon_y}\right] \tag{2.11}$$

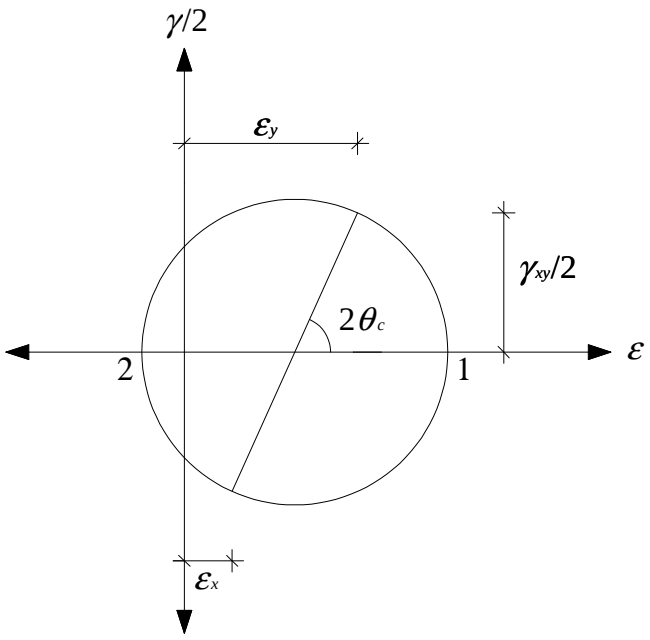

Figure 2.6. Mohr's circle for average strains

2.3.3. Equilibrium Conditions

The external forces applied to the reinforced concrete element are resisted by the stresses in concrete and the reinforcement. According to free-body diagram shown in Figure 2.7, the following equilibrium relations can be derived;

$$f_{cx} = f_{c1} - \frac{\nu_{cxy}}{\tan 2\theta_c} \tag{2.12}$$

$$f_{cy} = f_{c1} - \nu_{cxy} \tan 2\theta_c \tag{2.13}$$

$$\sigma_x = f_{cx} + \rho_x f_{sx} \tag{2.14}$$

$$\sigma_y = f_{cy} + \rho_y f_{sy} \tag{2.15}$$

where;

f_{cx}, f_{cy} : stress in concrete in *x*- and *y*-directions

υ_{cxy} : shear stress

f_{c1}, f_{c2} : stress in concrete in principal 1- and 2-directions

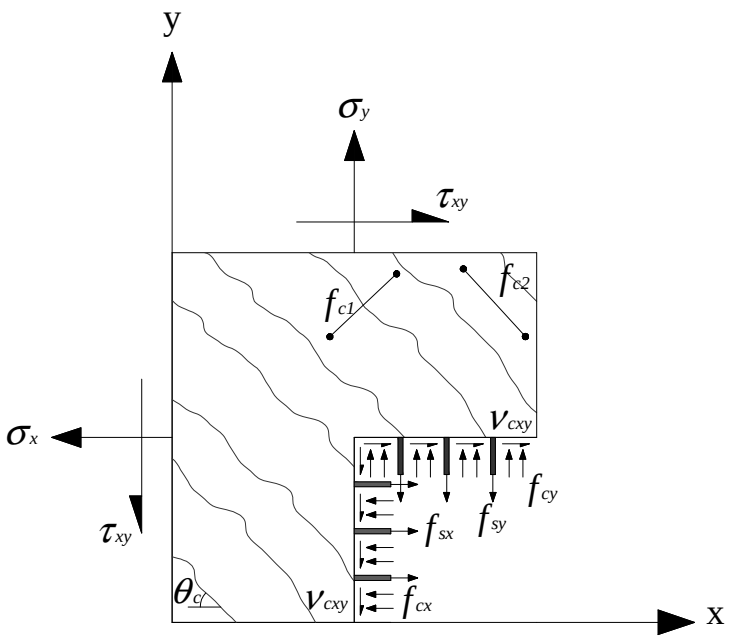

Figure 2.7. Free-body diagram of part of element

2.3.4. Constitutive Relations

Constitutive relationships are required to connect average stresses to average strains for both the reinforcement and the concrete. These relations may deviate considerably from the usual local stress-local strain relations determined from standard materials tests.

The principal compressive stress in concrete f_{c2} is a function of the principle compressive strain ε_{c2} and tensile strain ε_{c1}. The relationship as suggested by (Vecchio and Collins 1986) is;

$$f_{c2} = f_{c2max}\left[2\left(\frac{\varepsilon_{c2}}{\varepsilon_0'}\right) - \left(\frac{\varepsilon_{c2}}{\varepsilon_0'}\right)^2\right] \tag{2.16}$$

where ε_0 is the strain at the peak stress obtained from the standard cylinder test, and f_{c2max} is expressed as;

$$f_{c2max} = \frac{-f_c'}{0.8 - 0.34\frac{\varepsilon_{c1}}{\varepsilon_0}} \tag{2.17}$$

where f_c' is the peak compressive stress obtained from a standard cylinder test. The relation in Equation 2.16 would yield the same strain at the peak stress as obtained from a standard cylinder test. An alternative relationship where the reduction of the strain at the peak stress is considered can be expressed with respect to $\varepsilon_{c1}/\varepsilon_{c2}$ ratio as:

$$f_{c2} = f_p\left[2\left(\frac{\varepsilon_{c2}}{\varepsilon_p}\right) - \left(\frac{\varepsilon_{c2}}{\varepsilon_p}\right)^2\right] \tag{2.18}$$

where,

$$f_p = \beta_d f_c' \quad , \quad \varepsilon_p = \beta_d \varepsilon_0 \tag{2.19}$$

$$\beta_d = \frac{1}{1 + c_d} \leq 1.0 \tag{2.20}$$

$$c_d = 0.35\left[-\frac{\varepsilon_{c1}}{\varepsilon_{c2}} - 0.28\right]^{0.8} \tag{2.21}$$

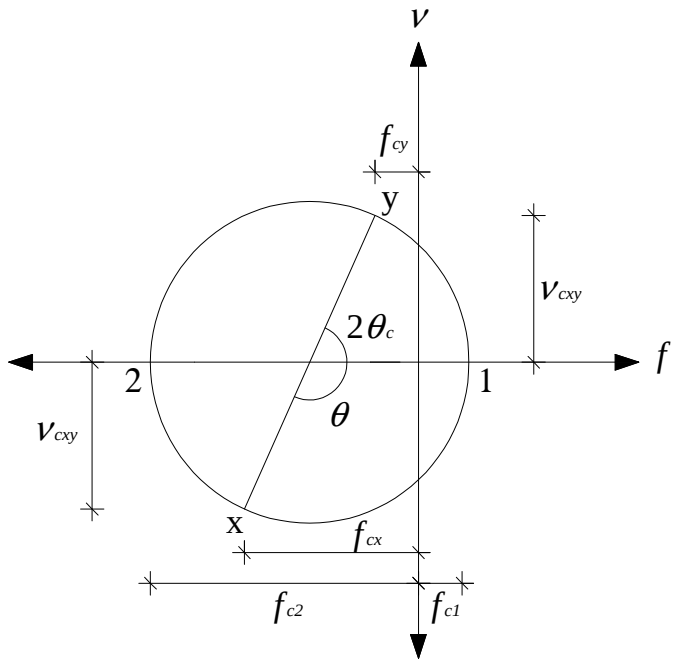

Figure 2.8. Mohr's circle of average concrete stresses

With regards to concrete in tension, the constitutive relationship relates the principal tensile stress, f_{c1}, to the principal tensile strain, ε_{c1}. It is first necessary to determine the uniaxial cracking strength, f'_t, and corresponding cracking strain, ε_{cr}. In the absence of information, they may be estimated as follows:

$$f_{c1} = E_c\varepsilon_{c1} \qquad \text{for} \quad 0 < \varepsilon_{c1} < \varepsilon_{cr} \tag{2.22}$$

where

$$E_c = \frac{2f'_c}{\varepsilon_0} \tag{2.23}$$

$$f'_t = 0.33\sqrt{f'_c} \tag{2.24}$$

$$\varepsilon_{cr} = \frac{f'_t}{E_c} \tag{2.25}$$

After cracking, stresses induced in concrete as a result of tension stiffening can be calculated as;

$$f_{c1} = \frac{f_t'}{1+\sqrt{c_t \varepsilon_{c1}}} \quad \varepsilon_{c1} > \varepsilon_{cr} \tag{2.26}$$

For reinforcing steel, the following constitutive relations can be used if strain hardening is neglected.

$$f_{sx} = E_s \varepsilon_{sx} \leq f_{yx} \tag{2.27}$$

$$f_{sy} = E_s \varepsilon_{sy} \leq f_{yy} \tag{2.28}$$

where f_{yx} and f_{yy} are the yield strength of reinforcement in *x*- and *y*-directions, respectively.

2.3.5. Consideration of Local Conditions

Given a compatible average strain condition, the relationships presented in the proceeding section can determine the average stresses in the concrete and reinforcement in equilibrium with the applied shear and normal stresses. However, it would be unconservative to ignore the possibility that the element response is governed by local yielding of the reinforcement at the crack or sliding shear failure along a crack. To address these possibilities, the MCFT limits the local stresses at the crack and the average concrete tensile stress transmitted across a crack.

Stresses fields in reinforced concrete vary from the average condition between cracks to the local condition at the crack. Consider Figure 2.9, which shows the average stresses at a section between cracks perpendicular to the principal tensile stress direction, and Figure 2.10, which shows the local stresses at the free surface of the crack.

At a free surface of a crack, the average concrete tensile stresses reduce virtually to zero. To transfer the average tensile stress across the crack, the reinforcement stress and strain must increase locally at the crack. Static equivalency of the average and local stresses in the direction normal to the crack surface results in the following equations;

$$\varepsilon_{scrx} = \varepsilon_{sx} + \Delta\varepsilon_{1cr}\cos^2\theta_{nx} f_{sx} = E_s\varepsilon_{sx} \le f_{yx} \tag{2.29}$$

$$\varepsilon_{scry} = \varepsilon_{sy} + \Delta\varepsilon_{1cr}\cos^2\theta_{ny} \tag{2.30}$$

$$f_{scrx} = E_s\varepsilon_{scrx} \le f_{yx} \tag{2.31}$$

$$f_{scry} = E_s\varepsilon_{scry} \le f_{yy} \tag{2.32}$$

$$f_{ci} = \sum_{i=x,y} \rho_i (f_{scri} - f_{si})\cos^2\theta_{ni} \tag{2.33}$$

where;

f_{scrx} : local stress at a crack of reinforcement parallel to the x-direction

f_{scry} : local stress at a crack of reinforcement parallel to the y-direction

θ_{nx} : angles between the normal to the crack and the reinforcement in the x-direction

θ_{ny} : angles between the normal to the crack and the reinforcement in the y-direction

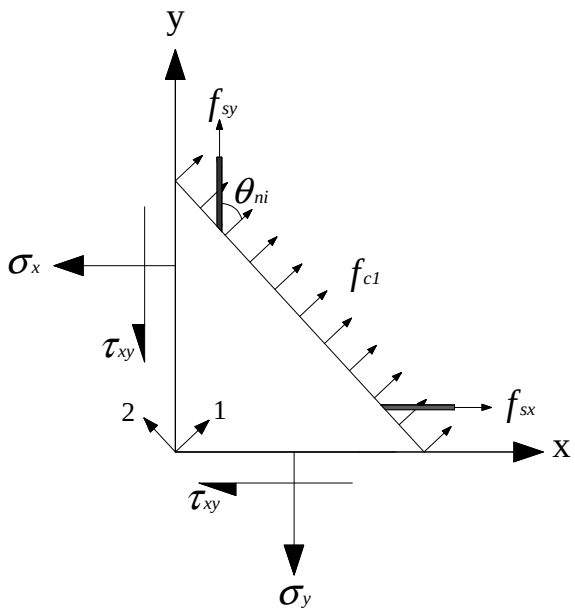

Figure 2.9. Average stress between crack

Since it is a principal plane, shear stresses are absent from the section in Figure 2.10. However, as the reinforcement generally crosses the crack at a skewed angle, local shear v_{ci}, are present on the crack surface as shown in Figure 2.10. Static equivalency of average and local stresses in the direction tangential to the crack determines the local shear stresses as follows:

$$\upsilon_{ci} = \sum_{i=x,y} \rho_i (f_{scri} - f_{si}) \cos\theta_{ni} . \sin\theta_{ni} \leq \upsilon_{cimax} = \frac{\sqrt{f_c'}}{0.31 + \frac{24w}{a+16}} \tag{2.34}$$

where;

υ_{ci} : local concrete shear at a crack

θ_{ni} : angles between the normal to the crack and the reinforcement

w : average crack width

a : maximum aggregate size

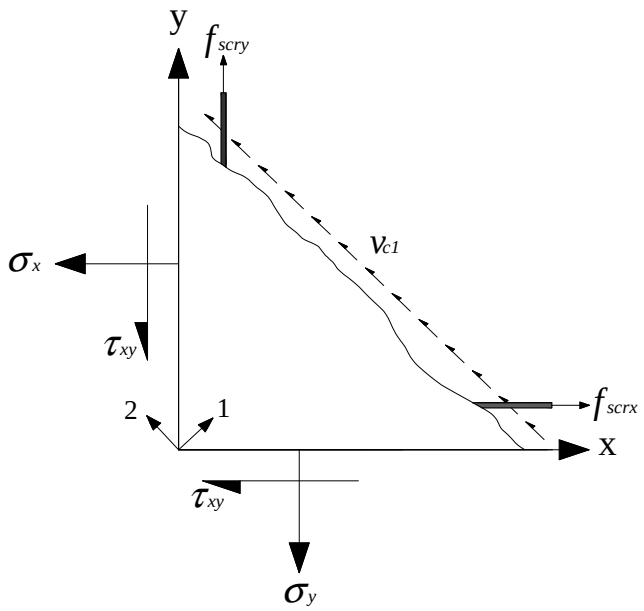

Figure 2.10. Local stresses at crack free surface

The average crack width w, is the product of principle concrete tensile strain and the average crack spacing perpendicular to the crack, s_θ, such as:

$$w = \varepsilon_{c1} s_\theta \tag{2.35}$$

where

$$s_\theta = \frac{1}{\frac{\cos\theta}{s_{mx}} + \frac{\sin\theta}{s_{my}}} \tag{2.36}$$

If either the maximum permitted average concrete tensile stress or local shear stress at a crack is exceeded, then the strain state of the element is modified to result in a lower average concrete tensile stress.

2.3.6. Finite Element Implementation

Displacement-based finite element methods for structural analysis result in a system of equations relating unknown nodal displacements to forces through the structure stiffness matrix. MCFT formulations derived for a single membrane element can be implemented into a finite element scheme (Vecchio and Wong 2002), as realized in VT2. VT2's algorithm for nonlinear finite element analysis is summarized by the flow chart given in Figure 2.11. The following discussion describes the details of some of these steps.

In general, at any point within the reinforced concrete continuum, the total strains, $[\varepsilon] = [\varepsilon_x \quad \varepsilon_y \quad \varepsilon_z]^T$, are related to stress, $[\sigma]$, by the composite material stiffness matrix, $[D]$, as follows;

$$[\sigma] = [D][\varepsilon] \tag{2.37}$$

The composite material stiffness matrix is the sum of the concrete material matrix, $[D_c]$, and the reinforcement component material stiffness matrices, $[D_s]$, such as;

$$[D] = [D_c] + \sum_{i=1}^{n} [D_s]_i \tag{2.38}$$

As the MCFT model reinforced concrete as an orthotropic material in the principal stress directions, it is necessary to formulate the concrete material stiffness matrix, $[D_c]'$, relative to these directions. If it is assumed that the Poisson's effect is negligible, then $[D_c]'$ is computed as follows;

$$[D_c]' = \begin{bmatrix} \bar{E}_{c1} & 0 & 0 \\ 0 & \bar{E}_{c2} & 0 \\ 0 & 0 & \bar{G}_c \end{bmatrix} \tag{2.39}$$

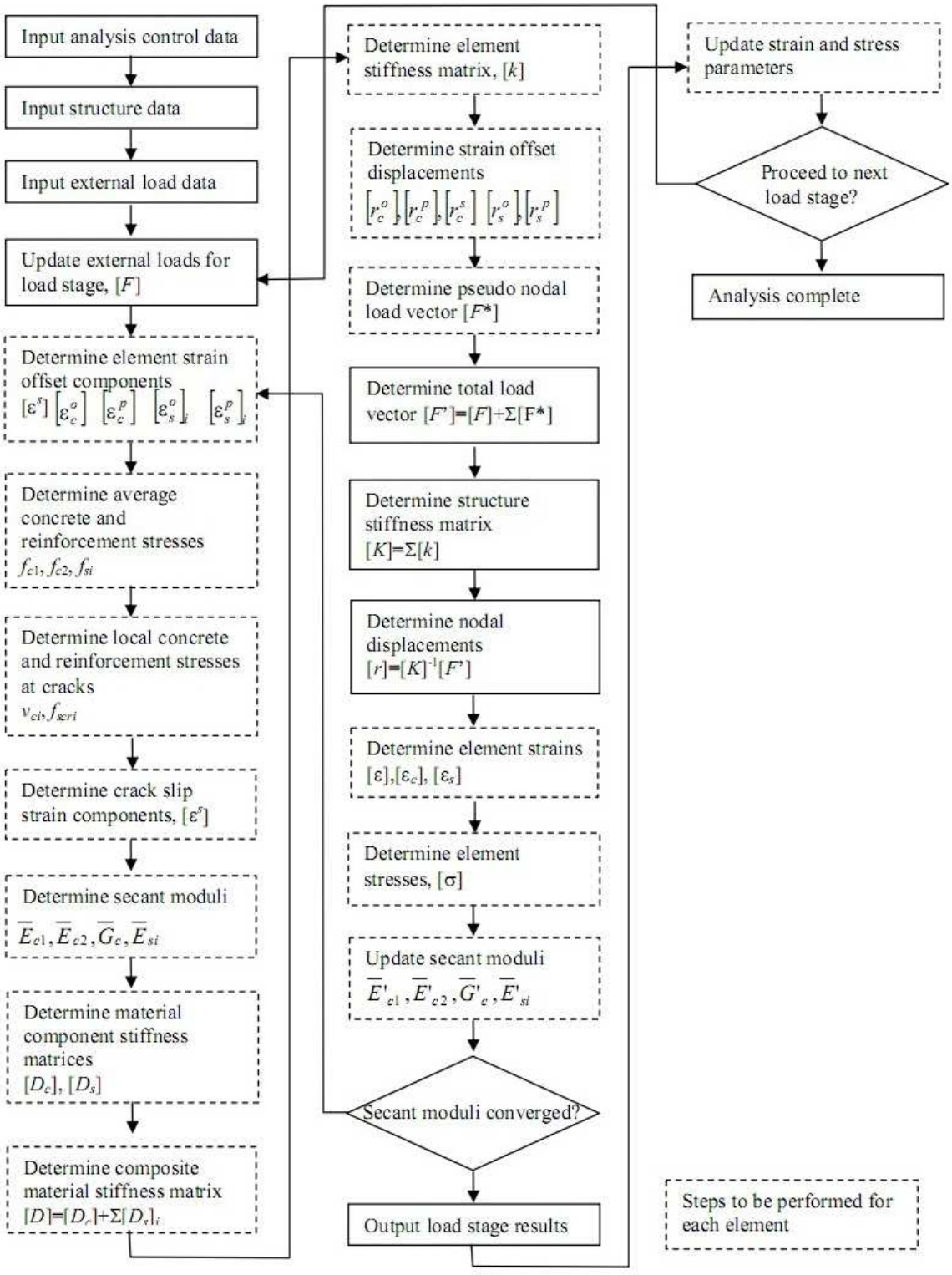

Figure 2.11. VT2 nonlinear finite element analysis algorithm
(Source: Vecchio and Wong 2002)

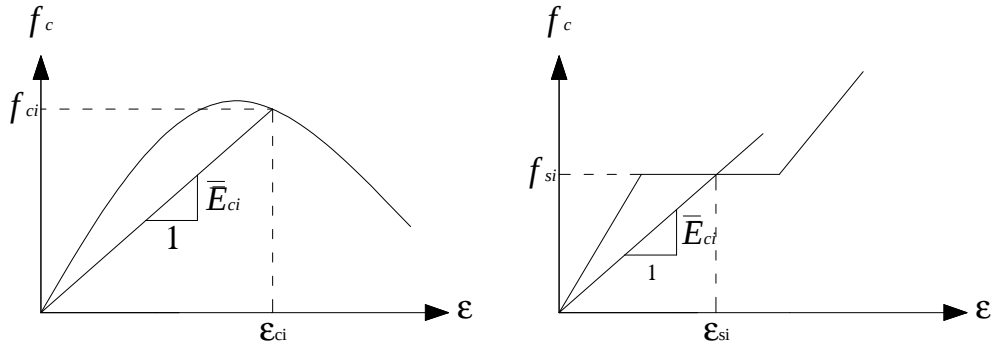

Figure 2.12. Definition of secant moduli for (a) concrete (b) reinforcement

The secant moduli $\bar{E}_{c1}$, $\bar{E}_{c2}$, $\bar{G}_c$, as shown in Figure 2.12 are computed from current values of the principal stresses, f_{c1} and f_{c2}, and the corresponding principal net concrete strains, ε_{c1} and ε_{c2}, as follows;

$$\bar{E}_{c1} = \frac{f_{c1}}{\varepsilon_{c1}} \tag{2.40}$$

$$\bar{E}_{c2} = \frac{f_{c2}}{\varepsilon_{c2}} \tag{2.41}$$

$$\bar{G}_c = \frac{\bar{E}_{c1} \cdot \bar{E}_{c2}}{\bar{E}_{c1} + \bar{E}_{c2}} \tag{2.42}$$

Similarly, material stiffness matrices $[D_s]_i{}'$ for each reinforcement component must first be determined relative to their longitudinal axes. As the reinforcement is assumed only to resist uniaxial stresses, $[D_s]_i{}'$ is computed as follows;

$$[D_s]_i{}' = \begin{bmatrix} \rho_i \bar{E}_{si} & 0 & 0 \\ 0 & 0 & 0 \\ 0 & 0 & 0 \end{bmatrix} \tag{2.43}$$

where ρ_i is the reinforcement ratio of the reinforcement component. The secant modulus $\bar{E}_{si}$, as shown in Figure 2.12b, is computed from its current value of stress, f_{si} and the corresponding strain, ε_{si} as follows;

$$\bar{E}_{si} = \frac{f_{si}}{\varepsilon_{si}}[D_s]_i{}' = \begin{bmatrix} \rho_i \bar{E}_{si} & 0 & 0 \\ 0 & 0 & 0 \\ 0 & 0 & 0 \end{bmatrix} \tag{2.44}$$

The material stiffness matrices, $[D_c]'$ and $[D_s]_i{}'$, are then transformed from their respective principal axes to the x, y axes by means of the transformation matrix, $[T]$, as follows;

$$[D_c]_i = [T_c]_i{}^T [D_c]_i [T_c]_i \tag{2.45}$$

$$[D_s]_i = [T_s]_i{}^T [D_s]_i [T_s]_i \tag{2.46}$$

$$[T] = \begin{bmatrix} \cos^2\psi & \sin^2\psi & \cos\psi \,.\, \sin\psi \\ \sin^2\psi & \cos^2\psi & -\cos\psi \,.\, \sin\psi \\ -2\cos\psi \,.\, \sin\psi & 2\cos\psi \,.\, \sin\psi & (\cos^2\psi - \sin^2\psi) \end{bmatrix} \tag{2.47}$$

For the concrete, the angle ψ is the inclination of the principal tensile stress axis, θ_σ, with respect to the positive x-axis. For the reinforcement, the angle ψ Figure 2.13 is the orientation, α_i, of each reinforcement component, with respect to the positive x-axis.

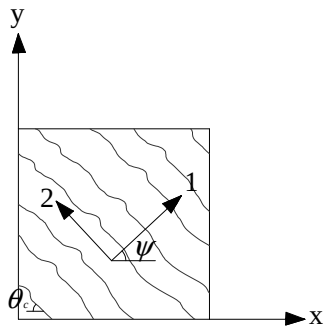

Figure 2.13. Angles in cracked element

The finite element implementation can be expanded to include dynamic analysis through inclusion of the mass and stiffness matrices and adaptation of a time integration scheme. Details of the dynamic algorithm can be found in Saatci and Vecchio (2009).

2.4. Static Analysis of Reinforced Concrete Beams

As will be explained in the following chapters, in this study, results of several impact tests performed on RC beams were used for evaluating the performance of nonlinear finite element methods in predicting the impact response of RC structures. In this section, static analyses of the specimens later used for impact modeling are presented. These static analyses are intended for testing the performance of the evaluated methods under static loads.

The static analyses presented in this section simulate the tests carried out by Saatci (2007) on RC beams. In Saatci's study, the RC beam specimens used for the impact tests were duplicated and tested under monotonically increasing loads at the mid-span to determine their static behavior. In this section, these static tests are modeled with the different analysis methods as described in preceding sections, and the analyses results are compared with the test results to evaluate their performance.

2.4.1. Test Specimens for Static Analysis

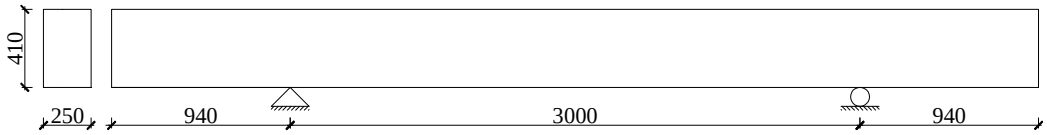

Figure 2.14. Specimen Dimensions

The test specimens used for the static analyses were duplicates of the impact specimens cast by Saatci (2007). These tests were performed after the completion of the impact test program. The test specimens constructed and modeled were four simply supported RC beams with identical longitudinal reinforcement and varying shear reinforcement. The dimension of the test specimens were 410 mm in height and 250 mm in width and 4880 mm in length. The specimens were tested under simply supported conditions with a shear span of 1500 mm, leaving 940 mm at each end (Figure 2.14).

The beams were reinforced with symmetric longitudinal reinforcement in height such that it would have equal moment capacity in positive and negative flexure. All

beams had the same amount of longitudinal reinforcement: two No.30 (area = 700 mm^2) steel bars placed with 38 mm clear cover at the bottom and top of the beam. Shear reinforcement was varied between the beams as the failure mechanism under impact loading was suggested to be shear critical, thus allowing a better understanding of how shear reinforcing affects the failure behavior. The four levels of shear reinforcement include no shear reinforcing steel, 0.1% shear reinforcement, 0.2% shear reinforcement, and 0.3% shear reinforcement as shown in Table 2.2. The type of shear reinforcement used in these tests were D8 reinforcing bar (area = 55 mm^2) whereas in impact tests, D6 reinforcing bars (area = 40 mm^2) were used. But the spacing of shear reinforcement remained same between the two tests. This discrepancy in shear reinforcement should only affect the outcome of MS1, since MS0 has no shear reinforcement and MS2 and MS3 will be moment critical beams.

d = 357 mm

ρ = 1.6 %

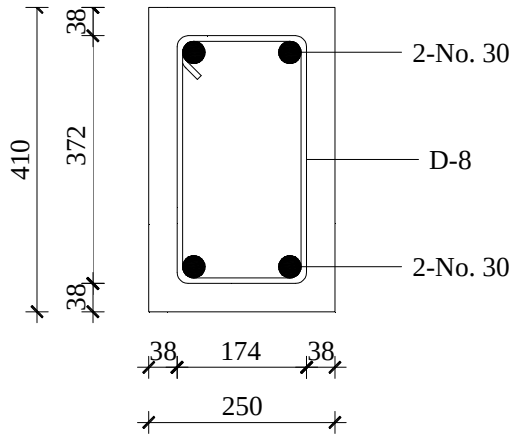

Figure 2.15. Specimen cross-section

Another variable in the testing relates to the time of testing in relation to casting of concrete. These tests, all four specimens were cast at the same time, and tested as soon as the compressive strength was within the required range.

Table 2.2. Transverse reinforcement ratios and stirrup spacing for beams

Specimen	**Transverse Reinforcement Ratio**	**Stirrup Spacing (mm)**
MS0	0.0%	-
MS1	0.1%	300
MS2	0.2%	150
MS3	0.3%	100

Compressive strength values to be used in analysis were obtained by testing cylinders that cured beside the formwork providing relatively similar in situ strength values. The concrete compressive strength of the beams at testing was approximately 50MPa. The material properties of reinforcements are given in Table 2.3.

All specimens were subjected to monotonically increasing loads at the mid-span, and the applied load and mid-span deflection were measured and recorded during the tests.

Table 2.3. Transverse reinforcement ratios and stirrup spacing for beams

	Area mm^2	**Yield Strain x10^{-3}**	**Yield Stress MPa**	**Ultimate Strength MPa**	**Young's Modulus MPa**	**ε_{sh} x10^{-3}**	**ε_u x10^{-3}**	**E_{sh} MPa**
No. 30	700	2.5	468	685	200000	12.5	80	3200
D-8	55	4.9	572	623	195000	5	50	1400

2.4.2. Plasticity Analysis of Saatci Beams using ANSYS

ANSYS (2009) was used to carry out the plasticity analysis of the beams using Willam-Warnke model (Willam and Warnke 1975). In ANSYS model, a total of 1000 brick elements were used to represent concrete and support plates, and 248 truss bar elements were used to model longitudinal steel reinforcement. The mesh included 2162 nodes. Taking advantage of the symmetric load and support conditions, only half of the beams were modeled. All nodes at centerline of the beam were restrained against in the x-direction displacements (Figure 2.18).

The 120 mm wide steel bearing plate at the support and the 160 mm wide steel bearing plate at applied load area were modeled with four elements. SOLID45 element type in ANSYS library was used for modeling of support plates. Material properties for steel were chosen as linear isotropic with elasticity modulus of $2x10^5$ MPa and Poisson's ratio of 0.20.

A total of 992 brick elements were used to model the concrete. The dimensions of the elements were varied in the model to accommodate the nodal locations in accordance with the locations of the truss bars representing the longitudinal reinforcements and the elements representing the support plates. The SOLID65 element

type was used for modeling of concrete with and without smeared transverse reinforcement. This solid element was capable of cracking in tension and crushing in compression. For linear isotropic part, material properties were chosen as $34.3x10^3$ MPa for elasticity modulus, and 0.15 for Poisson's ratio. Concrete crushing strength was specified as 49 MPa and cracking stress was specified as 2.3 MPa. Other concrete material parameters were left with ANSYS defaults.

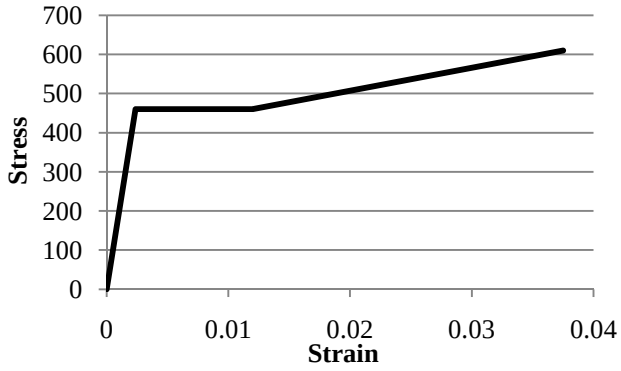

Figure 2.16. Stress-strain relations for steel

A total 248 truss bar elements were used to model longitudinal steel reinforcement. LINK8 was a spar element which used as steel reinforcement. Material properties were chosen as linear isotropic elasticity modulus $1.9x10^5$ MPa, and Poisson's ratio 0.15. The stress-strain relation for steel was described as in Figure 2.16 as found from steel coupon tests. Shear reinforcement, where present, were introduced as smeared reinforcement with specified volumetric ratio in concrete SOLID65 elements.

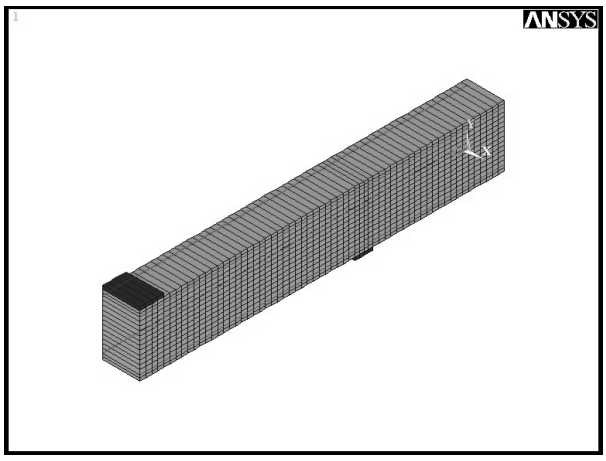

Figure 2.17. Finite element model in 3D

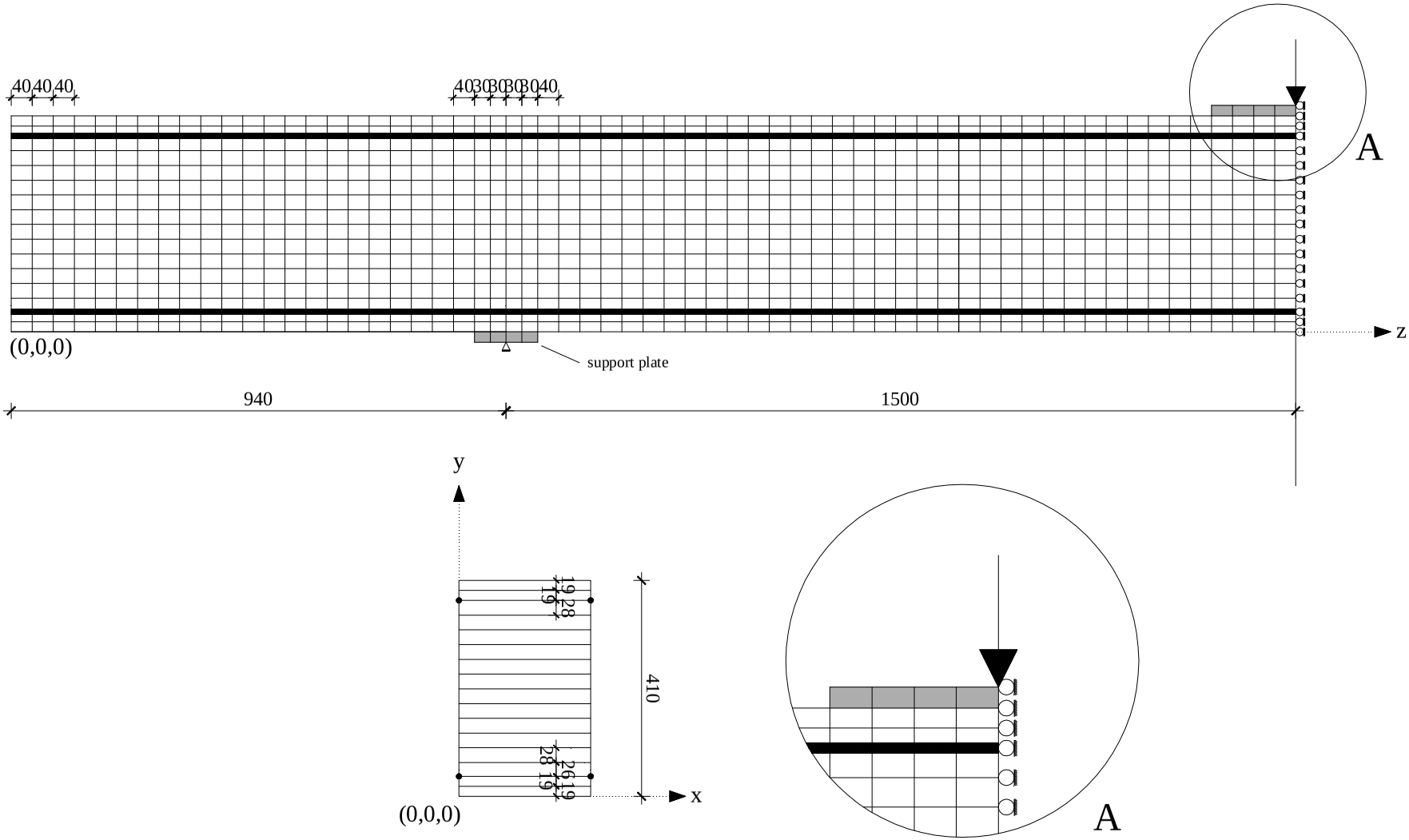

Figure 2.18. Finite Element Model for ANSYS

The finite element model used in analyses is presented in Figure 2.17 and 2.18. The static load was modeled as increasing displacements at the arrow shown in Figure 2.18. The default nonlinear analysis options were used in analyses.

Predicted Response of MS0 using ANSYS

The predicted response of MS0 was found to be relatively similar to the actual response viewed in the test. ANSYS modeled the beam to be slightly stiffer than the actual response, but the peak load and crack pattern predicted were similar to the observed values. The main variation in behavior between the predicted and the observed results can be viewed after the peak load was reached, where ANSYS found that the beam lost its entire capacity as soon as the peak load was reached, whereas the actual beam sustained some load (Figure 2.19).

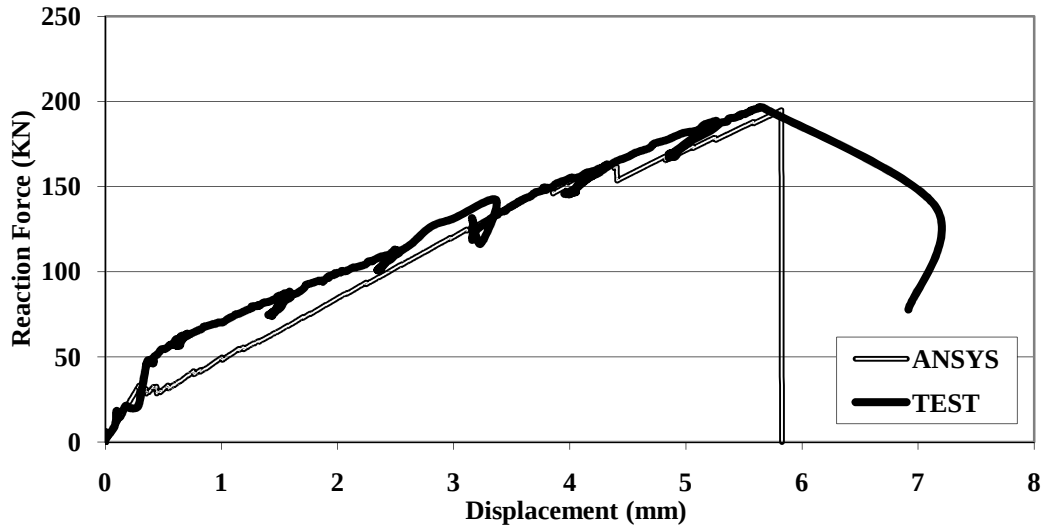

Figure 2.19. Reaction force - mid span displacement curve for MS0

Predicted Response of MS1 using ANSYS

The predicted response of MS1 was found to be similar to the actual response viewed in the test. ANSYS modeled the beam to be slightly stiffer than the actual response, but the load reached a peak and major cracks developed earlier than the test values. The predicted crack development is approximately flexure cracking at mid span, but formation and propagation of shear cracks developed as the beam approached the ultimate load. ANSYS found the beam would sustain a larger force but fail at a displacement much smaller than actually observed (Figure 2.20).

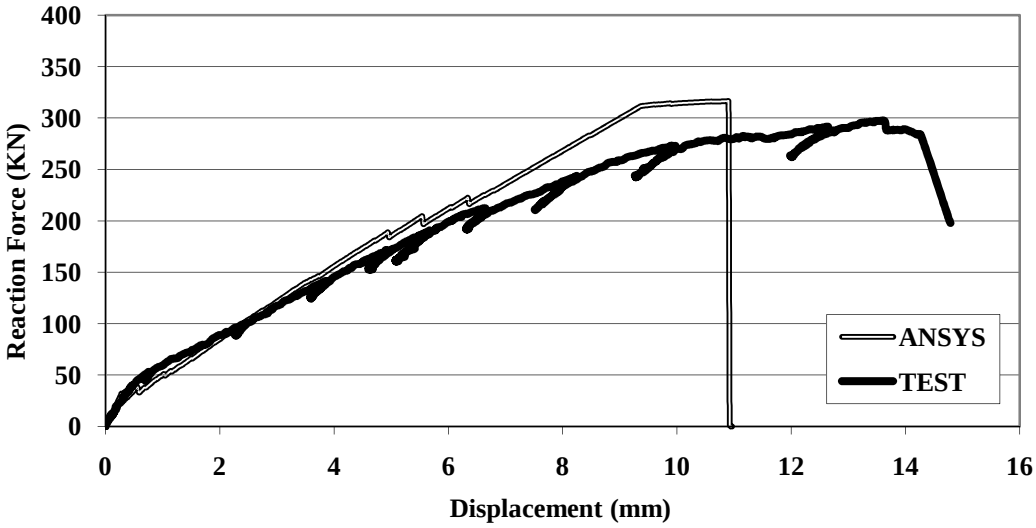

Figure 2.20. Reaction force - mid span displacement curve for MS1

Predicted Response of MS2 using ANSYS

Up to the yielding of longitudinal reinforcement, the predicted response of MS2 was found to be very similar to the actual response observed in the test. The yielding point was estimated well. However, the ductility of the beam was severely underestimated. In the model, the beam failed a little after yielding (Figure 2.21).

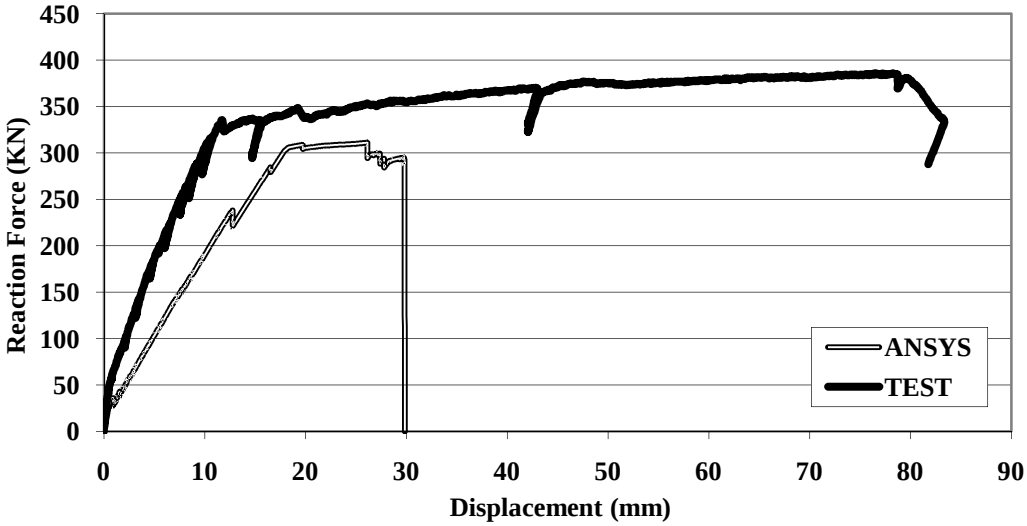

Figure 2.21. Reaction force - mid span displacement curve for MS2

Predicted Response of MS3 using ANSYS

Similar to the analysis of MS2, ANSYS predicted the initial stiffness of the beam and the displacement and the force at the time of longitudinal reinforcement yielding well. However, the ductility was severely underestimated. ANSYS model failed to converge a solution when the applied displacement kept increasing (Figure 2.22).

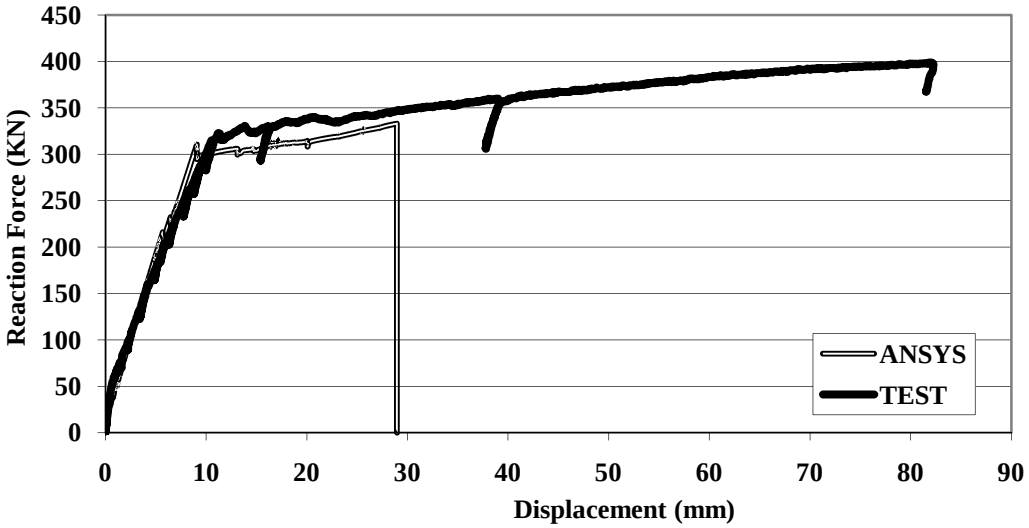

Figure 2.22. Reaction force - mid span displacement curve for MS3

2.4.3. Compression Field Theory Analysis of Saatci Beams using VecTor2

The mesh chosen for VT2 model was similar to the one shown in Figure 2.18, except that VT2 model is two-dimensional plane stress mesh. The results presented here were adopted from Saatci (2007). The model proposed by Palermo and Vecchio (2002) was used to model the hysteretic response of concrete. All other material and behavioral models used for concrete were the default models of VT2, which are summarized in Table 2.4. All the material and behavioral models used for steel reinforcement were the default models of VT2, as summarized in Table 2.5. Details on the formulations of these models can be found in Vecchio and Wong (2002).

Table 2.4. Material and behavioral models used for concrete

Material Property	Material Model
Concrete Compression Base Curve	Popovics (NSC)
Concrete Compression Post-Peak	Modified Park-Kent
Concrete Compression Softening	Vecchio 1992-A
Concrete Tension Stiffening	Modified Bentz
Concrete Tension Softening	Linear
Concrete Tension Splitting	Not Considered
Concrete Confinement Strength	Kupfer / Richart
Concrete Dilatation	Variable - Kupfer
Concrete Cracking Criterion	Mohr-Coulomb (Stress)
Concrete Crack Width Check	Crack Limit (Agg/5)
Concrete Hysteresis	NL w/ Decay (Palermo)
Slip Distortion	Vecchio-Lai

Table 2.5. Material and behavioral models used for steel reinforcement

Material Property	Material Model
Steel Hysteresis	Seckin Model
Rebar Dowel Action	Tassios (Crack Slip)
Rebar Buckling	Asatsu Model

The force-mid-span displacement results obtained from the analyses are presented in Figure 2.26 to Figure 2.29. As seen in the figures, in all analyses, the initial stiffnesses were somewhat overestimated. However, peak forces were estimated with greater accuracy. The ductility of MS2 and MS3 were estimated well.

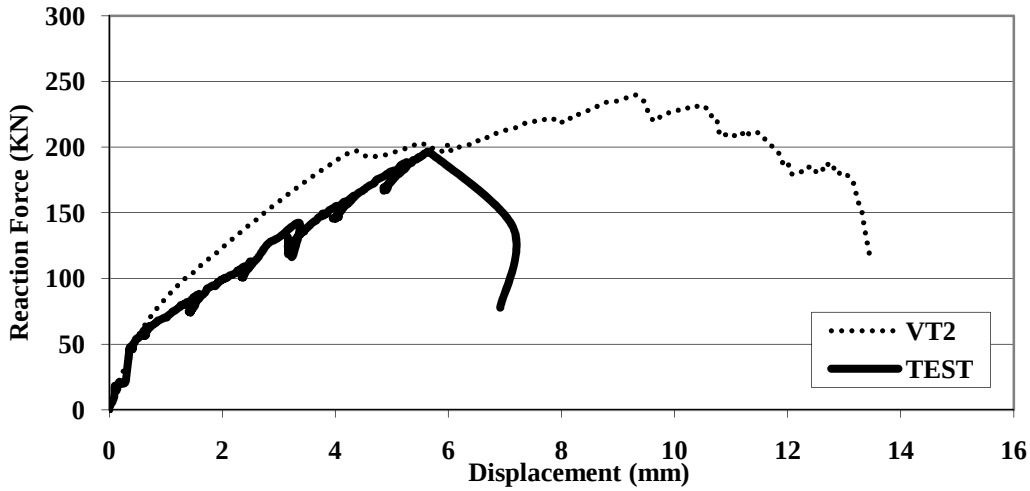

Figure 2.23. Reaction force - mid span displacement curve for MS0

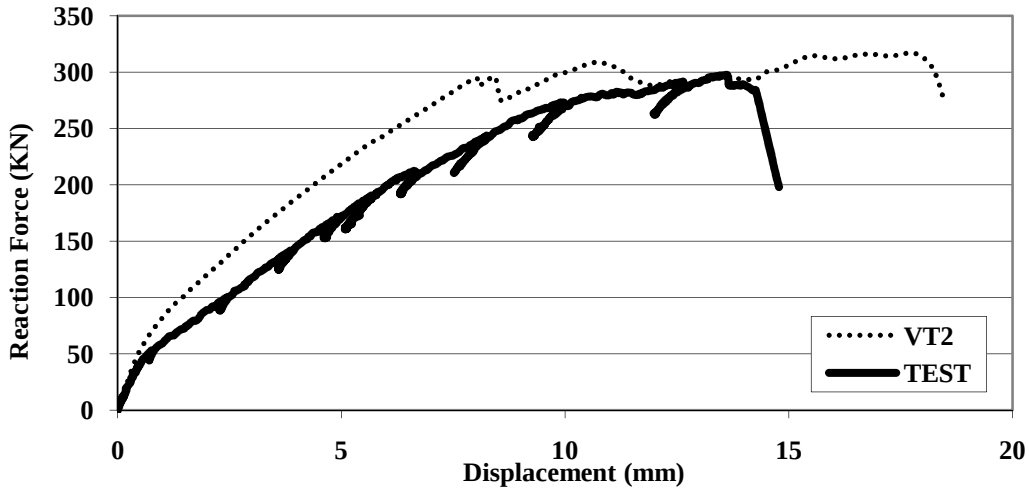

Figure 2.24. Reaction force - mid span displacement curve for MS1

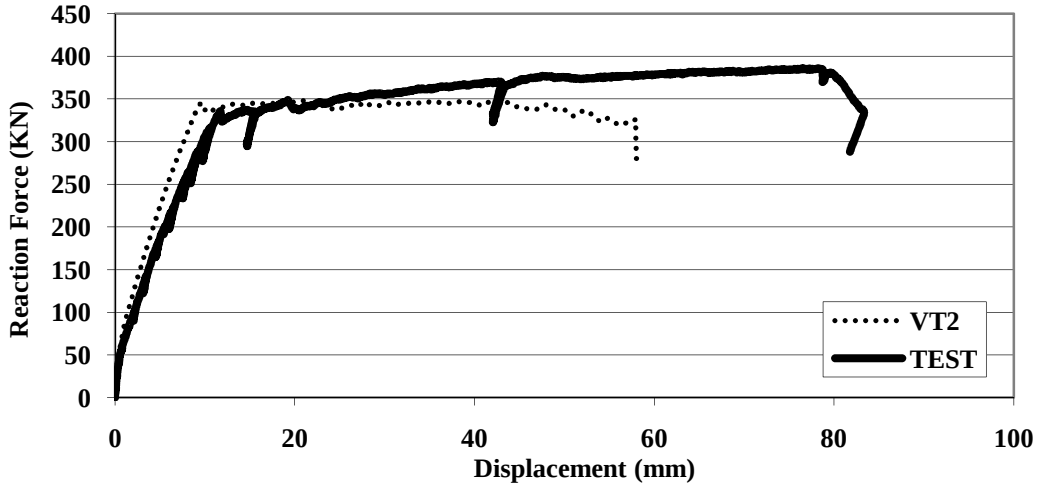

Figure 2.25. Reaction force - mid span displacement curve for MS2

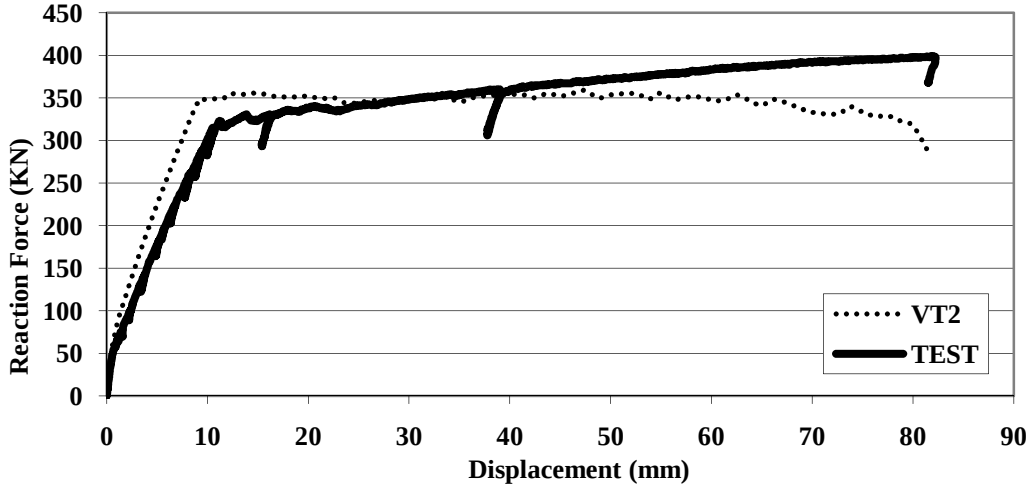

Figure 2.26. Reaction force - mid span displacement curve for MS3

2.4.4. Comparison of the Results of Static Analysis of Saatci Beams

The analyses results obtained using two different methods can be compared. The following figures present the comparisons of mid-span displacements, as observed in the tests and computed with ANSYS and VT2. Peak displacements are summarized in Table 2.6.

As seen in the figures, ANSYS performed better with the beam without any stirrups. However, VT2 was able to simulate some post-peak response, whereas ANSYS model failed abruptly. For the beam with little shear reinforcement, MS1, ANSYS predicted a higher stiffness and lower ductility. On the other hand, as seen in Figure 2.29 and Figure 2.30, VT2 performed much better in predicting the ductility of the beams. ANSYS appeared to fail predicting the response when extensive cracking and damage occur. Such a behavior for the ANSYS Willam-Warnke model was reported in some other similar studies as (Fanning 2001). In general, ANSYS appears to predict the behavior better when cracking is limited, or the failure becomes shortly after the appearance of the first crack, such as the case in MS0. However, VT2 is more successful in predicting the response when extensive cracking occurs and in the post-peak region. ANSYS's deficiencies can be attributed to the Willam-Warnke model used, since this model reportedly performs better mostly in cases of uniform stresses (Course notes by Vecchio), and its simplistic treatment of failed elements by multiplying the stiffness of failed elements with a very small number. On the other hand, VT2 has a better and more detailed approach to the post-cracking behavior.

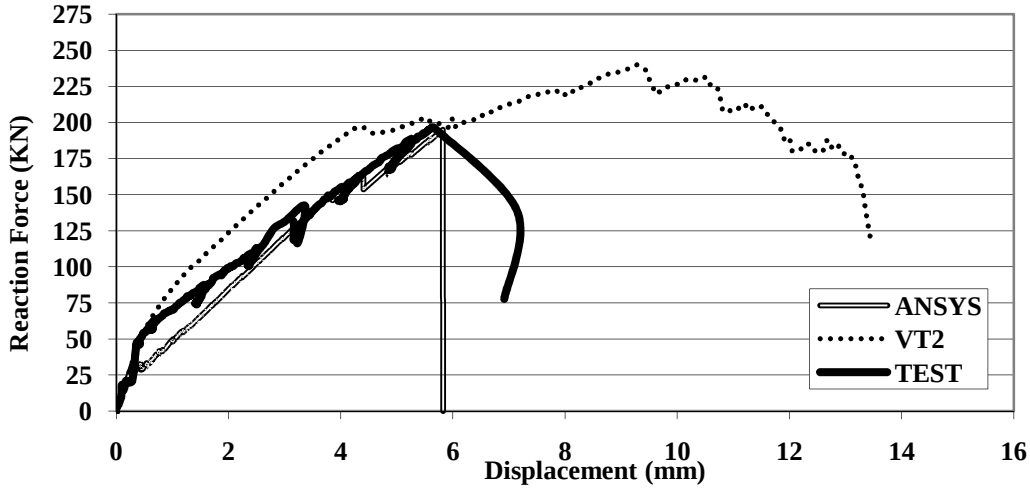

Figure 2.27. Comparison of observed and computed responses, MS0

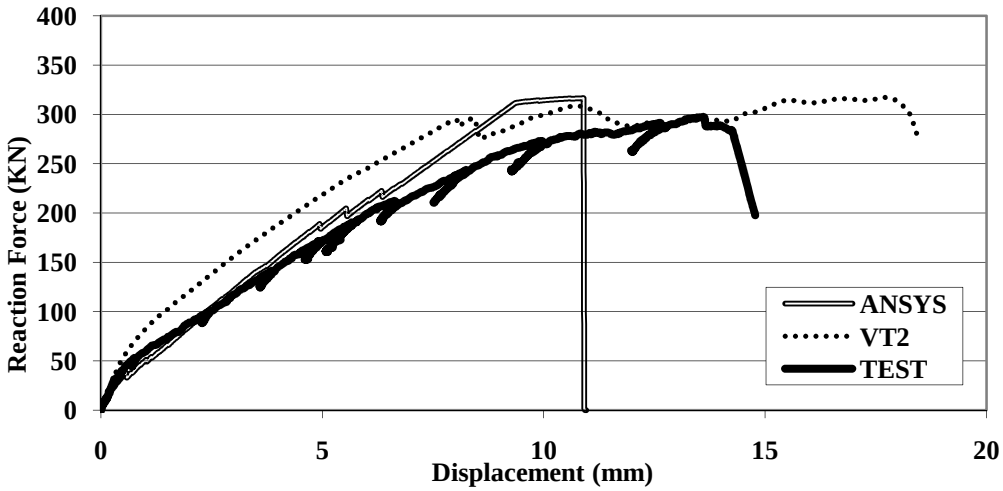

Figure 2.28. Comparison of observed and computed responses, MS1

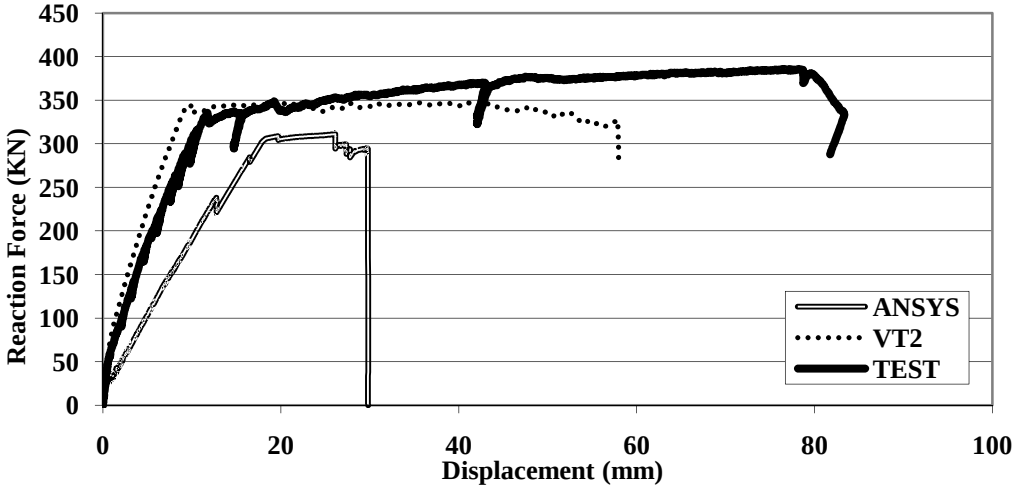

Figure 2.29. Comparison of observed and computed responses, MS2

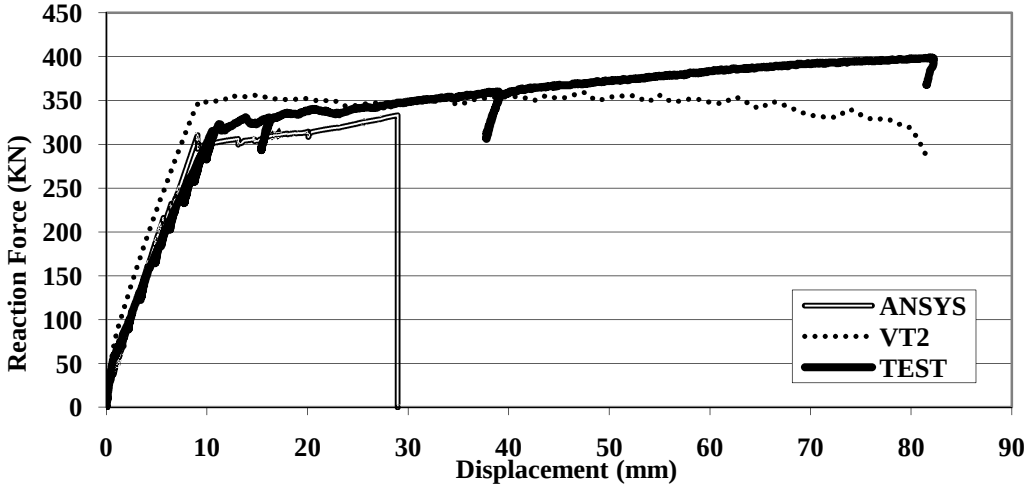

Figure 2.30. Comparison of observed and computed responses, MS3

Table 2.6. Peak values as obtained from the tests and analyses

Test	TEST RESULTS		ANSYS				VT2 RESULTS			
	Max. Displacement (mm)	Max. R.Force (ms)	Max. Displacement (mm)	Max. R.Force (ms)	Error in Max. Displ. (%)	Error in Max.R.Force (%)	Max. Displacement (mm)	Max. R.Force (ms)	Error in Max. Displ. (%)	Error in Max.R.Force (%)
MS0	5.63	196.68	5.82	194.93	-3.42	0.89	9.30	239.80	-65.18	-21.92
MS1	13.46	297.00	10.90	316.35	19.04	-6.51	17.75	317.20	-31.84	-6.80
MS2	76.38	385.68	26.10	311.02	65.83	19.36	21.00	347.80	72.50	9.82
MS3	81.81	398.94	28.97	333.18	64.59	16.48	47.50	358.80	41.94	10.06

CHAPTER 3

IMPACT MODELING USING IMPLICIT FINITE ELEMENT METHODS

3.1. Introduction

In this chapter, falling-weight impact test results conducted on reinforced concrete (RC) beams are compared with the finite element programs VecTor2 (VT2) and VecTor3 (VT3) using the Modified Compression Field Theory (MCFT) (Vecchio and Collins 1986). Shear-critical members were selected since modeling the shear behavior of RC structures presents a challenge. In addition to the Saatci beams mentioned in Section 2.4.1, impact tests conducted by Kishi et al. (2002) on shear-critical beams were also analyzed with VT2 to predict the behavior of RC beams subjected to impact loads.

This chapter documents the finite element models used by the computer programs and the predicted behavior of RC beams subjected to impact loads. Section 3.2 gives details of test specimens of Saatci and Kishi beams. Section 3.3 gives details of analysis of Saatci and Kishi beams with VT2, whereas Section 3.4 gives details of impact analysis of Saatci beams with VT3.

3.2. Test Specimens

3.2.1. Saatci Beams

The test specimens used in impact tests in Saatci's study (2007) were similar to the ones explained in Section 2.4.1. In impact tests, two different drop-weights (211 kg and 600 kg) were used for the testing. The test specimens constructed and modeled were eight simply supported reinforced concrete beams with identical longitudinal reinforcement, and varying shear reinforcement. The dimension of the test specimens were 410 mm in height, 250 mm in width, and 4880 mm in length. The specimens were

tested under simply supported conditions with a shear span of 1500 mm, leaving 940 mm at each end (Figure 2.14)

For impact test program, it was decided to have a duplicate of each specimen in order to investigate the effects of different impact drop-weights on undamaged specimens. Therefore, the specimens were cast as four pairs; that is, with identical geometry and reinforcement.

d= 357 mm

ρ = 1.6 %

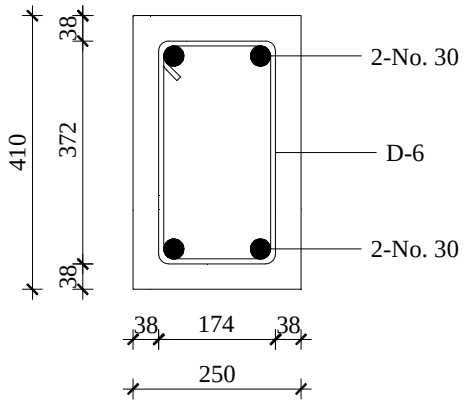

Figure 3.1. Specimen cross-section

Table 3.1. Transverse reinforcement rations and stirrup spacing for beams

Specimen	**Transverse Reinforcement Ratio**	**Stirrup Spacing (mm)**
SS0a, SS0b	0.0%	-
SS1a, SS1b	0.1%	300
SS2a, SS2b	0.2%	150
SS3a, SS3b	0.3%	100

Table 3.2. Cylinder test results

	28th day		**At the time of testing**	
	Peak compressive stress, f'_c (MPa)	**Strain at peak stress (ε_0)**	**Peak compressive stress, f'_c (MPa)**	**Strain at peak stress (ε_0)**
SS0a, SS0b	39.9	Not measured	50.1	2.32×10^{-3}
SS1a, SS1b	34.9	1.83×10^{-3}	44.7	2.36×10^{-3}
SS2a, SS2b	39.4	1.65×10^{-3}	47.0	2.42×10^{-3}
SS3a, SS3b	37.6	1.70×10^{-3}	46.7	2.51×10^{-3}

The specimens were reinforced with equal amounts of longitudinal reinforcement such that they would have equal moment capacity in positive and negative flexure. Therefore, these specimens had the same longitudinal reinforcement of two No. 30M steel bars placed with 38 mm cover at the bottom and top of the beam. The shear reinforcement was varied between the beams since the failure mechanism under impact loading was predicted to be shear critical, thus allowing a better understanding of how shear reinforcing affects the failure behavior. The four levels of shear reinforcement include no shear reinforcing steel, 0.1% shear reinforcement, 0.2% shear reinforcement, and 0.3% shear reinforcement as shown in Table 3.1. The type of shear reinforcement used in this test was D6 reinforcing bars.

Compressive strength values to be used in analysis were obtained by testing cylinders that cured beside the formwork providing relatively similar in situ strength values. The material properties are given in Table 3.2, Table 3.3, and Table 3.4.

Table 3.3. Steel coupon test results

	Area (mm^2)	**Nominal Diameter (mm)**	**Yield Strain, ε_y ($x10^{-3}$)**	**Yield Stress, f_y (MPa)**	**Ultimate strength, f_u (MPa)**	**Modulus of Elasticity, E_s (MPa)**
No.30	700	29.9	2.38	464	630	195 000
D-6	38.71	7.0	3.18	605	652	190 250

Table 3.4. Material densities

Material	**Density**
Concrete (SS3a, SS3b)	2425 kg/m^3
Concrete (SS2a, SS2b)	2420 kg/m^3
Concrete (SS1a, SS1b)	2473 kg/m^3
Concrete (SS0a, SS0b)	2437 kg/m^3
Steel (No.30 bar)	5.3 kg/m
Steel (D-6 stirrup)	0.48 kg/stirrup

Two different drop-weights were used for the testing; a lighter weight of 211 kg (beams identified as a-series) and a heavier weight of 600 kg (beams identified as b-series). The contact velocities of the drop-weights were 8 m/s.

3.2.2. Kishi Beams

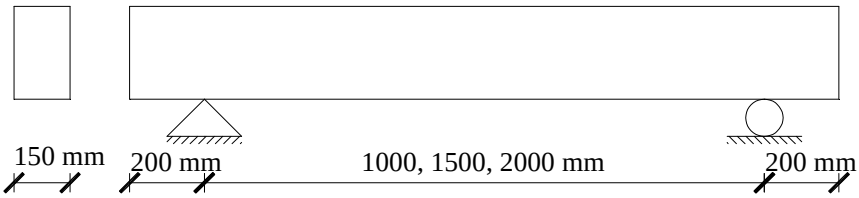

Figure 3.2. Specimen dimensions

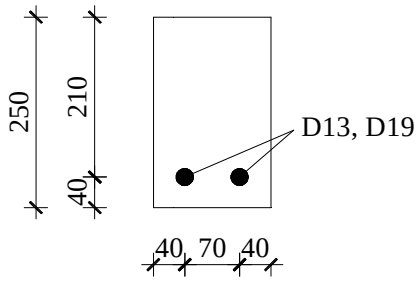

D13
Diameter = 10.31 mm
Area = 83.48 mm²
D19
Diameter = 12.47 mm
Area = 122.58 mm²

Figure 3.3. Specimen cross-section

The test specimens tested by Kishi et al. (2001) were six simply supported reinforced concrete beams with identical longitudinal reinforcement and no shear reinforcement. The dimensions of the test specimens were 250 mm in height, 150 mm in width and varying lengths of 1000, 1500 and 2000 mm (Figure 3.2). The shear-span ratio a/d and static shear bending capacity ratio α, span length, and main rebar's diameter were varied as shown in Figure 3.3. The static design values for all RC beams are calculated according to Japanese code (JSCE 1996). RC beams used in the study were designated using two variables: main rebar ratio ρ_t (A: 0.0182, B: 0.0080); and the value of 10 times shear-span ratio a/d (a: shear span; d: effective depth of cross section). Static shear capacity V_{usc} and static bending capacity P_{usc} were calculated using conventional prediction equations (JSCE 1996), and the static shear-bending capacity ratio α was obtained by dividing V_{usc} by P_{usc}. The average concrete compressive strength and yield strength of the main rebar were approximately 33 MPa and 393 MPa, respectively.

Table 3.5. List of static design values for specimen

Specimen	Rebar ratio p_t	Shear-span ratio a/d	Shear-span a(mm)	Effective depth d(mm)	Static shear capacity V_{usc}(KN)	Static bending capacity P_{usc}(KN)	Capacity ratio α ($=V_{usc}/P_{usc}$)	Impact velocity V(m/s)
A24	0.0182 (A)	2.4	1000	210	70.8	165.2	0.43	1.3-6
A36		3.6	1500	210	70.8	110.1	0.64	1.3-5
A48		4.8	2000	210	70.8	82.6	0.86	1.3-5
B24	0.0080 (B)	2.4	1000	210	70.8	78.8	0.68	1-5
B36		3.6	1500	210	70.8	52.5	1.08	1.3-5
B48		4.8	2000	210	70.8	39.4	1.37	1.3-6

Each RC beam was simply supported and fixed on its top and bottom surface at point 200 mm inside the ends. A single impact load was applied to the mid-span of the RC beam by dropping a free-falling 300 kg steel weight. One specimen of each kind of RC beam was tested at 1 m/s impact velocity to investigate the elastic impact behavior. The other specimens were tested at impact velocity of V>1 m/s to investigate the behavior of RC beams from the elastro-plastic region to the ultimate state.

3.3. Impact Analysis of Reinforced Concrete Beams using VecTor2

3.3.1. Impact Analysis of Saatci Beams using VecTor2

In this section, the analysis carried out by Saatci and Vecchio (2009) using VT2 are presented for comparison. For these analyses, a total of 1008 rectangular elements were used to represent to concrete and support plates, and 124 truss bar elements were used to model longitudinal steel reinforcement. The mesh included 1098 nodes. Taking advantage of the symmetric load and support conditions, only half of a beam was modeled. All nodes at centerline of the beam were restrained against in the x-direction (Figure 3.4).

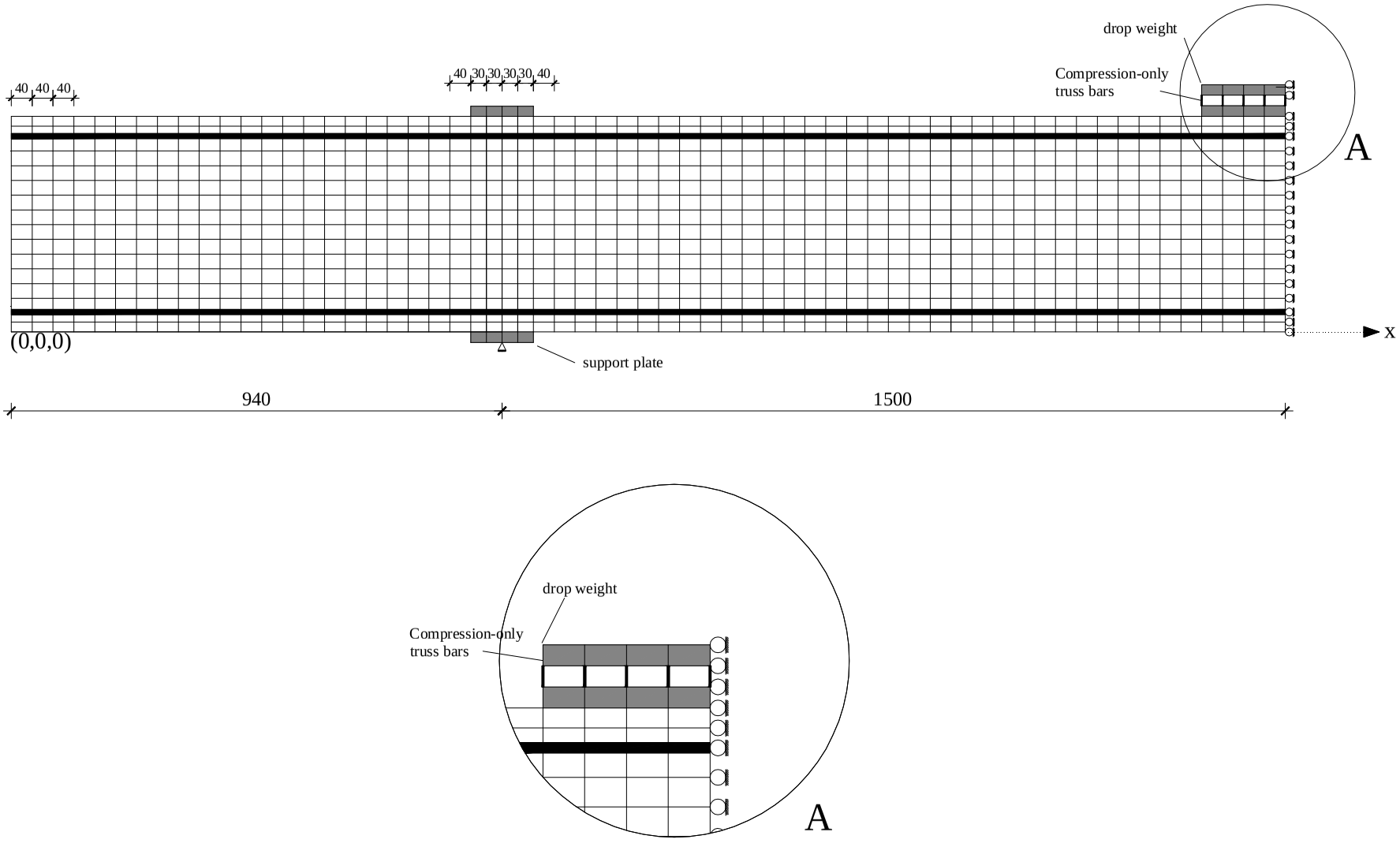

Figure 3.4. Finite element model for VT2

The 120 mm wide steel bearing plates at the supports were modeled with four elements placed at the top and bottom of support points. The drop weight was modeled using four rigid rectangular elements each 40x20 mm in size. The elements modeling the drop-weight were connected to the specimen by five compression-only truss bars, so that when the drop-weight bounced back, it will not pull up on specimen. These truss bars were also assigned very high stiffness properties, and they were connected to the element representing the steel placed at the point of impact (Figure 3.4).

A total of 992 rectangular elements were used to model the concrete. The dimensions of the elements were varied in the model to accommodate the nodal locations in accordance with the locations of the truss bars representing the longitudinal reinforcements and the elements representing the support plates.

The impact loads on the test specimens were simulated by assigning the impact velocity of the drop-weight to the nodal masses representing the drop-weight. The following figures present the comparisons of mid-span displacements, as observed and computed with VecTor2. Peak displacements are summarized in Table 3.6.

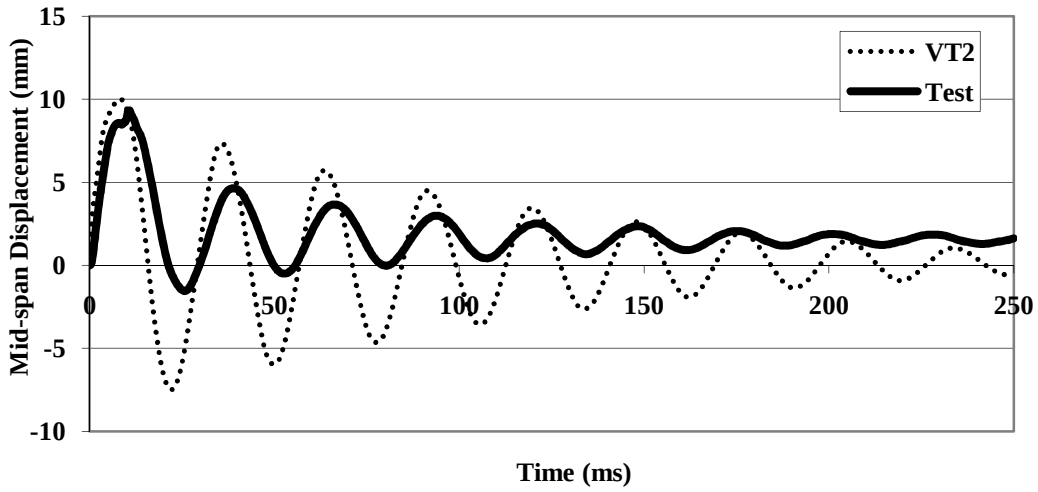

Figure 3.5. Comparison of observed and computed responses, SS0a

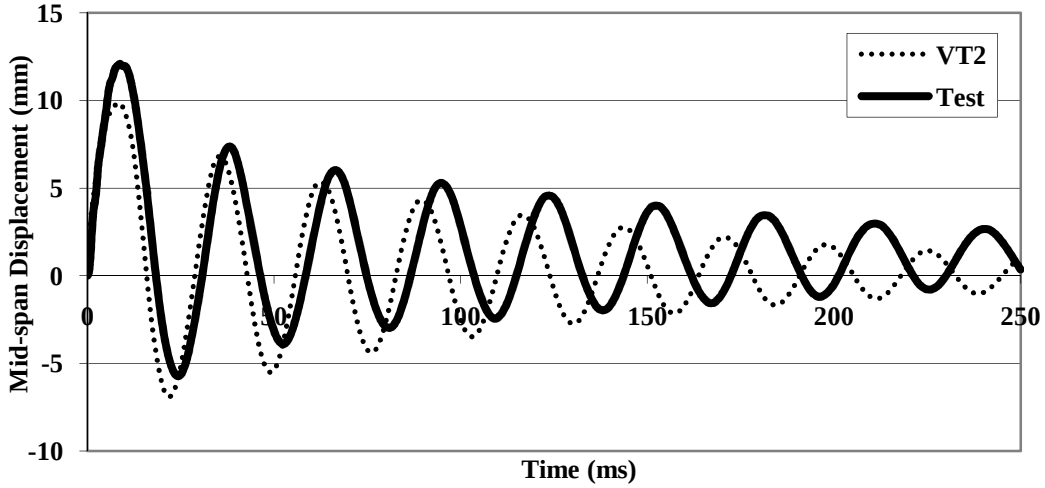

Figure 3.6. Comparison of observed and computed responses, SS1a

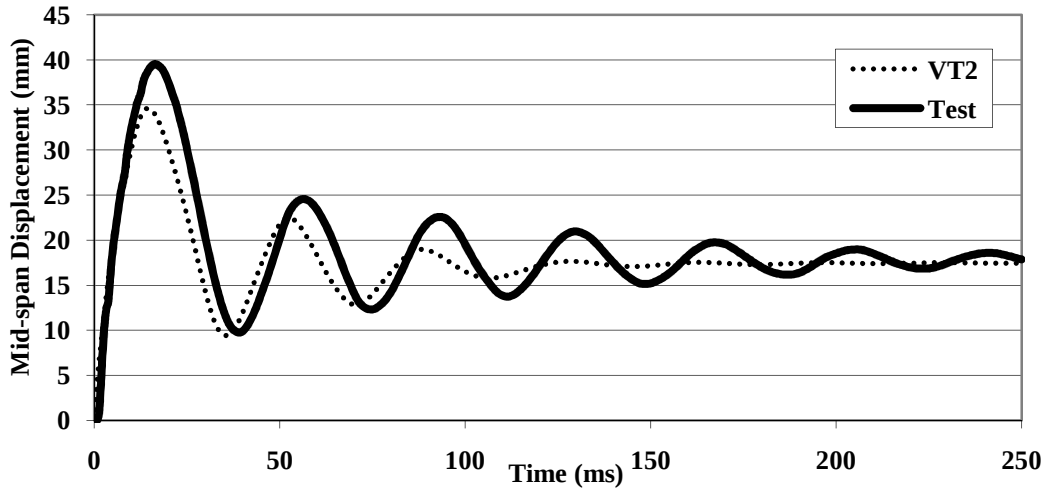

Figure 3.7. Comparison of observed and computed responses, SS1b

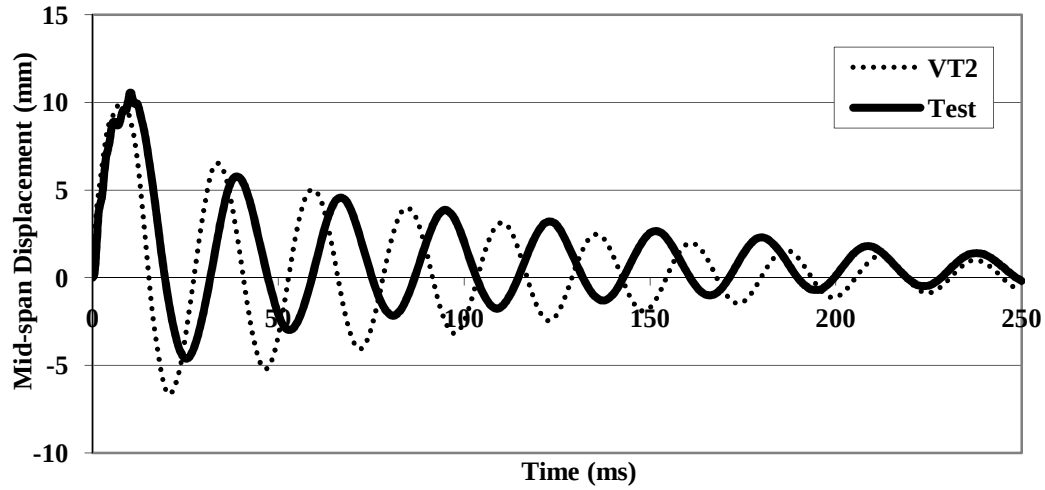

Figure 3.8. Comparison of observed and computed responses, SS2a

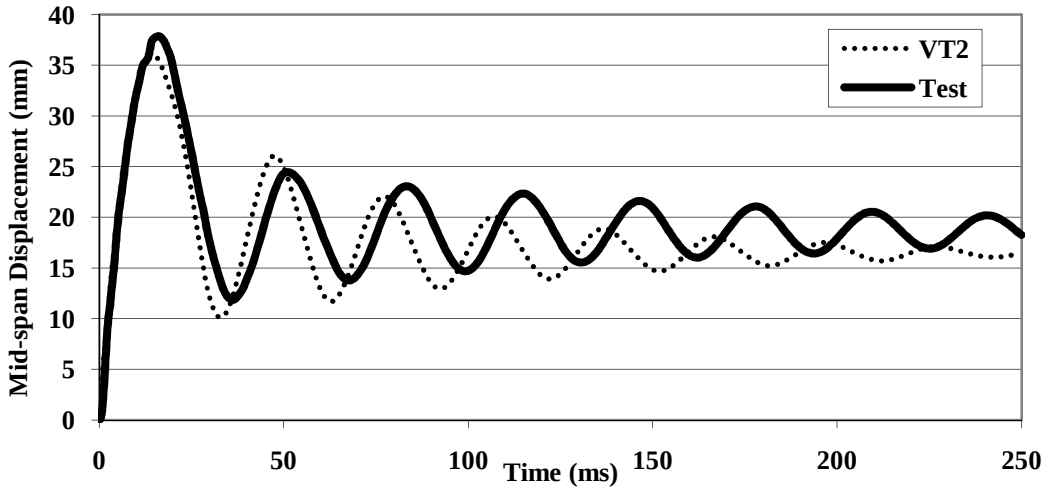

Figure 3.9. Comparison of observed and computed responses, SS2b

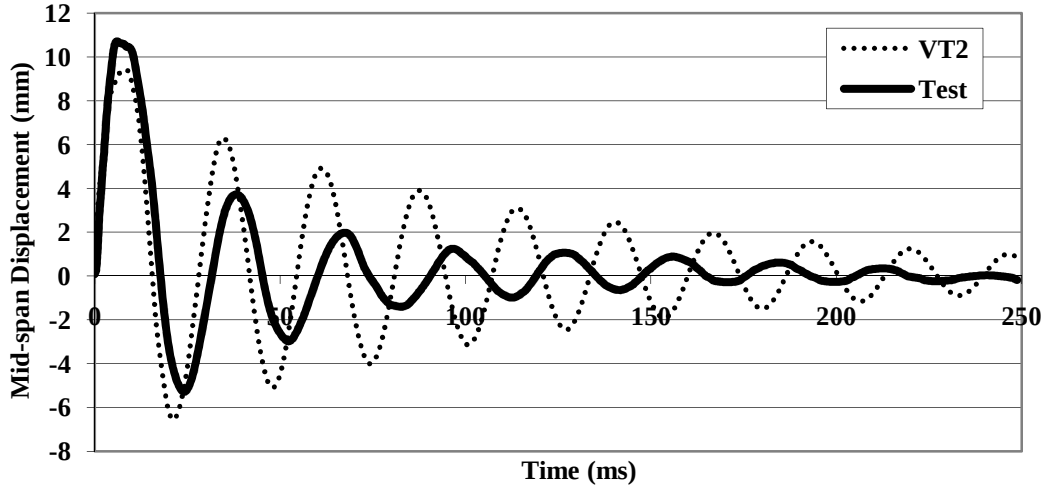

Figure 3.10. Comparison of observed and computed responses, SS3a

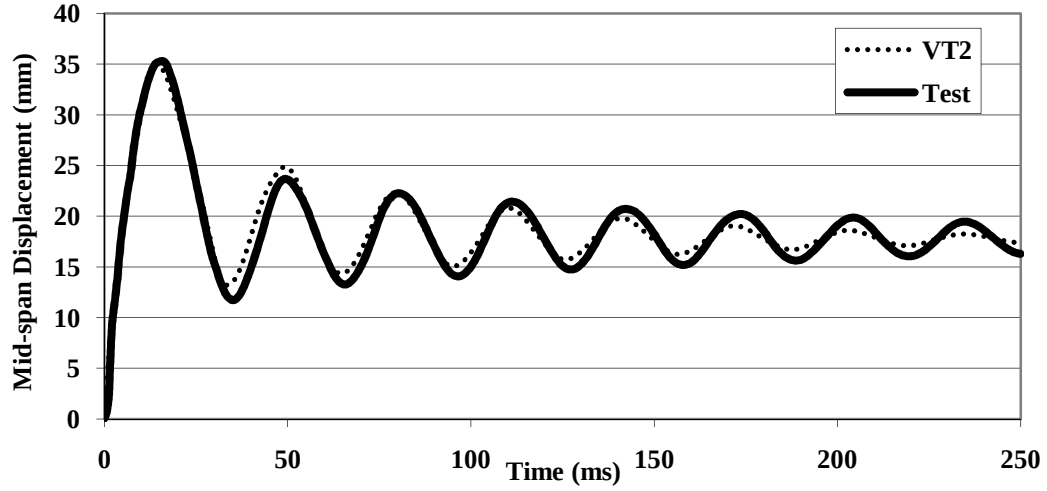

Figure 3.11. Comparison of observed and computed responses, SS3b

Table 3.6. Peak values as obtained from the tests, VT2 (first impact)

Test	TEST RESULTS		VT2 RESULTS		
	Max. Displacement (mm)	**Time at Max. Displacement (ms)**	**Max. Displacement (mm)**	**Time at Max. Displacement (ms)**	**Error in Max. Displ. (%)**
SS0a	9.32	10.83	10.02	8.50	-7.52
SS1a	12.08	8.75	9.86	8.50	18.34
SS1b	39.55	16.25	34.63	14.50	12.43
SS2a	10.54	10.42	9.93	7.50	5.82
SS2b	37.86	16.25	36.06	14.00	4.77
SS3a	10.70	6.25	9.44	8.50	11.83
SS3b	35.29	15.83	34.93	14.50	1.04

As seen in the figures and in the table, VT2 predicted the impact response of the beams well. Peak displacements were captured well in general. However, discrepancies in the post-peak vibrations, especially in the damping characteristics were also observed.

3.3.2. Impact Analysis of Kishi Beams using VecTor2

Tests carried out by Kishi et al. (2001) are modeled with VT2. To observe the suitability of the modeling techniques employed, shear- and flexural-critical specimens were selected for modeling. Only the extreme cases were considered in this study. Thus, the beams with the smallest and the largest span were selected. Test showed that, the beams subjected to 5 m/s impact load collapsed in a short time and showed no elastro-plastic deformation. Therefore, this study does not include the results of 5 m/s impact load.

For all analyses, crack profiles calculated by VecTor2 were visualized by a post-processor program called Augustus (Bentz 2003). Calculated and observed crack profiles for test are compared. It should be noted that, as a result of MCFT's rotating crack approach (Vecchio and Collins 1986), the crack direction at a load stage is determined by the principal axis of stress calculated for that load stage. In other words, the direction of cracks constantly changes, and Augustus does not sketch the crack

directions of the preceding load stages in the output. Therefore, a calculated crack profile does not reflect the cracking history of the structure, but, rather, relates only to that particular load stage. For this reason, several load stages need to be examined for a complete analysis of the estimated crack pattern. Moreover, the crack condition is calculated for each concrete element, whereas the cracks in the specimen would develop singly over a region. Hence, the calculated crack directions for individual elements should be regarded as an estimate of the inclination and width of a typical crack over that region. The crack profiles estimated at the initial stages of the response, negative moment phase as discussed by (Saatci and Vecchio 2009), at the time the peak midspan displacement occurred, and at the final resting stage of the specimen, are presented and compared with the crack profiles obtained from the test results. Note that the crack profiles observed after the tests relate to the final resting stage of the specimen. The crack widths calculated by VecTor2 for the time when the peak midspan displacement occurred are also presented to give an indication of the levels of predicted maximum crack widths.

Model and Analysis of beam A24&B24

The beams A24 and B24 were the ones with the smallest span tested by Kishi et al. Both beams had a shear span of 500 mm. A24 had 0.0182 longitudinal reinforcement ratio, whereas B24 had 0.0080, and both beams were shear-critical. For these analyses a total of 318 rectangular elements were used to represent concrete and support plates, and 27 truss bar elements were used to model longitudinal steel reinforcement. The mesh included 362 nodes. Taking advantage of the symmetric load and support conditions, only half of the beams were modeled. All nodes at the centerline of the beam were restrained against displacements in the x-direction (Figure 3.12).

The 40 mm wide steel bearing plates at the supports were modeled with two elements placed at the bottom of support points. The drop weight was modeled using two rigid rectangular elements each 30x20 mm in size. The elements modeling the drop-weight were connected to the specimen by three compression-only truss bars, so that when the drop-weight bounced back, it will not pull up on specimen. These truss bars were also assigned very high stiffness properties, and they were connected to the element representing the steel plate placed at the point of impact. A total of 314 rectangular elements were used to model concrete. The dimensions of the elements were

varied in the model to accommodate the nodal locations in accordance with the locations of the truss bars representing the longitudinal reinforcements and the elements representing the support plates.

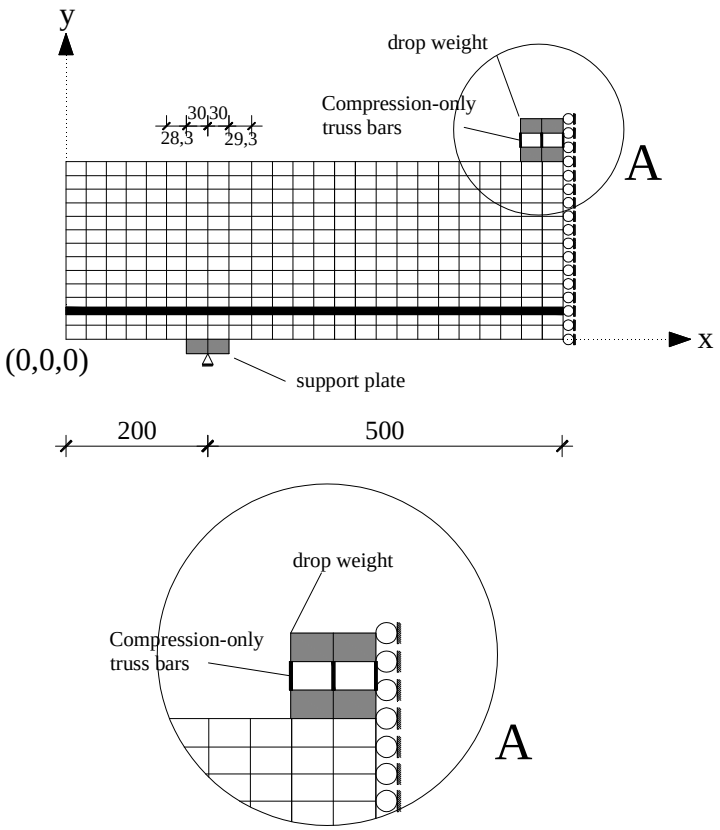

Figure 3.12. Finite element model for VT2 (A24&B24)

The impact loads on the test specimens were simulated by assigning the impact velocity of the drop-weight to the nodal masses representing the drop-weight. The following figures present the comparisons of mid-span displacements, as observed and computed with VecTor2. Estimated crack profiles by VT2 at the time of peak mid-span displacement are also presented. Peak displacements are summarized in Table 3.7 and Table 3.8.

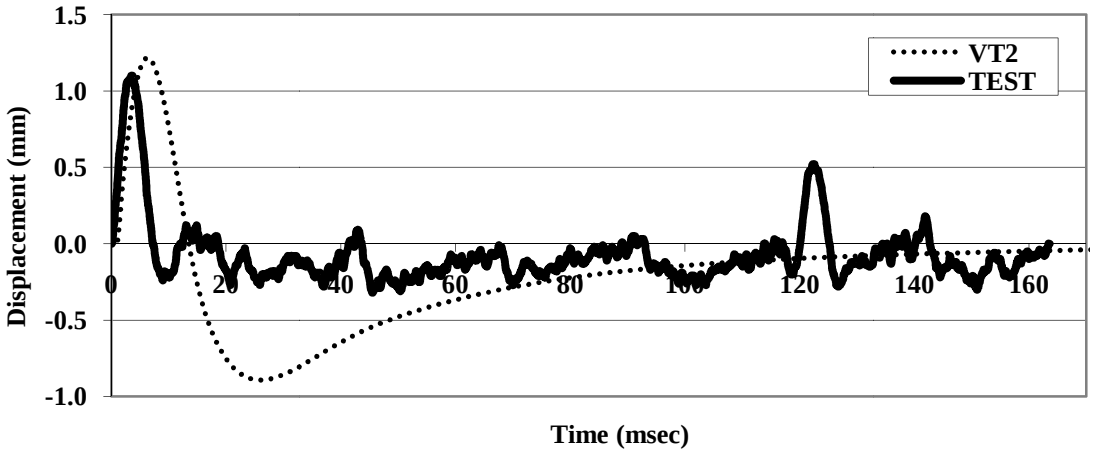

Figure 3.13. Comparison of observed and computed responses, A24 - V=1 m/s

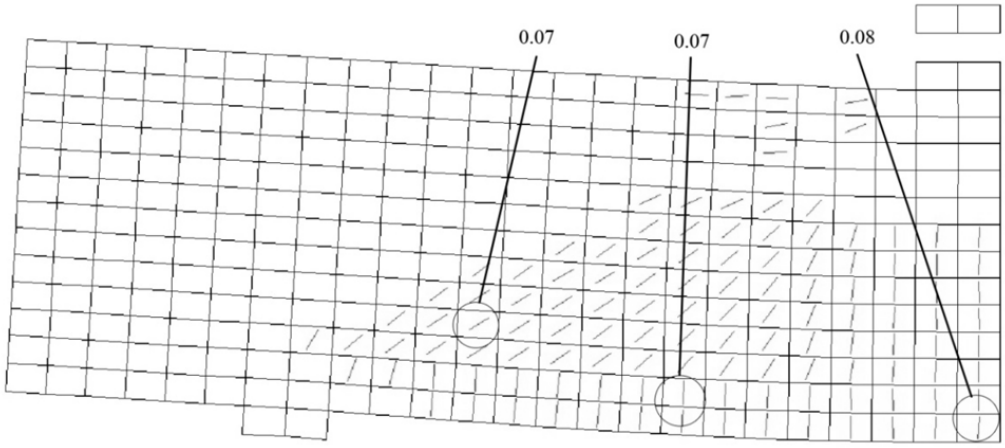

Figure 3.14. Calculated crack profile at peak point, A24 - V=1 m/s

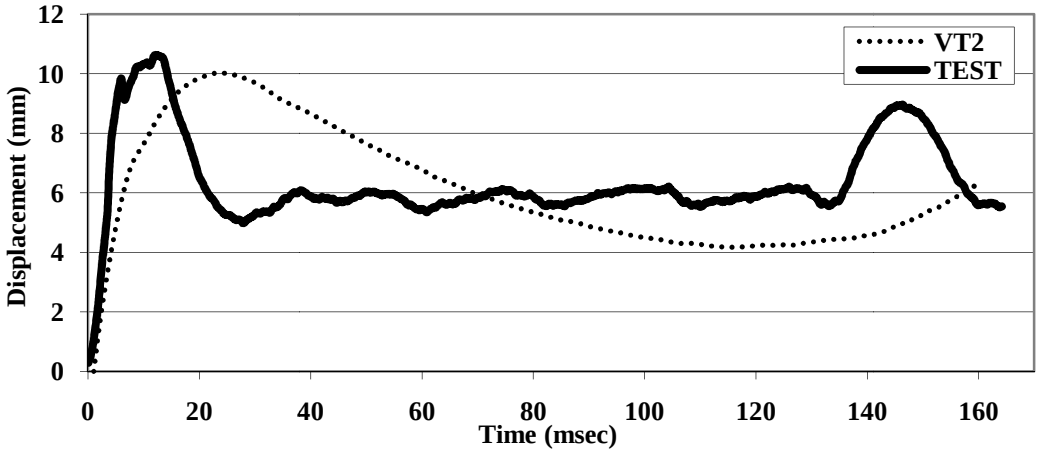

Figure 3.15. Comparison of observed and computed responses, A24 - V=3 m/s

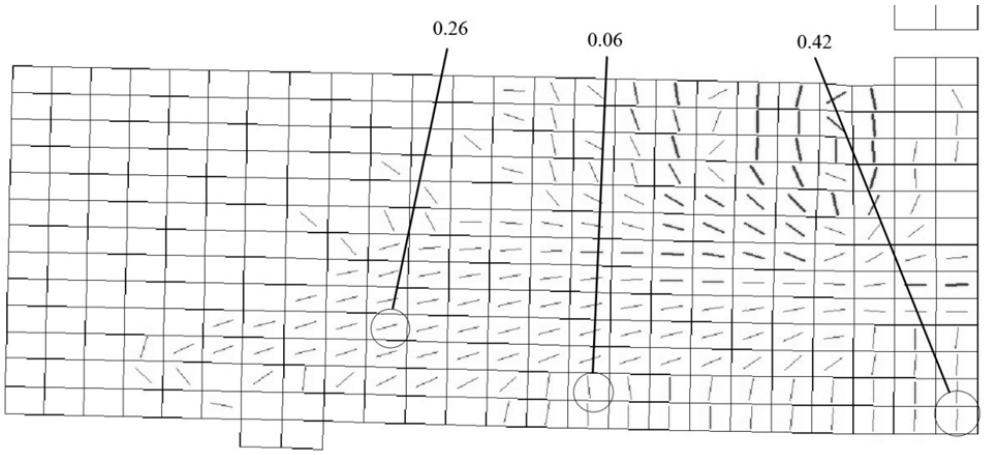

Figure 3.16. Calculated crack profile at peak point, A24 - V=3 m/s

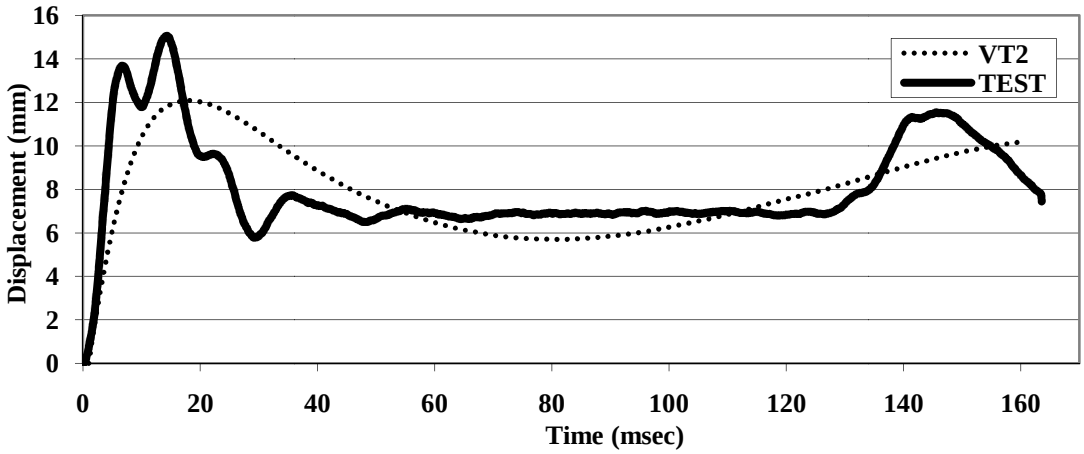

Figure 3.17. Comparison of observed and computed responses, A24 - V=4 m/s

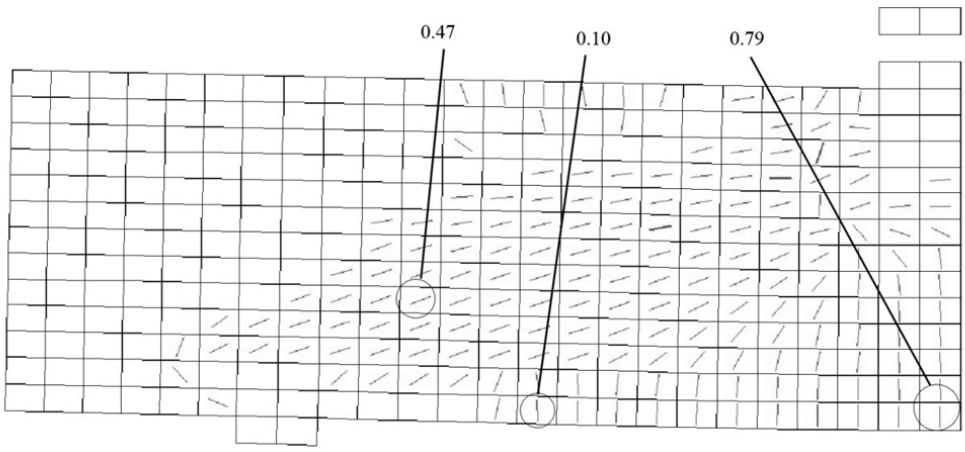

Figure 3.18. Calculated crack profile at peak point, A24 - V=4 m/s

Table 3.7. Peak values as obtained from the tests and VT2 analyses for A24

Test	V (m/s)	TEST RESULTS		VT2 RESULTS		
		Max. Displacement (mm)	Time at Max. Displacement (ms)	Max. Displacement (mm)	Time at Max. Displacement (ms)	Error in Max. Displ. (%)
A24	**1**	1.10	3.50	1.21	6.00	-10.27
A24	**3**	10.63	12.40	10.03	24.00	5.67
A24	**4**	15.07	14.30	12.09	18.00	19.79

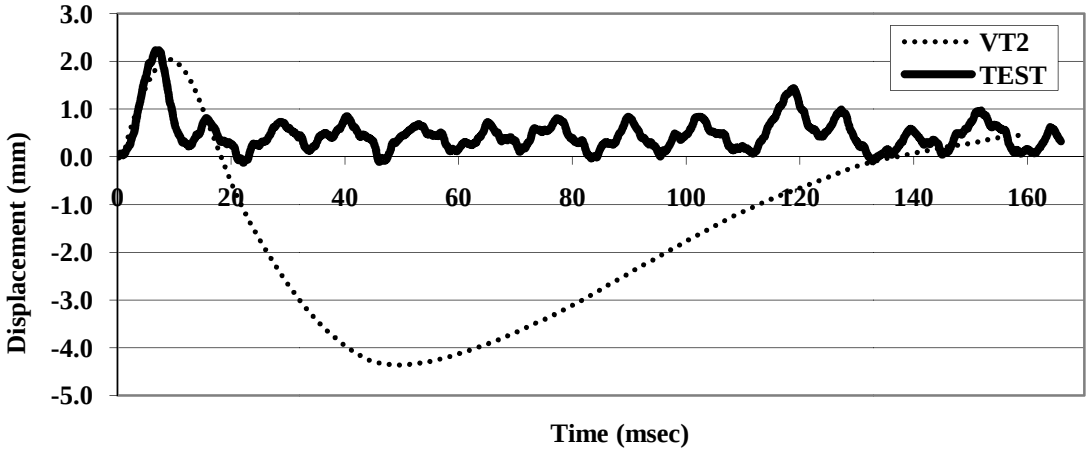

Figure 3.19. Comparison of observed and computed responses, B24 - V=1 m/s

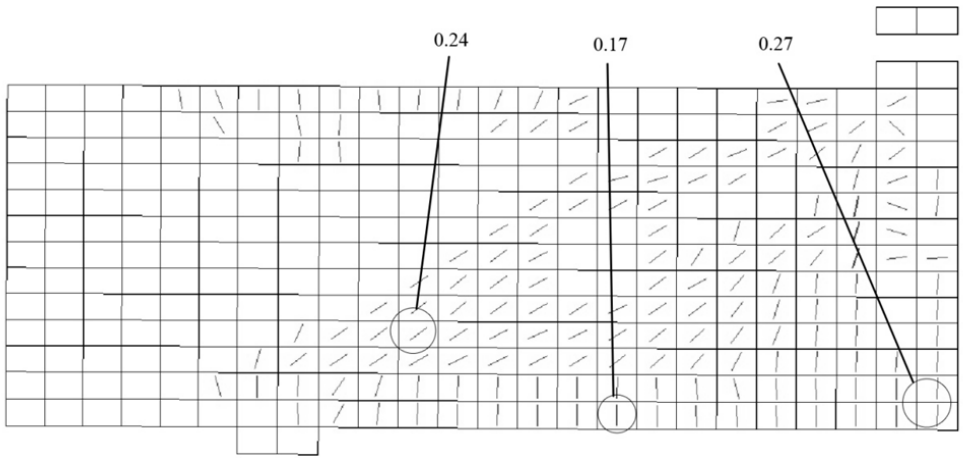

Figure 3.20. Calculated crack profile at peak point, B24 - V=1 m/s

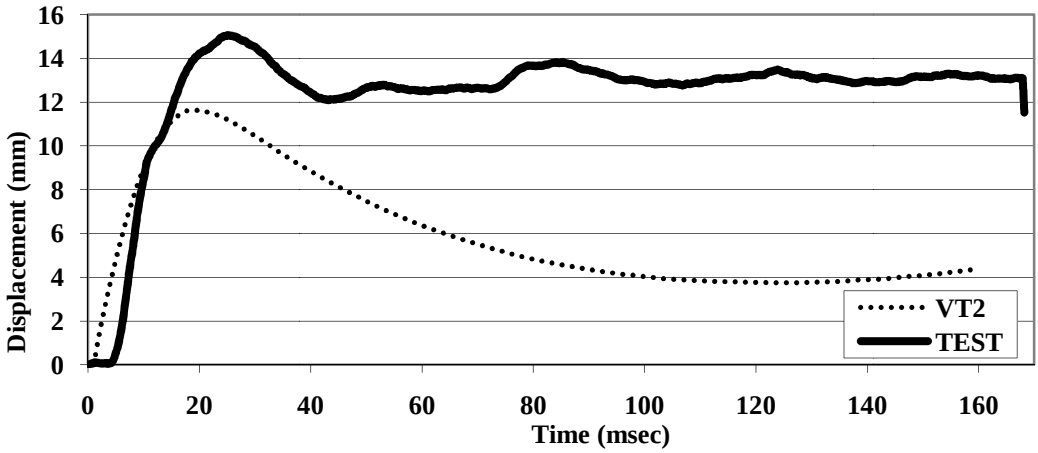

Figure 3.21. Comparison of observed and computed responses, B24 - V=3 m/s

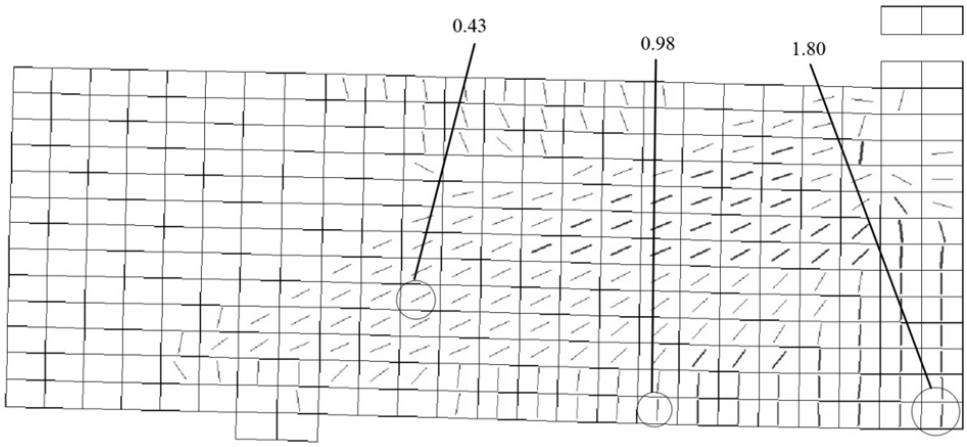

Figure 3.22. Calculated crack profile at peak point, B24 - V=3 m/s

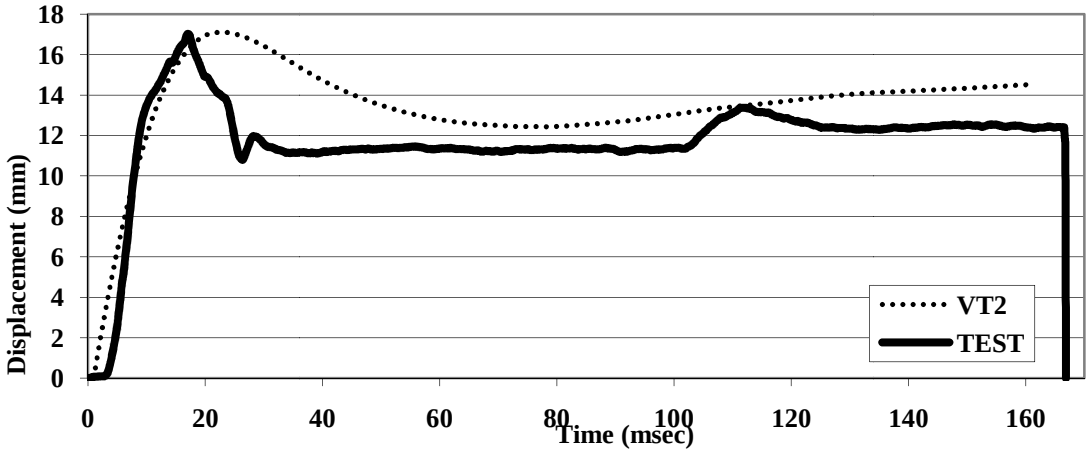

Figure 3.23. Comparison of observed and computed responses, B24 - V=4 m/s

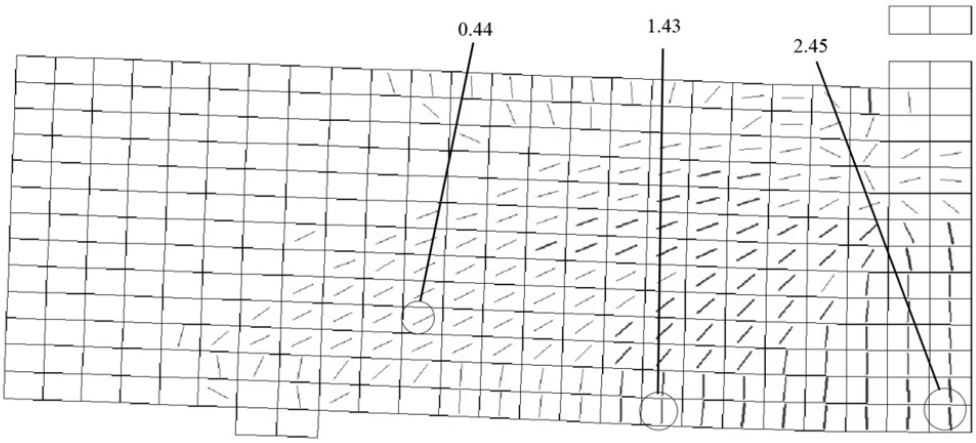

Figure 3.24. Calculated crack profile at peak point, B24 - V=4 m/s

Table 3.8. Peak values as obtained from the tests and VT2 for B24

Test	V (m/s)	TEST RESULTS		VT2 RESULTS		
		Max. Displacement (mm)	Time at Max. Displacement (ms)	Max. Displacement (mm)	Time at Max. Displacement (ms)	Error in Max. Displ. (%)
B24	**1**	2.23	6.70	2.04	9.00	8.48
B24	**3**	15.06	25.00	11.63	19.00	22.75
B24	**4**	17.02	17.10	17.11	23.00	-0.55

Model and Analysis of beam A48&B48

The beams A48 and B48 were the ones with the largest span tested by Kishi et al. Both beams had a shear span of 1000 mm. A48 had 0.0182 longitudinal reinforcement ratio, whereas B48 had 0.0080. A48 was still shear-critical due to it's the large amount of longitudinal reinforcement it had, where as B48 was flexural-critical. For this analysis a total of 526 rectangular elements were used to represent to concrete and support plates, and 43 truss bar elements were used to model longitudinal steel reinforcement. The mesh included 586 nodes. Taking advantage of the symmetric load and support conditions, only half of a beam was modeled. All nodes at centerline of the beam were restrained against displacements in the x-direction (Figure 3.25).

The 40 mm wide steel bearing plates at the supports were modeled with two elements placed at the bottom of support points. The drop weight was modeled using two rigid rectangular elements each 30x20 mm in size. The elements modeling the drop-weight were connected to the specimen by three compression-only truss bars, so

that when the drop-weight bounced back, it will not pull up on specimen. These truss bars were also assigned very high stiffness properties, and they were connected to the elements representing the steel placed at the point of impact.

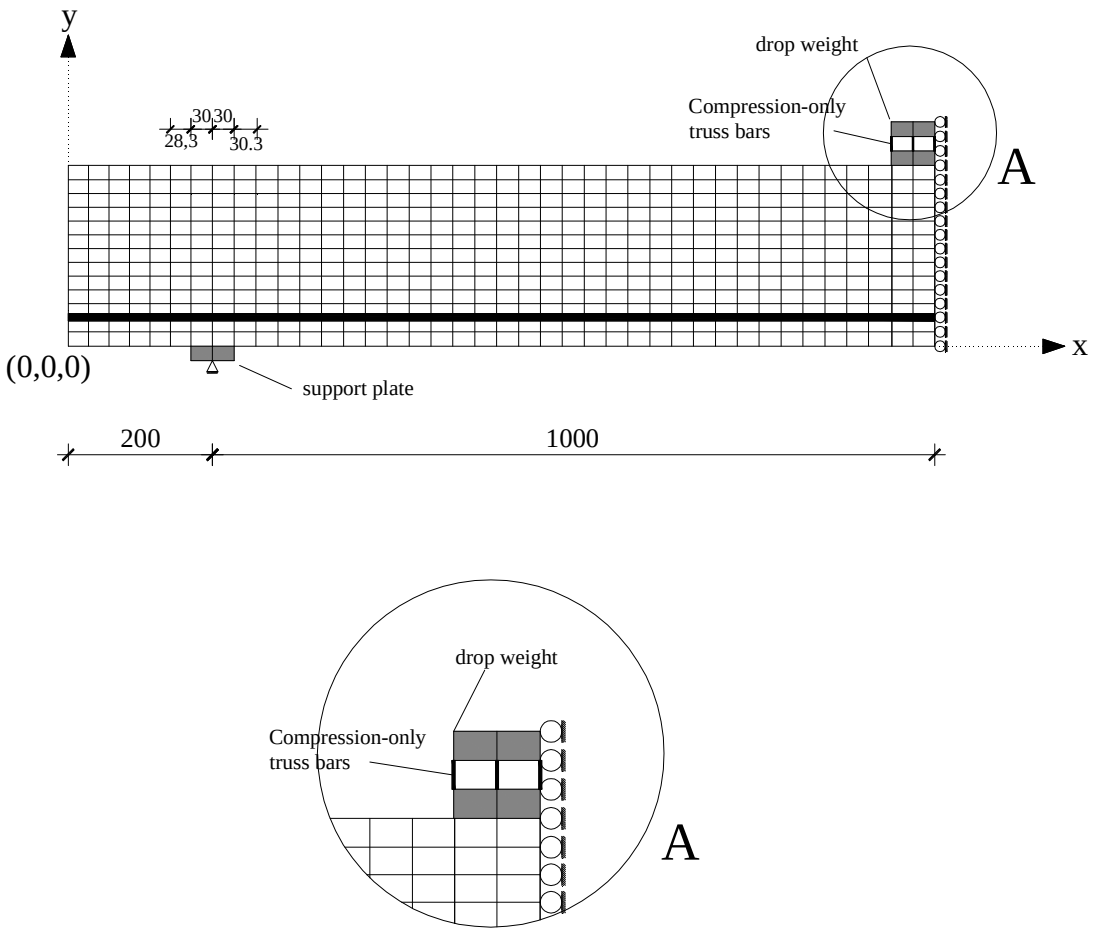

Figure 3.25. Finite element model for VT2 (A48 and B48)

A total of 520 rectangular elements were used to model the concrete. The dimensions of the elements were varied in the model to accommodate the nodal locations in accordance with the locations of the truss bars representing the longitudinal reinforcements and the elements representing the support plates.

The impact loads on the test specimens were simulated by assigning the impact velocity the drop-weight to the nodal masses representing the drop-weight. The following figures present the comparisons of mid-span displacements, as observed in the tests and computed with VecTor2. Peak displacements are summarized in Table 3.9

and Table 3.10. The crack profiles at the time of peak mid-span displacement are also presented.

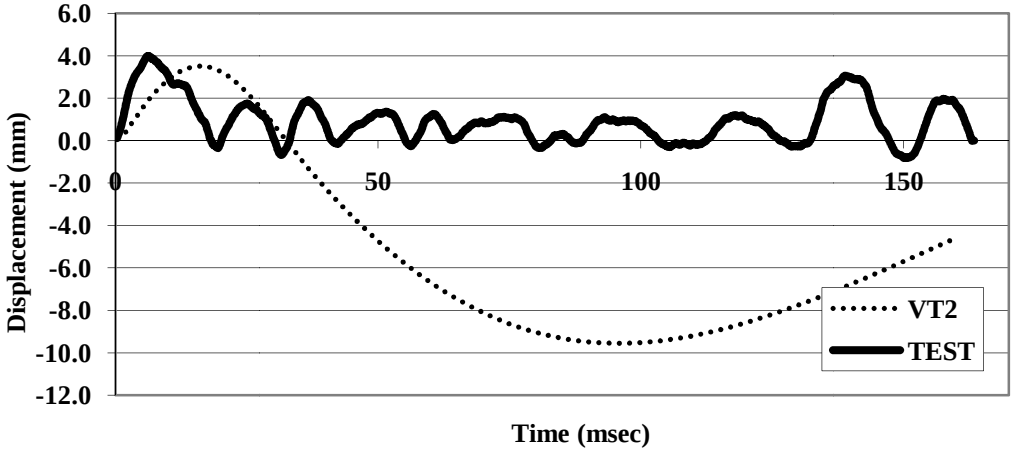

Figure 3.26. Comparison of observed and computed responses, A48 - V=1 m/s

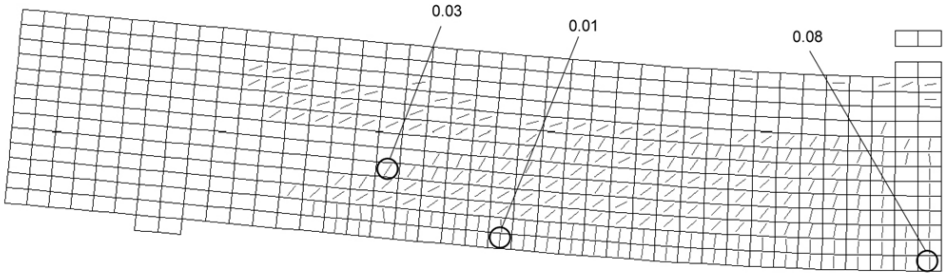

Figure 3.27. Calculated crack profile at peak point, A48 - V=1 m/s

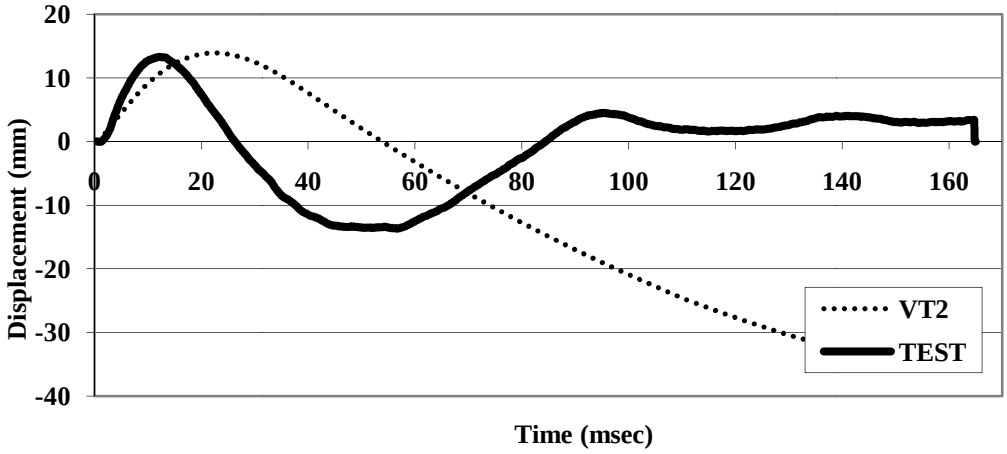

Figure 3.28. Comparison of observed and computed responses, A48 - V=3 m/s

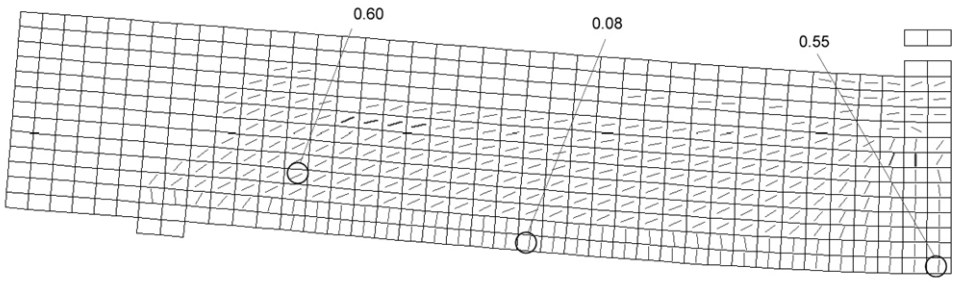

Figure 3.29. Calculated crack profile at peak point, A48 - V=3 m/s

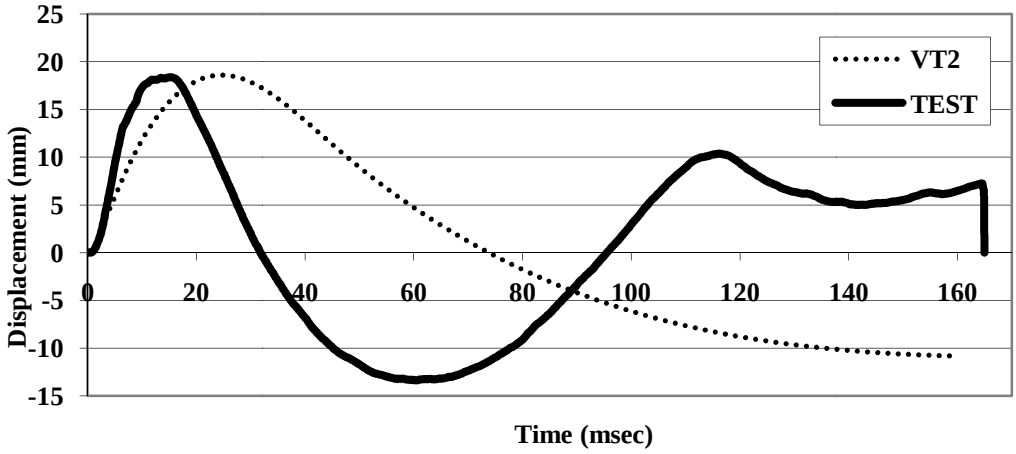

Figure 3.30. Comparison of observed and computed responses, A48 - V=4 m/s

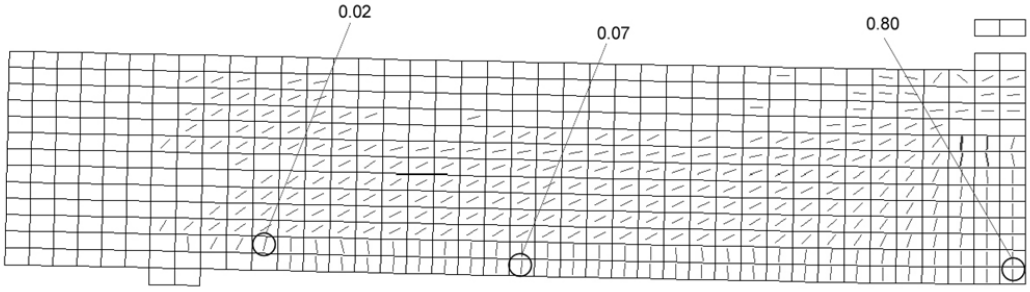

Figure 3.31. Calculated crack profile at peak point, A48 - V=4 m/s

Table 3.9. Peak values as obtained from the tests, VT2 (first impact)

Test	V (m/s)	TEST RESULTS		VT2 RESULTS		
		Max. Displacement (mm)	Time at Max. Displacement (ms)	Max. Displacement (mm)	Time at Max. Displacement (ms)	Error in Max. Displ. (%)
A48	**1**	3.98	6.10	3.51	16.00	11.93
A48	**3**	13.27	12.40	13.89	23.00	-4.67
A48	**4**	18.38	15.10	18.61	25.00	-1.25

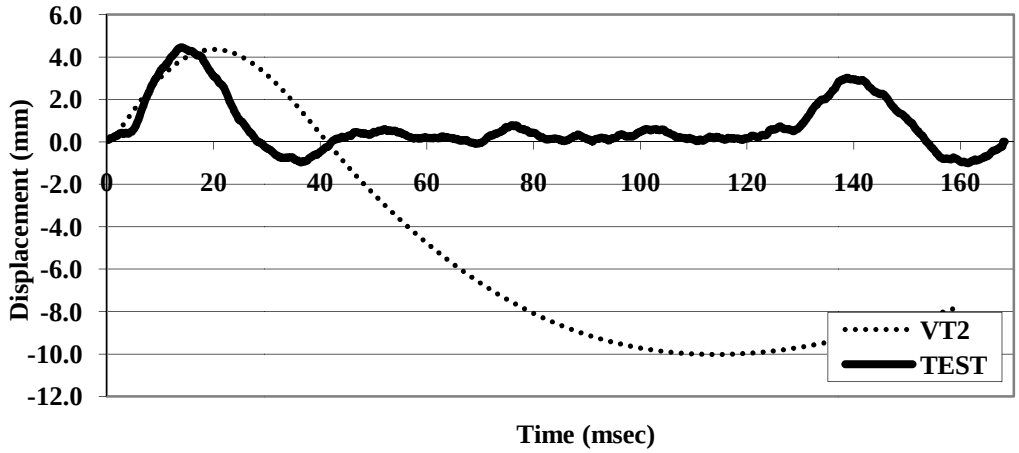

Figure 3.32. Comparison of observed and computed responses, B48 - V=1 m/s

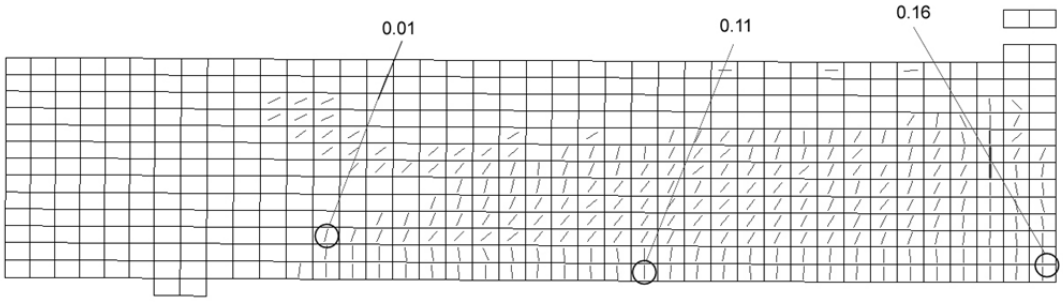

Figure 3.33. Calculated crack profile at peak point, B48 - V=1 m/s

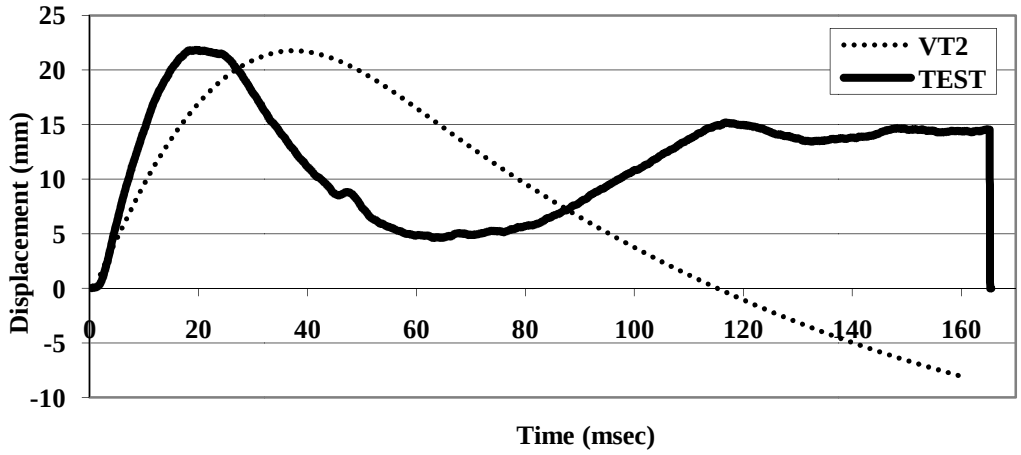

Figure 3.34. Comparison of observed and computed responses, B48 - V=3 m/s

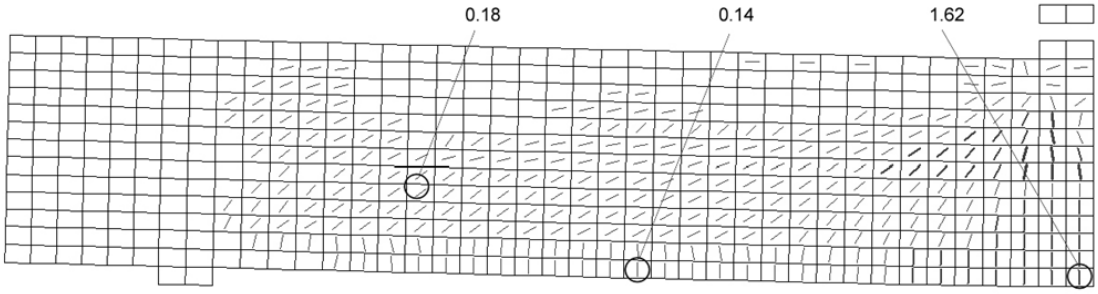

Figure 3.35. Calculated crack profile at peak point, B48 - V=3 m/s

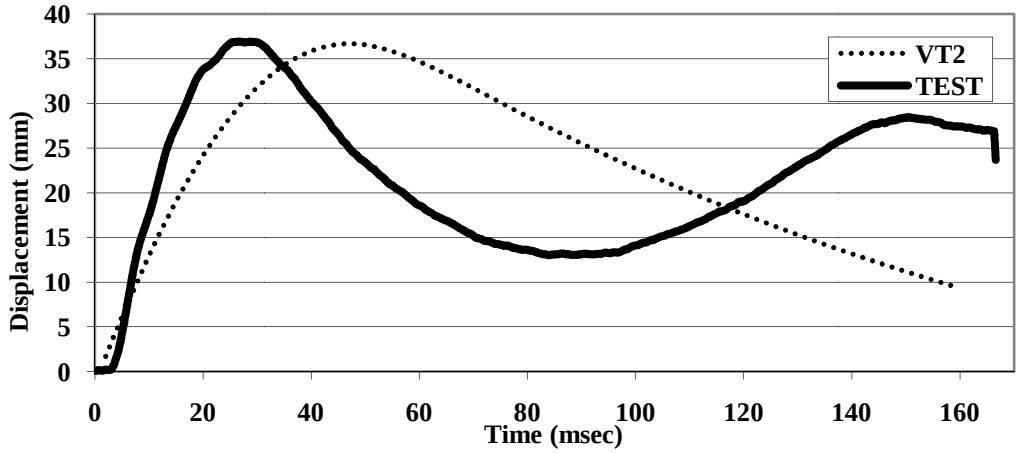

Figure 3.36. Comparison of observed and computed responses, B48 - V=4 m/s

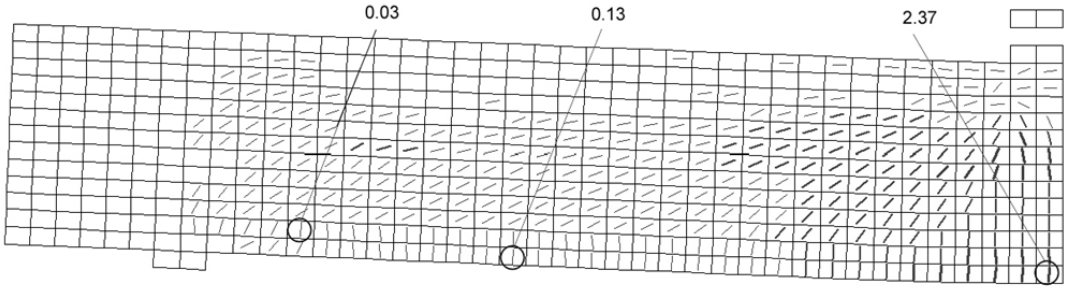

Figure 3.37. Calculated crack profile at peak point, B48 - V=4 m/s

Table 3.10. Peak values as obtained from the tests, VT2 (first impact)

Test	V (m/s)	TEST RESULTS		VT2 RESULTS		
		Max. Displacement (mm)	Time at Max. Displacement (ms)	Max. Displacement (mm)	Time at Max. Displacement (ms)	Error in Max. Displ. (%)
B48	**1**	4.46	13.90	4.36	20.00	2.20
B48	**3**	21.83	19.40	21.76	37.00	0.31
B48	**4**	36.90	26.80	36.68	47.00	0.61

As seen in the tables and figures, VT2 performed well in general. Peak displacements were captured with great accuracy almost for all cases. The errors in predicting the maximum displacements were minimal and well within the range of acceptable accuracy for reinforced concrete structures. Such good predictions were observed in shear-critical members as well, demonstrating VT2's ability in modeling shear behavior. However, the predictions for post-peak vibrations were generally poor. Such poor predictions can be attributed to the deficiencies in modeling the contact between the drop-weight and the specimens, as well as modeling the hysteretic behavior of concrete. It also has to be noted that minimal information was available regarding the details of the test setup and the support conditions of the beams. Since VT2 performed significantly better with Saatci beams for which all testing details were available and considered in modeling, greater part of the error encountered in predictions can be attributed to the lack of detailed information about the testing conditions.

3.4. Impact Analysis of Reinforced Concrete Beams using VecTor3

3.4.1. Impact Analysis of Saatci Beams using VecTor3

The analysis carried in Section 3.3.1 are repeated with the three-dimensional mesh using VecTor3. For this analysis a total of 1008 hexahedral elements were used to represent to concrete and support plates, and 262 truss bar elements were used to model longitudinal steel reinforcement. The mesh included 2196 nodes. Taking advantages of the symmetric load and support conditions, only half of a beam was modeled. All nodes at centerline of the beam were restrained against displacements in the x-direction (Figure 3.38)

The 120 mm wide steel bearing plate at the supports was modeled with four elements placed at the top and bottom of support points. The drop weight was modeled using four rigid hexahedral elements each 40x20 mm in size. The elements modeling the drop-weight were connected to the specimen by ten compression-only truss bars, so that when the drop-weight bounced back, it will not pull up on specimen. These truss bars were also assigned very high stiffness properties, and they were connected to the element representing the steel placed at the point of impact.

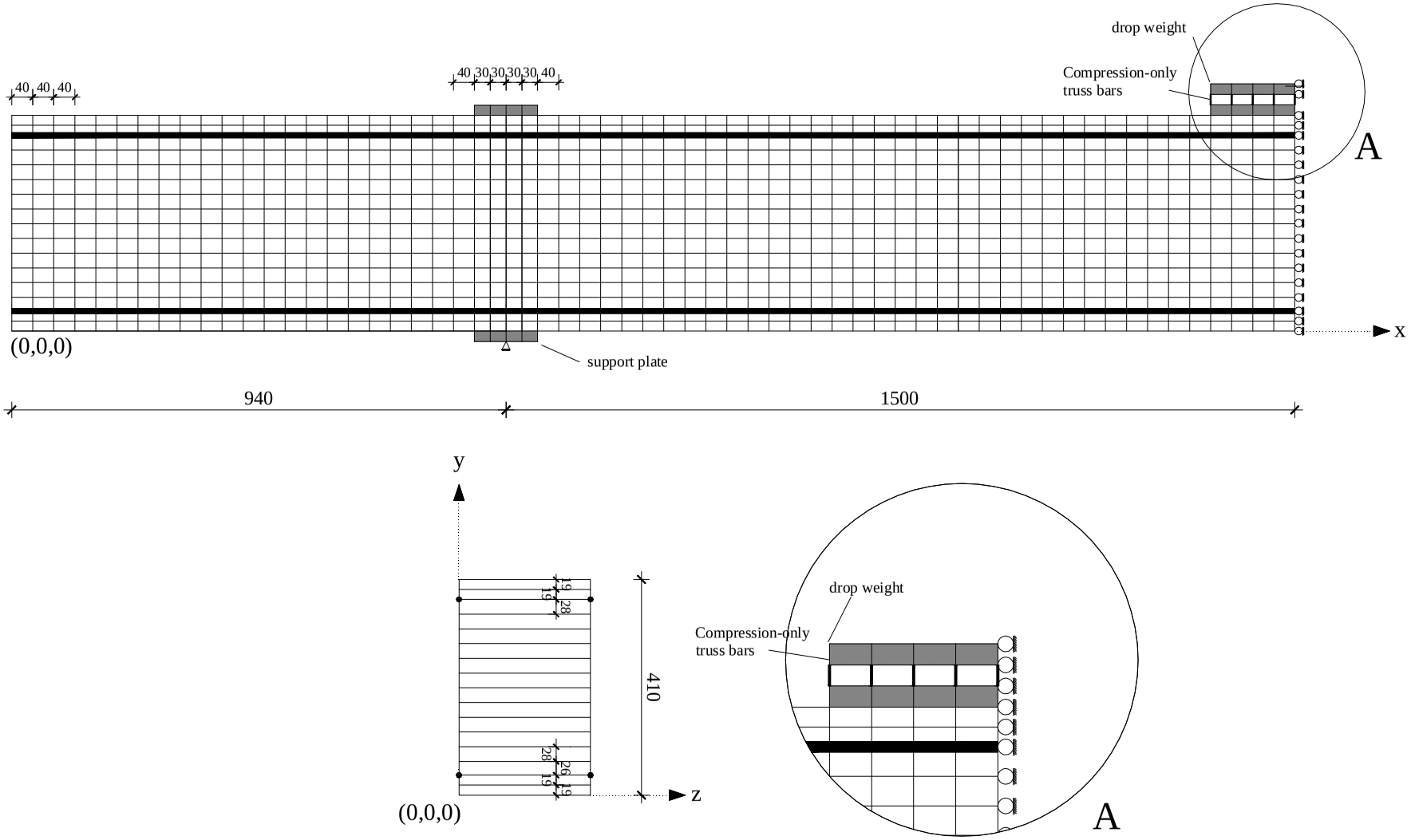

Figure 3.38. Finite element model for VT3

A total of 992 rectangular elements were used to model the concrete. The dimensions of the elements were varied in the model to accommodate the nodal locations in accordance with the locations of the truss bars representing the longitudinal reinforcements and the elements representing the support plates.

The impact loads on the test specimens were simulated by assigning the impact velocity of the drop-weight to the nodal masses representing the drop-weight. The following figures present the comparisons of mid-span displacements, as observed in tests and computed with VecTor3. Peak displacements are summarized in Table 3.11.

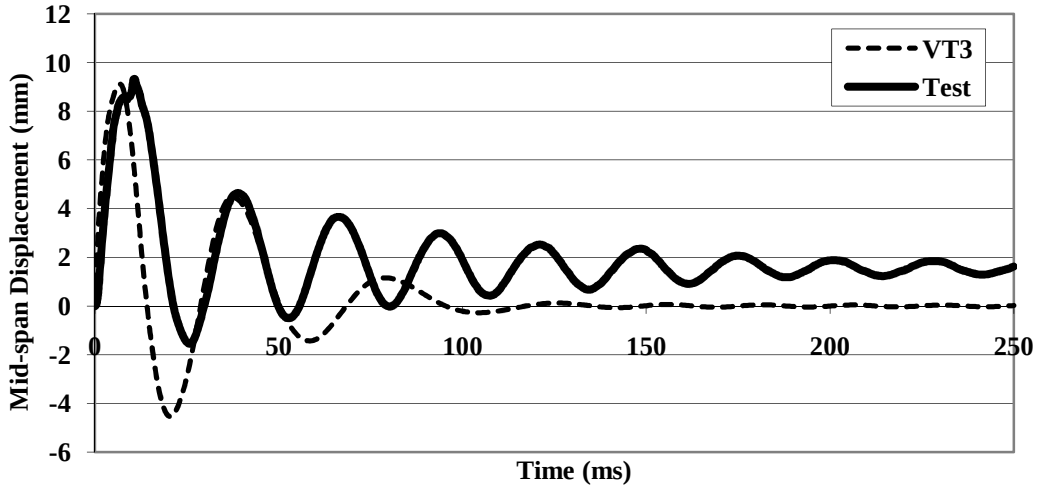

Figure 3.39. Comparison of observed and computed responses, SS0a

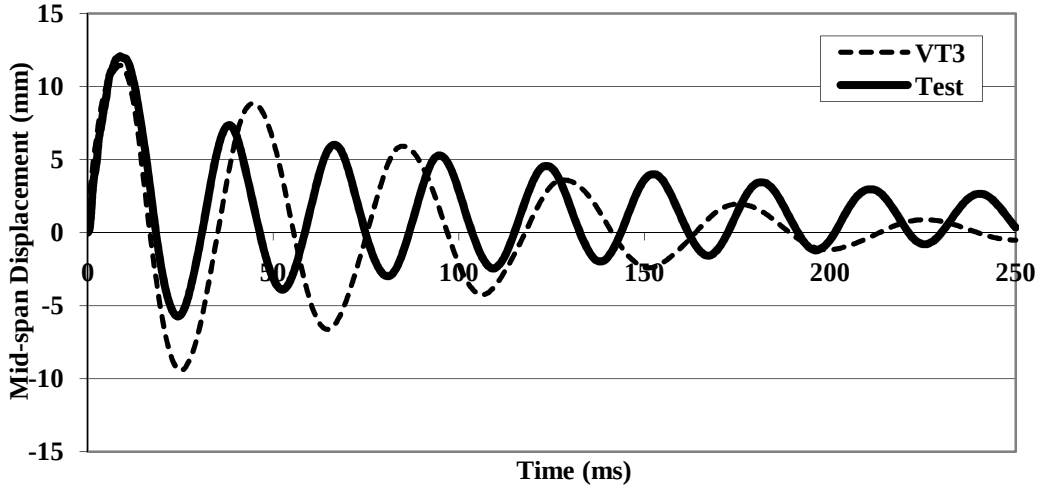

Figure 3.40. Comparison of observed and computed responses, SS1a

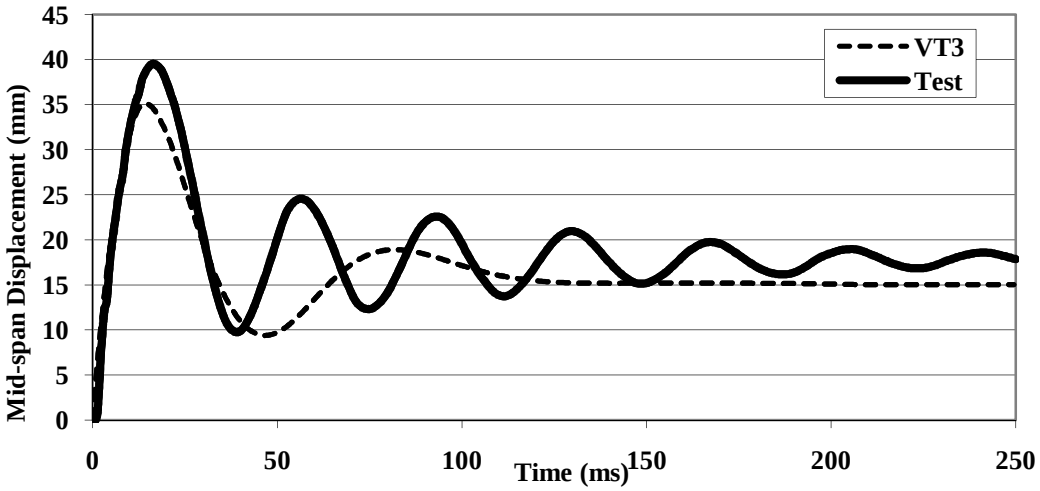

Figure 3.41. Comparison of observed and computed responses, SS1b

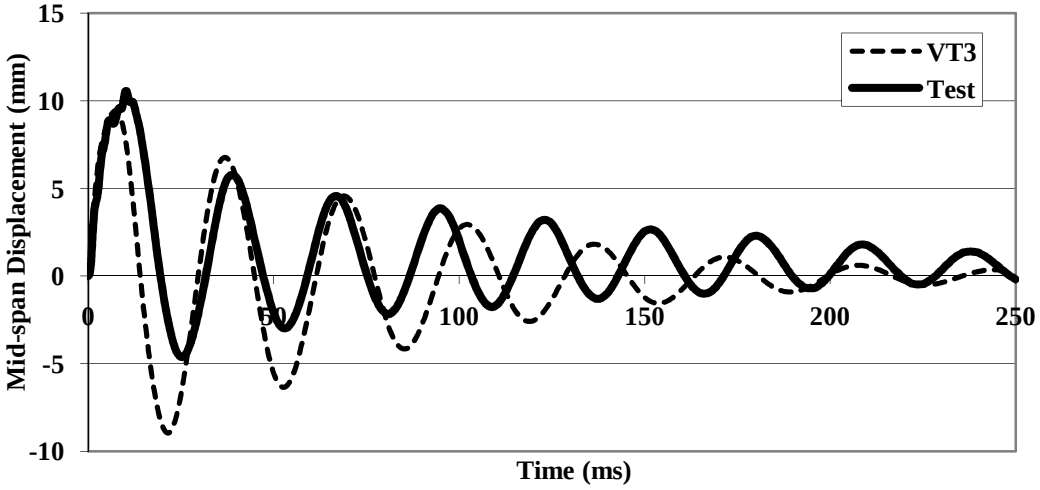

Figure 3.42. Comparison of observed and computed responses, SS2a

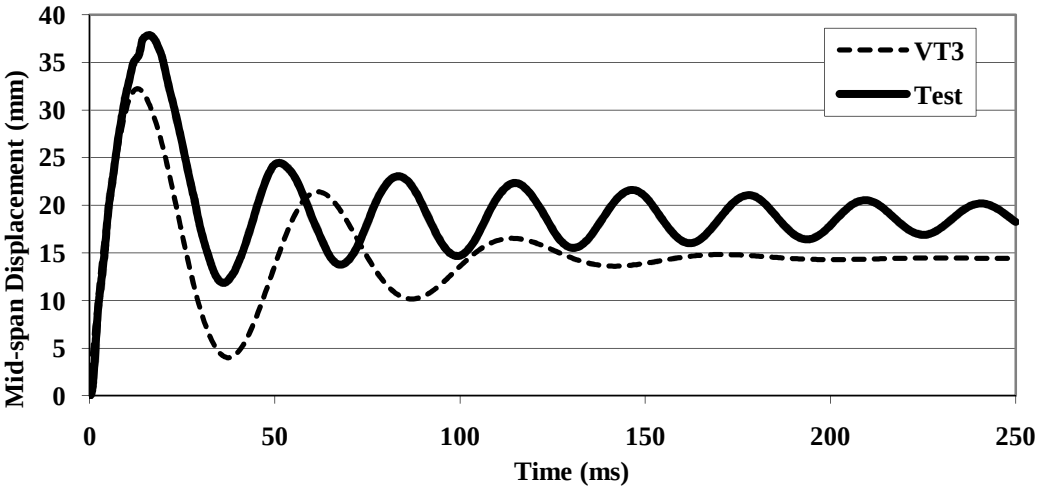

Figure 3.43. Comparison of observed and computed responses, SS2b

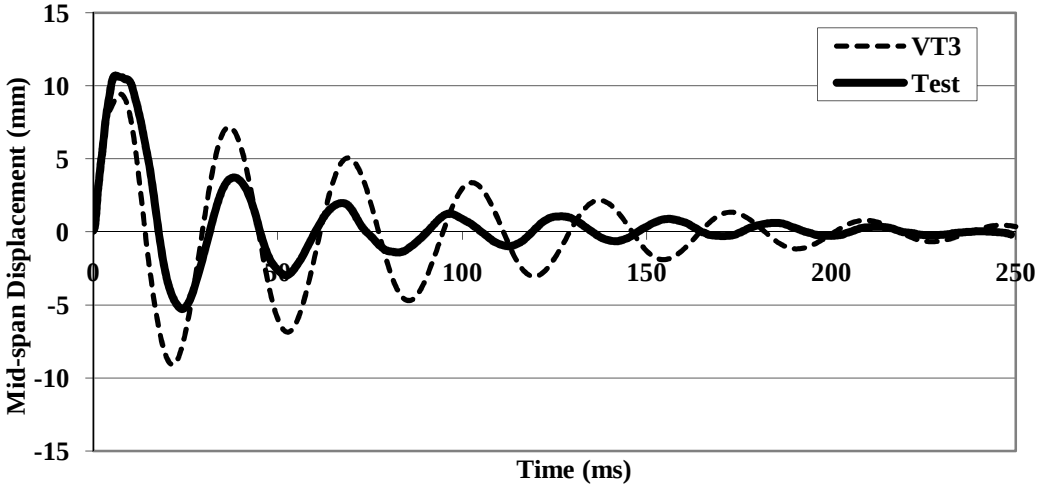

Figure 3.44. Comparison of observed and computed responses, SS3a

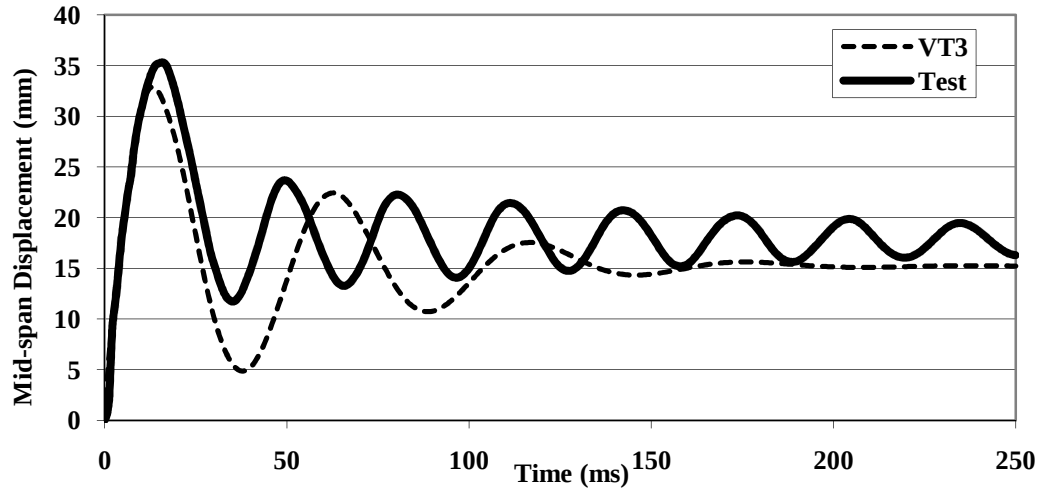

Figure 3.45. Comparison of observed and computed responses, SS3b

Table 3.11. Peak values as obtained from the tests and VT3

Test	TEST RESULTS		VT3 RESULTS		
	Max. Displ. (mm)	Time at Max. Displ. (ms)	Max. Displ. (mm)	Time at Max. Displ. (ms)	Error in Max. Displ. (%)
SS0a	9.32	10.83	9.11	7.00	2.25
SS1a	12.08	8.75	11.43	9.00	5.35
SS1b	39.55	16.25	35.10	14.50	11.23
SS2a	10.54	10.42	9.44	7.50	10.49
SS2b	37.86	16.25	32.24	13.00	14.84
SS3a	10.70	6.25	9.44	7.50	11.84
SS3b	35.29	15.83	32.88	13.00	6.83

3.5. Comparison of the Results of Impact Analysis of Saatci Beams

VT2 and VT3 essentially use the same methodology of MCFT. However, they may produce different results. The following figures compare both solutions for the same specimens. Peak displacements are summarized in Table 3.12. As seen in figures, both VT2 and VT3 made very similar predictions for the peak displacements. However, since VT2 has an advanced treatment of the drop-weight with regards to its connection to the specimen with compression-only truss bars, it yielded better predictions in the post-peak range. The algorithm for the compression-only truss bars in VT3 has some deficiencies, causing some tension in these bars. This problem was eliminated in VT2, but remained in VT3 for the time being. On the other hand, VT3 model produced no significant out-of-plane stress or deformation, suggesting that the two-dimensional model employed by VT2 was sufficient for an accurate modeling.

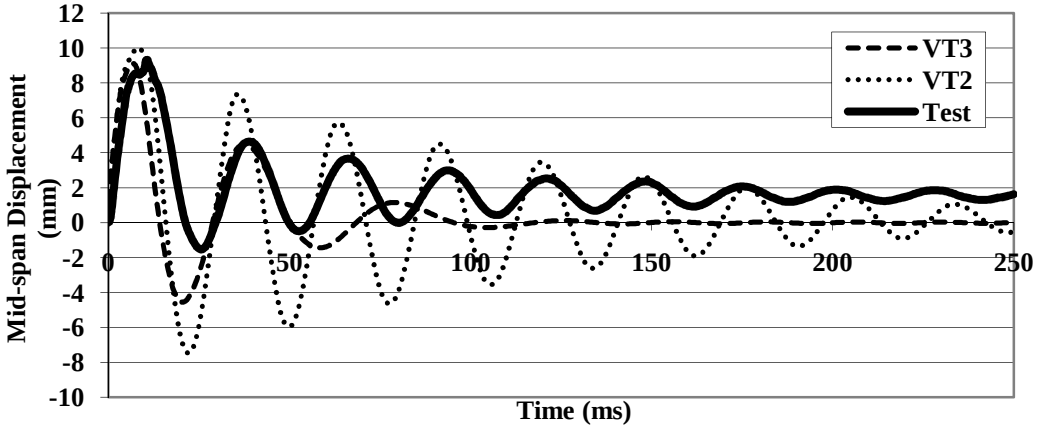

Figure 3.46. Comparison of observed and computed responses, SS0a

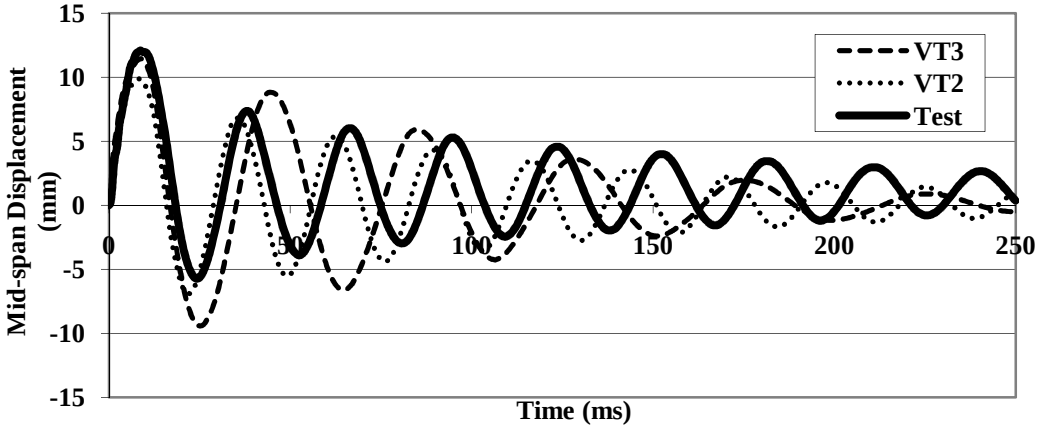

Figure 3.47. Comparison of observed and computed responses, SS1a

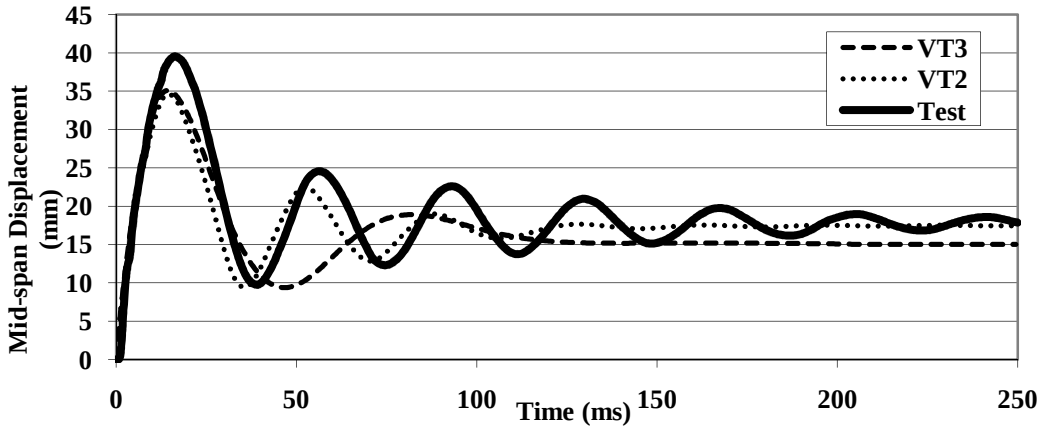

Figure 3.48. Comparison of observed and computed responses, SS1b

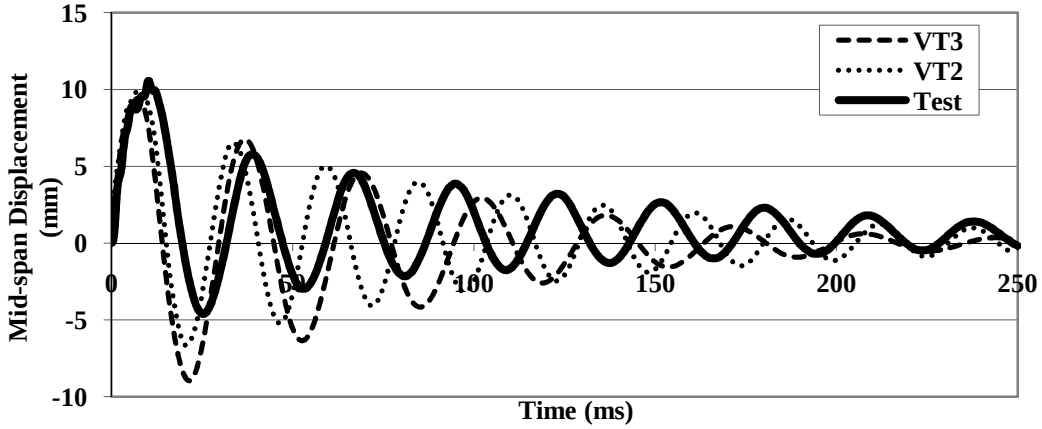

Figure 3.49. Comparison of observed and computed responses, SS2a

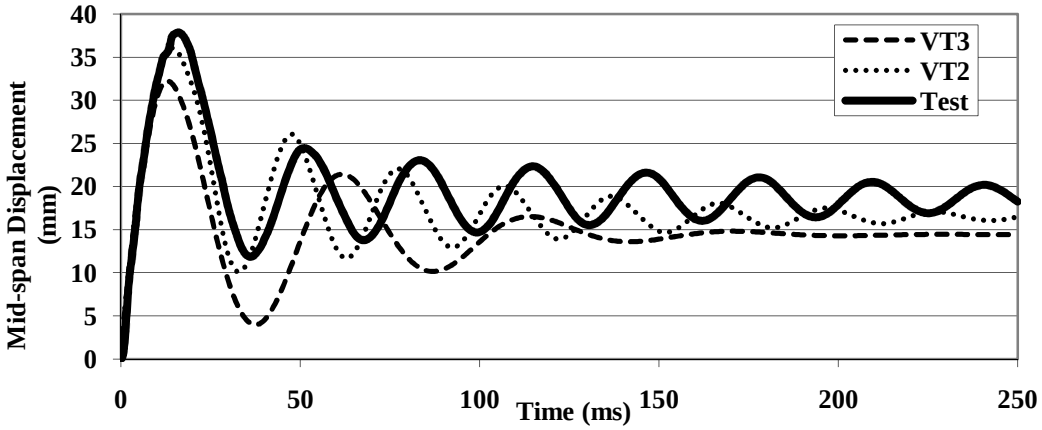

Figure 3.50. Comparison of observed and computed responses, SS2b

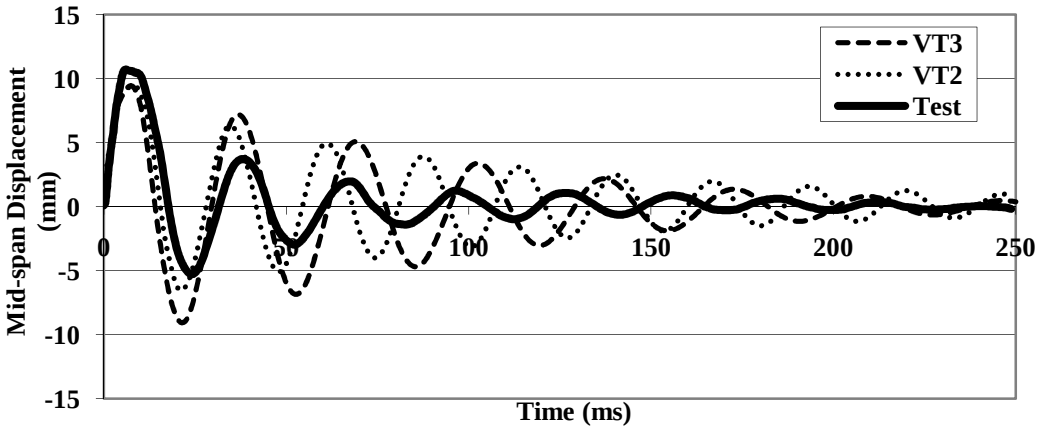

Figure 3.51. Comparison of observed and computed responses, SS3a

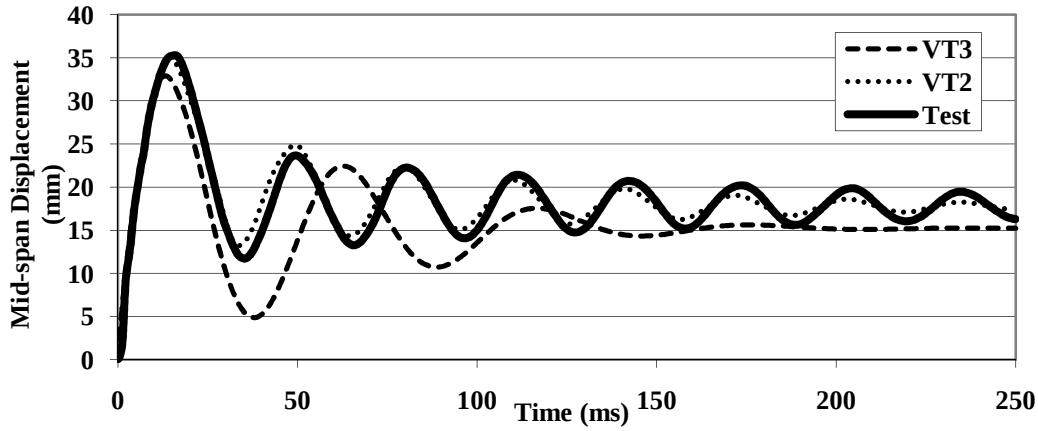

Figure 3.52. Comparison of observed and computed responses, SS3b

Table 3.12. Peak values as obtained from VT2 and VT3

Test	VT3 RESULTS			VT2 RESULTS		
	Max. Disp. (mm)	Time at Max. Disp. (ms)	Error in Max. Displ. (%)	Max. Disp. (mm)	Time at Max. Disp. (ms)	Error in Max. Displ. (%)
SS0a	9.11	7.00	2.25	10.02	8.50	-7.52
SS1a	11.43	9.00	5.35	9.86	8.50	18.34
SS1b	35.10	14.50	11.23	34.63	14.50	12.43
SS2a	9.44	7.50	10.49	9.93	7.50	5.82
SS2b	32.24	13.00	14.84	36.06	14.00	4.77
SS3a	9.44	7.50	11.84	9.44	8.50	11.83
SS3b	32.88	13.00	6.83	34.93	14.50	1.04

3.6. Modeling Considerations for VecTor2 and VecTor3 Analyses

In this section, certain considerations regarding the modeling choices and analysis parameters presented in the preceding sections are discussed.

3.6.1. Effect of Damping Parameters

VecTor programs use Rayleigh damping method to include the viscous damping into the solutions. Hence, although the solution is not obtained through a modal analysis, an eigenvalue analysis is carried out and vibrational modes and periods are found. Then, viscous damping ratios are assigned to these modes and corresponding coefficients for mass and stiffness matrices are found to establish the damping matrix. Since VecTor2 was capable of modeling the majority of energy dissipating mechanisms, only a minimal amount of viscous damping was needed to stabilize the numerical solutions. Before finalizing the analyses, a parametric study was carried out to determine the damping ratios to be assigned to the first two vibrational modes. The damping ratios for the first and second modes of vibration were continuously reduced, until the solutions lost their stability. The smallest amount of viscous damping that resulted in a stable solution was selected for the final analyses of the test specimens. These values are summarized in Table 3.13 and Table 3.14. Note that since the structure was reduced to exploit symmetry, the vibrational modes found do not reflect the actual modes in the structure. However, since a precise damping was not required and these modes were only used to determine the two coefficients for mass and stiffness matrices, such an error is acceptable.

The effects of damping parameters on the solutions are presented Figure 3.53 and Figure 3.54, for A24 (V=3 m/s) and SS3b. Note that the legends in these figures show the damping ratios assigned to the first and second modes. As can be seen in the figure, low levels of damping rendered the solutions unstable, causing an unbounded increase of displacements; a stable solution could only be achieved by increasing the viscous damping. Increasing the damping further beyond this stability limit simply decreased the displacement response. This method of introducing damping was found to be quite effective and accurate, especially considering that the analyses carried out with these limiting damping ratios also resulted in the best estimates of the actual response.

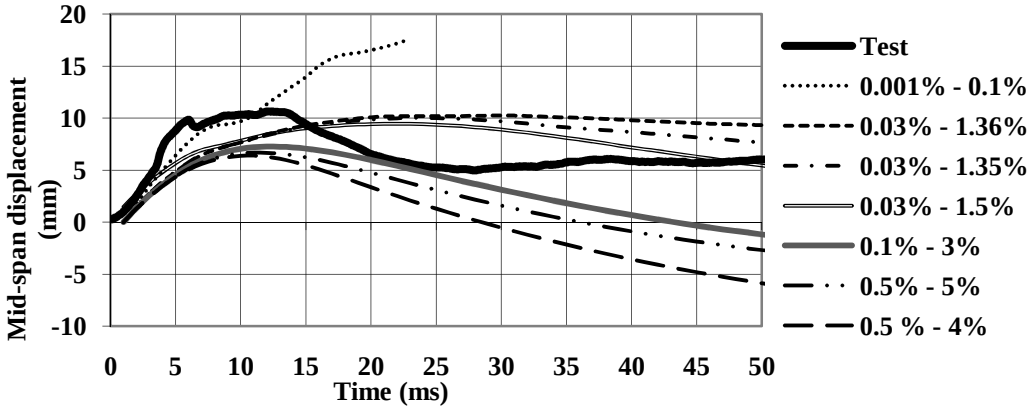

Figure 3.53. Effect of damping on computed response of A24, *V*=3 m/s (VT2)

Table 3.13. Damping properties used in analyses (VT2)

Specimen	*V* (m/s)	1st Mode Damping (% of critical)	2nd Mode Damping (% of critical)
A24	1	8.00	9.00
	3	0.03	1.35
	4	0.30	4.00
B24	1	0.10	0.40
	3	0.50	3.00
	4	0.50	8.00
A48	1	0.50	0.80
	3	0.50	3.00
	4	3.00	8.00
B48	1	0.40	4.00
	3	0.70	5.00
	4	0.50	5.00

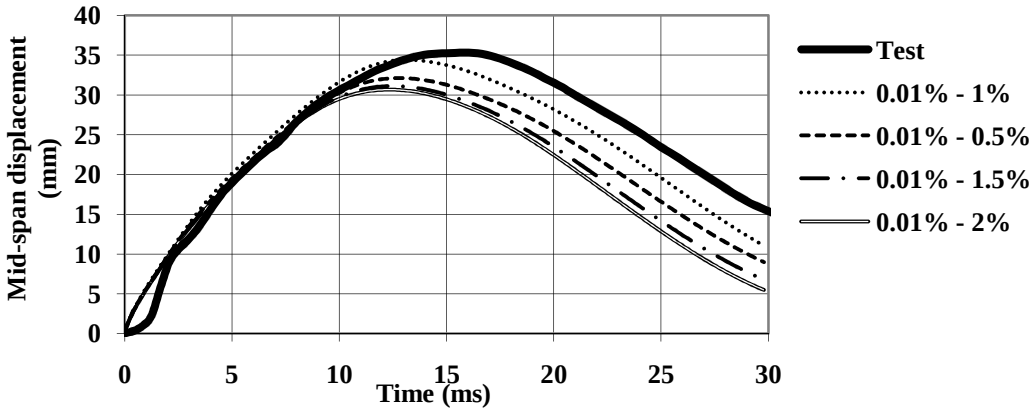

Figure 3.54. Effect of damping on computed response of SS3b (VT3)

Table 3.14. Damping properties used in analyses (VT3)

Specimen	1st Mode Damping (% of critical)	2nd Mode Damping (% of critical)
SS0a	0.50	1.50
SS1a	0.01	0.20
SS1b	0.01	0.50
SS2a	0.01	0.90
SS2b	0.01	0.60
SS3a	0.01	0.75
SS3b	0.01	1.00

3.6.2. Effect of Exploiting Symmetry Conditions

In this study, taking advantage of the symmetric load and support conditions, only half of the beams were modeled. All nodes at the centerline of the beam were restrained against displacements in the x-direction (Figure 3.55). However, since dynamic analyses were carried out on the beams, it is of importance to ensure that the calculated responses were not affected with this modeling choice. In other words, it has to be verified that no vibrational modes of significant importance was missed with this decision. Therefore, one of the dynamic analyses, B24 of Kishi beams tested with 4 m/s impact velocity, was repeated with a full mesh without exploiting the symmetry conditions in VecTor2 (Figure 3.56). To duplicate the entire analysis conditions, damping matrix coefficients found in the half-mesh were fed into the full-mesh analysis. The drop-weight was also restrained in the x-direction. The results obtained from these two analysis are compared in Figure 3.57. As seen from the figure, both analyses gave essentially identical results. Only at the late stages of the response, some diversions were observed due to local numerical instabilities. This result was expected since these beams were heavily damaged under the impact load and only first vibrational modes played a significant role in the response which was not affected by the half-mesh modeling. Therefore, exploiting the symmetry conditions was very beneficial in reducing the calculation time without altering the accuracy of the results obtained.

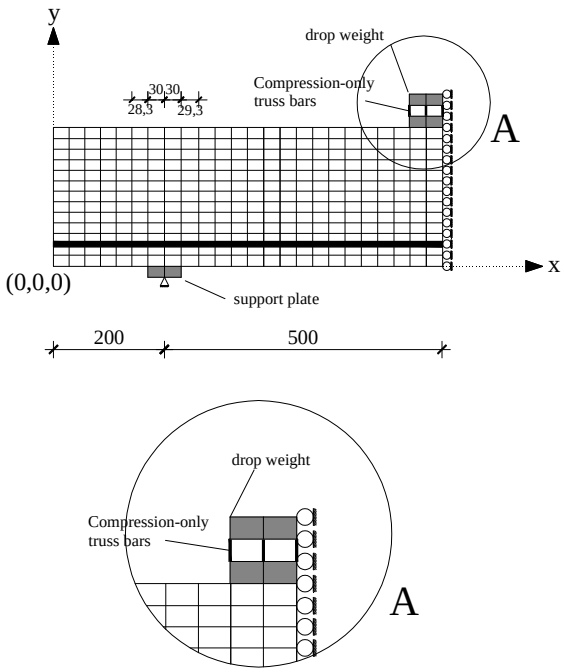

Figure 3.55. Finite element model for VT2 (B24 - half)

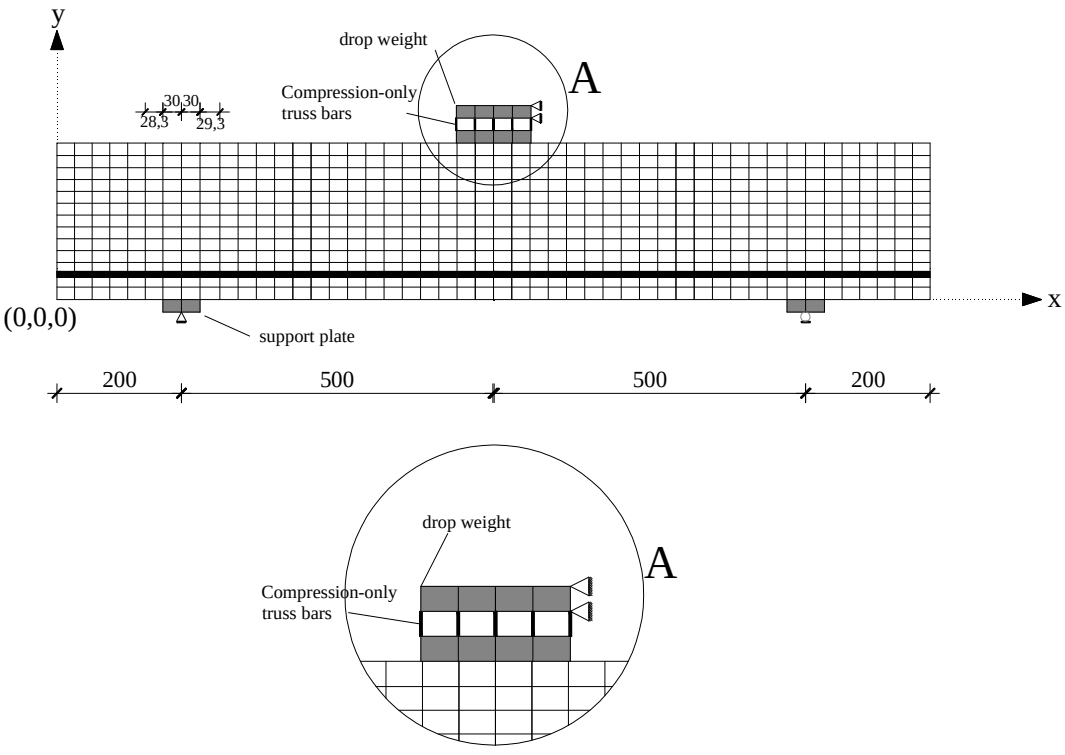

Figure 3.56. Finite element model for VT2 (B24 - full)

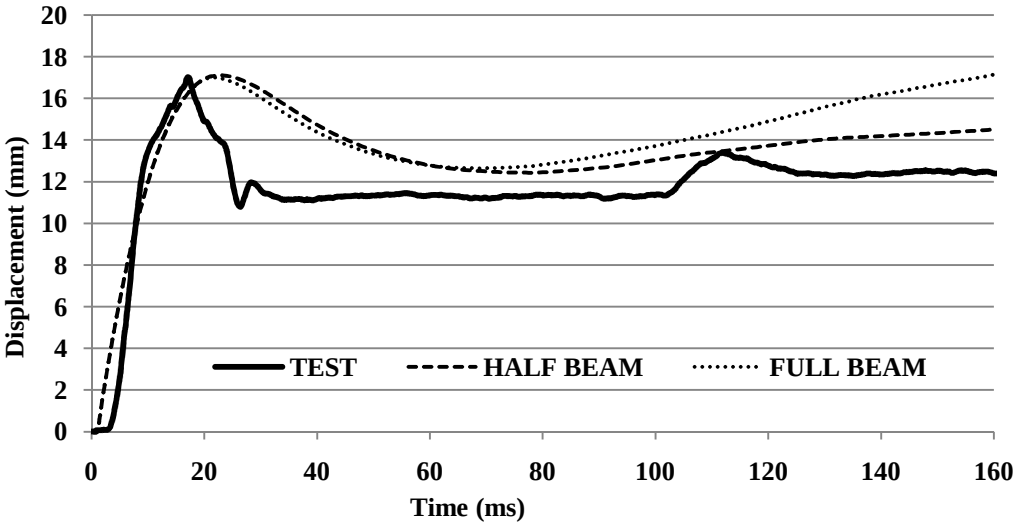

Figure 3.57. Comparison of observed and computed responses, B24 - V=4 m/s

3.6.3. Effect of Finite Element Mesh Size

To observe the effect of the size of the finite element mesh in the solutions, one of the static analyses, MS0, was repeated with a finer meshes. Model M1 (Figure 3.59a), Model M2 (Figure 3.59b), Model M2 (Figure 3.59c) were used for comparison. For M1, cross-section in the xy-plane had 1X16 elements, and in total the number of elements was 1000 (Figure3.59). On the other hand, for M2, cross-section in the xy-plane had 5X16 elements and in total the number of elements was 5000, and for M3, cross-section in the xy-plane had 8X16 elements and in total the number of elements was 8248 (Figure3.59). The analysis for MS0 was repeated with the mesh M2 and the mesh M3 for comparison.

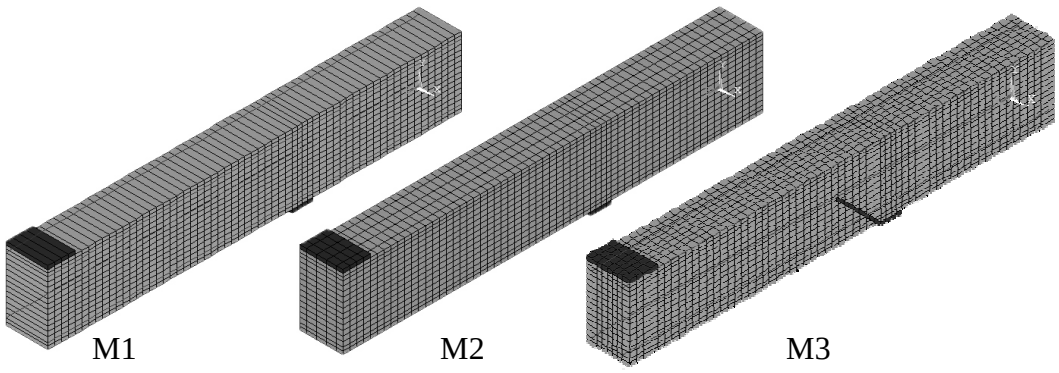

Figure 3.58. Three-dimensional view of finite element meshes

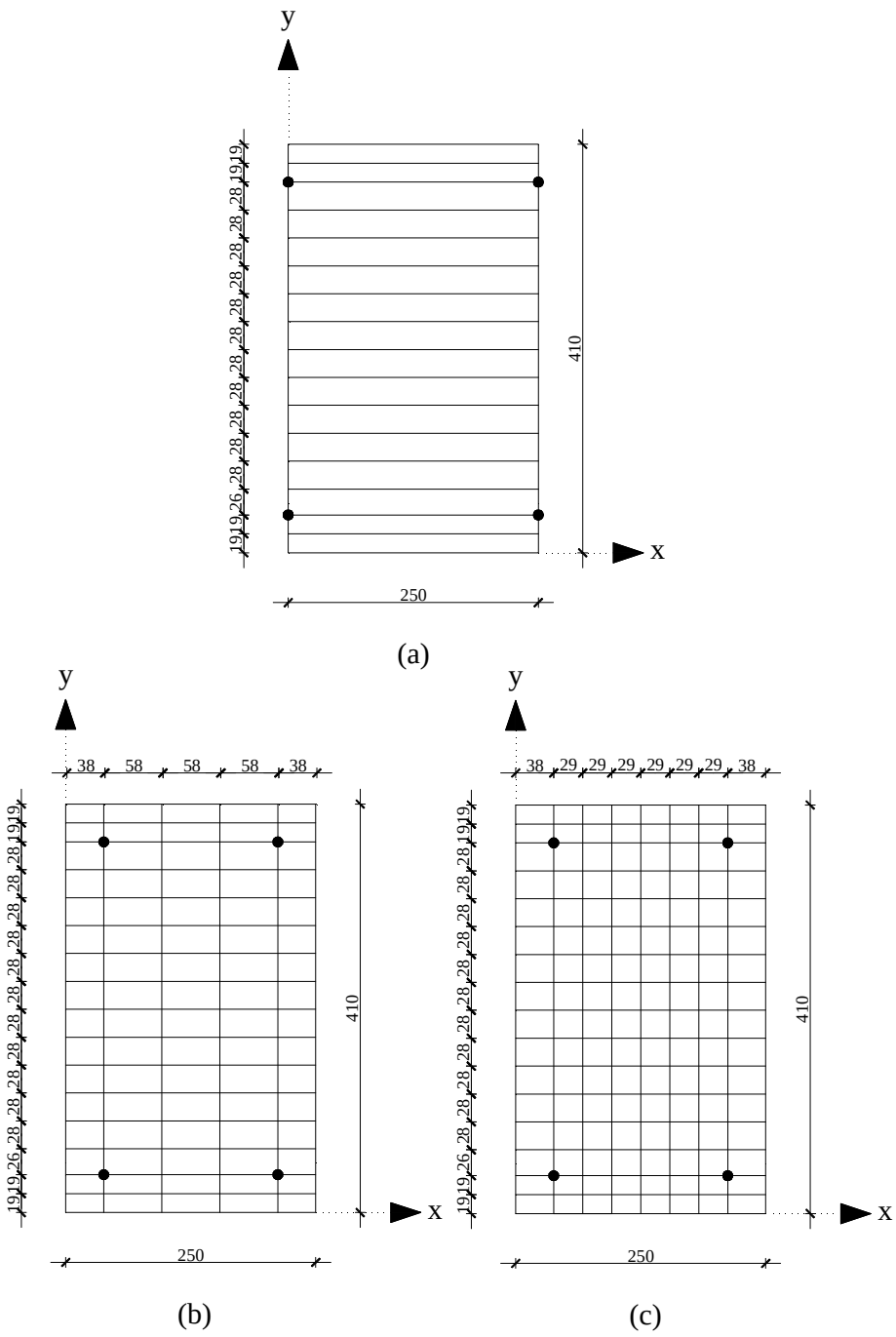

Figure 3.59. (a) Section for M1 (b) Section for M2 (c) Section for M3

As seen in Figure 3.60, the solution obtained both from M1, M2, and M3 were in close agreement. Therefore, it can be said that the chosen mesh size for the analyses were appropriate. Hence, M1 was confidently used in further analyses reduce the computation time.

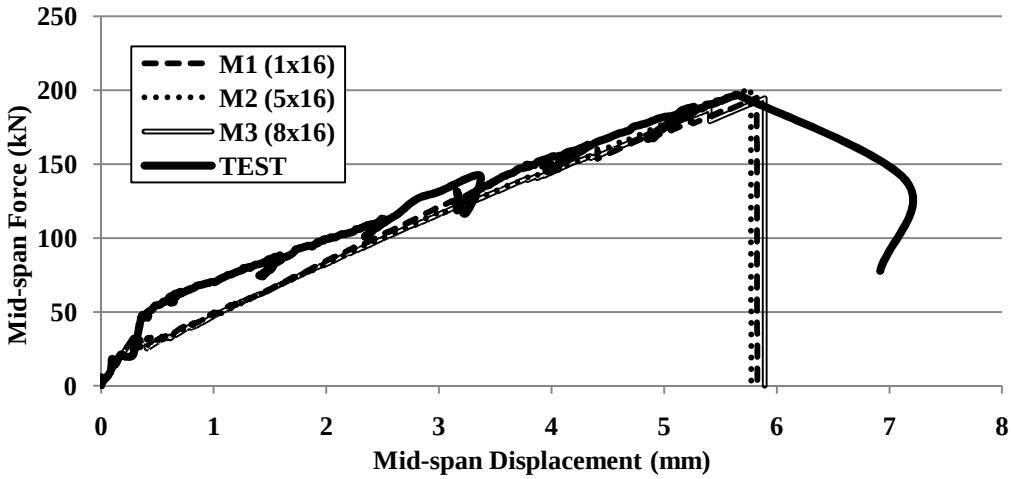

Figure 3.60. Comparison of model M1, M2, and M3 (MS0)

CHAPTER 4

IMPACT MODELING USING MASS-SPRING MODELS

4.1. Introduction

Due to the complicated and time consuming nature of a nonlinear finite element analysis (NLFEA), alternative simpler methods were also developed in the literature that consider the nonlinear behavior of the reinforced concrete structures under impact loading. Although this study has a focus on NLFEA, investigating these simpler methods and comparing their results with NLFEA is also beneficial in evaluating the efficiency of the NLFEA methods studied. In this chapter, a commonly used mass-spring model is described as an alternative simple modeling technique, and falling-weight impact test results conducted on reinforced concrete (RC) beams are compared with the results obtained from the analyses using this technique.

Section 4.2 gives details of the mass-spring model as recommended by CEB (CEB Comite Euro-International Du Beton 1988) and Section 4.3 gives details and results of analyses of Saatci beams using this model.

4.2. CEB Formulations

The mass-spring model is formed by collision of two masses, m_1 and m_2, representing the structure and the colliding body, respectively, a contact spring R_2 between two masses simulating the force which is raised by the counter deforming bodies after contact, and another spring R_1 which representing the deformation and activated resisting force of the structure. In general, both springs have nonlinear force-deformation relations.

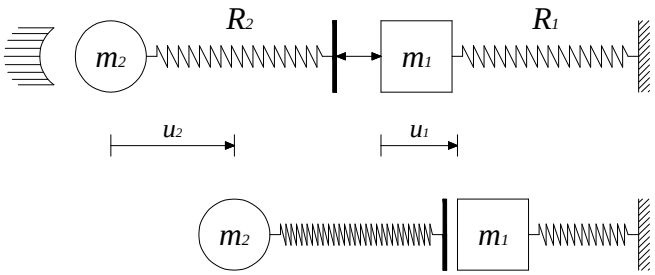

Figure 4.1. Simple mechanical model of two-mass system

The model, as shown in Figure 4.1, is formulated by the following two differential equations of equilibrium written for the two masses, m_1 and m_2;

$$m_2\ddot{u}_2 + R_2(u_2 - u_1) = 0 \tag{4.1}$$

$$m_1\ddot{u}_1 - R_2(u_2 - u_1) + R_1(u_1) = 0 \tag{4.2}$$

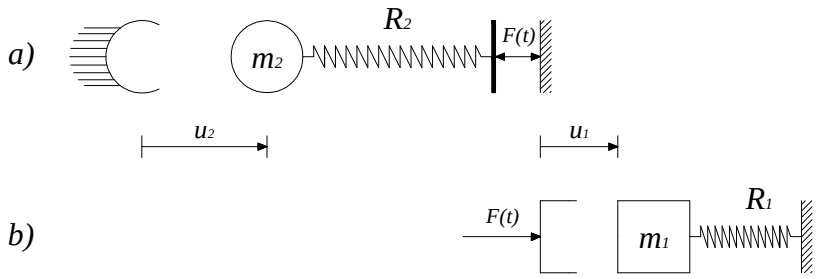

Figure 4.2. Divided response of a two-mass system

In cases where $u_2 \gg u_1$ the relations is expressed as;

$$m_2\ddot{u}_2 + R_2(u_2) = 0 \tag{4.3}$$

$$m_1\ddot{u}_1 + R_1(u_1) = R_2(u_2(t)) = F(t) \tag{4.4}$$

This situation is also called *Soft Impact* (Figure 4.3a) where the kinetic energy of the striking body is completely transferred into deformation energy of the striking body, while the rigidly assumed resisting structure remains undeformed.

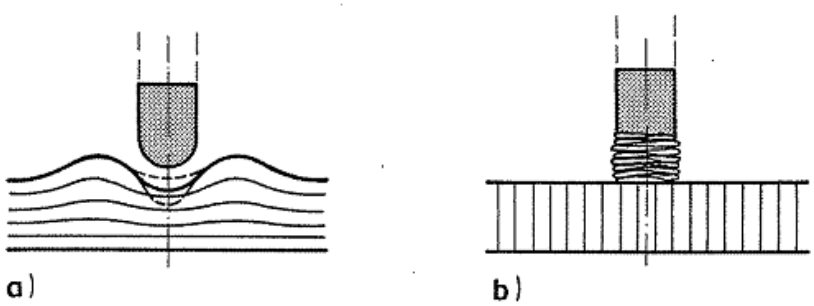

Figure 4.3. Hard and soft impact
(Source : CEB 1988)

The opposite response is called *Hard Impact* (Figure 4.3b) and occurs when the striking body is relatively rigid. In this case the kinetic energy of the striker is to a large extent absorbed by deformation of the struck body, which normally is the structure. Accordingly, the beams subjected to impact loads in this study exposed hard impact conditions. Hard impact conditions require the local behavior of the target body to be considered, as well as its general deformations (Figure 4.4).

The spring R_2 represents the contact characteristics of between the structure and the striking body. The general load-deformation pattern in the contact zone of a solid is shown in Figure 4.4. This pattern may be influenced by strain rate effects. Elastic compression take place in the range of $0 < \Delta u < \Delta u^1$ followed by an elasto-plastic situation for $\Delta u^1 < \Delta u < \Delta u^2$ where permanent internal damage occurs. For $\Delta u > \Delta u^2$ a further compaction or even liquefaction may follow with very high values of $\partial F / \partial [\Delta u]$.

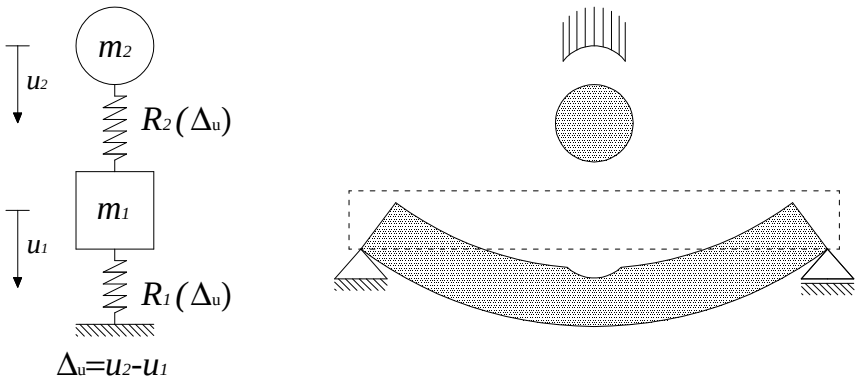

Figure 4.4. Hard impact

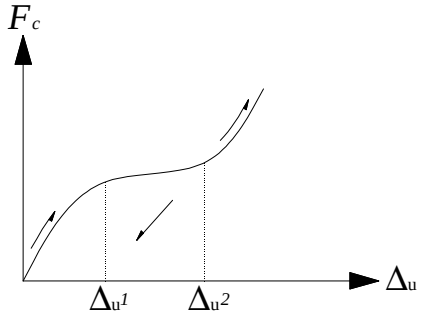

Figure 4.5. Load-deformation pattern of contact zone R_2 (Δ_u)

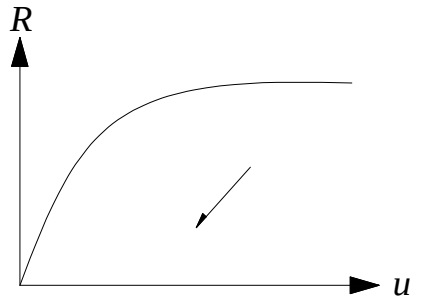

Figure 4.6. Characteristic load-deformation behavior of the struck body R_1 (u_1)

The stiffness and strength of the structure is represented by the spring R_1. Although R_1 can be linearly elastic, for a typical reinforced concrete structure, a nonlinear force-deformation relationship is more realistic as shown in Figure 4.6. Further details can also be incorporated into the behavior of the structure, such as the loading-unloading relationships and hysteresis rules. In this study, hysteresis rules defined by Takeda et al. (1970) are used to define the behavior of spring R_1. The static response was idealized by defininining a primary curve for initial loading and a set of rules for reversals as described in Figure 4.7. Using such a set of loading-unloading rules, the structural response under dynamic loads can be defined in considerable detail.

As mentioned earlier, the mass m_2 represents the mass of the striking body. Mass m_1, representing the mass of the structure, requires calculation of a “participating mass”, based on the estimated shape of deformation of the structure under the impact load, as given in Equation 4.5 and 4.6.

$$m_1 = \int_0^L \bar{m} \cdot \Phi^2(\mathrm{x})\, \mathrm{dx} \tag{4.5}$$

$$P(t) = \int_0^L p(t,x) \cdot \Phi \quad (\mathrm{x})\, \mathrm{dx} \tag{4.6}$$

$\bar{m}$: distributed mass

Once all properties are determined, the response under the impact loading can be determined by the simultaneous solution of Equations 4.1 and 4.2 through a finite difference scheme defined in time domain, as shown below.

$$m_2 \ddot{u}_2 + R_2 = 0 \tag{4.7}$$

$$m_1 \ddot{u}_1 + R_1 - R_2 = 0 \tag{4.8}$$

where

$$R_1 = R_1(u_1)\,; \quad R_2 = R_2(\Delta u_2)\,; \quad \Delta u_2 = u_2 - u_1 \tag{4.9}$$

Therefore, using the finite difference method for nonlinear springs,

$$v_2^{t+1} = v_2^t - \frac{\Delta t}{m_2} \cdot R_2(\Delta u_2^t) \tag{4.10}$$

$$u_2^{t+1} = u_2^t + v_2^{t+1} \cdot \Delta t \tag{4.11}$$

$$v_1^{t+1} = v_1^t + \frac{\Delta t}{m_1} \cdot [(R_2 \Delta u_2^t) - (R_1 u_1^t)] \tag{4.12}$$

$$u_1^{t+1} = u_1^t + v_1^{t+1} \cdot \Delta t \tag{4.13}$$

and with the initial conditions at $t = 0$;

$$v_1 = 0\,;\ u_1 = 0\,;\ \ v_2 = v_0\,;\ \ u_2 = 0 \tag{4.14}$$

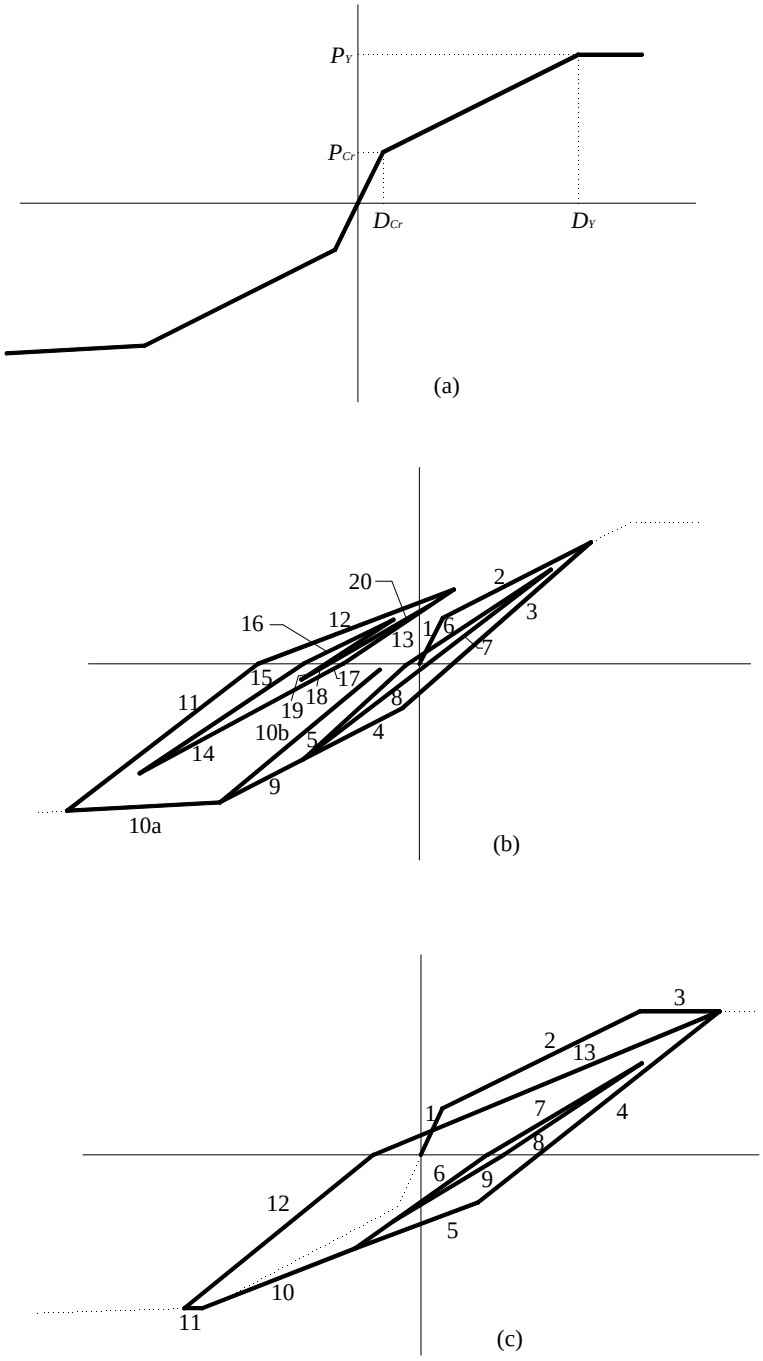

Figure 4.7. Examples of assumed static load-deflection relationship

For this study, a FORTRAN program was developed to calculate the structural response based on the hysteresis rules defined by Takeda et al. and carry out the time-stepping algorithm described in Equations 4.7 to 4.13. The listing for this code is given in the Appendix A.

4.3. Impact Analysis of Reinforced Saatci Beams using CEB Formulations

In this section, impact tests carried out by Saatci are simulated with the procedure described in the preceding section. The approximation made to predict the behavior of a struck beam is shown in Figure 4.8.

The input file for the developed FORTRAN program includes Analysis Parameters, Structural Parameters, and Impacting Mass Parameters as shown in Table 4.1. Total duration of response was taken as 0.25 s and number of time steps was taken as 20000. Structural Parameters, such as cracking and yielding points, are taken from static test results presented previously in Section 2.4. It should be noted that these parameters can be acquired from the VecTor or ANSYS analysis. To consider the strain rate effects caused by the rapid loading under impact, cracking loads were multiplied with 1.5, yield loads were multiplied with 1.2, and ultimate loads were multiplied with 1.2, based on the estimated strain rates and recommendations by CEB. Impacting masses were 211 kg for a lighter drop-weight (beams identified as a-series), and 600 kg for heavier drop-weight (beams identified as b-series). The contact velocity 8 m/s was assigned as an initial velocity for the drop-weights. The contact stiffness was determined by calculating the stiffness of the drop-weight according to its structural properties as 50 kN/mm. The local crushing of concrete was ignored in determining the contact stiffness.

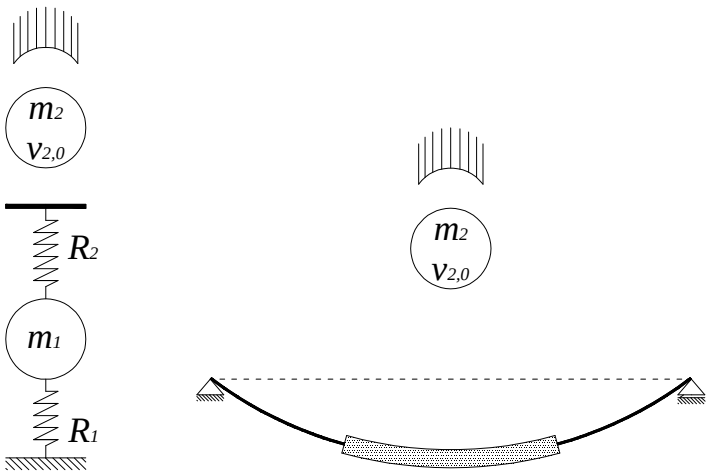

Figure 4.8. Two mass model for hard impact

Table 4.1. The input file parameters

Analysis Parameters	Structural Parameters	Impacting Mass Parameters
	Cracking load (kN)	
	Cracking displacement (mm)	
Total duration (s)	Yield Load (kN)	Impacting mass (kg)
No. of time steps	Yield Displacement (mm)	Contact velocity (m/s)
Record every Nth time step	Ultimate load (kN)	Contact stiffness (kN/mm)
	Ultimate displacement (mm)	
	Effective mass (kg)	

The following figures present the comparisons of mid-span displacements, as observed in tests and computed with Spring Model (SM). Peak displacements are summarized in Table 4.2.

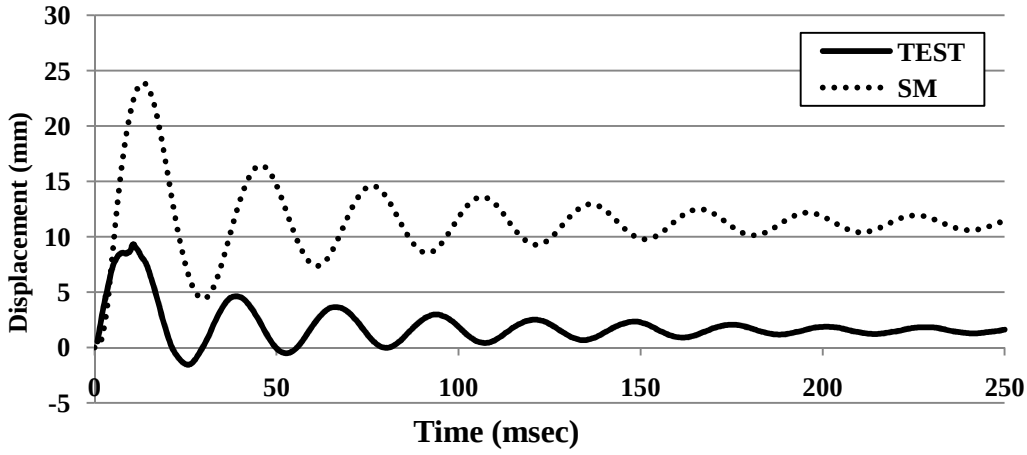

Figure 4.9. Comparison of observed and computed responses, SS0a

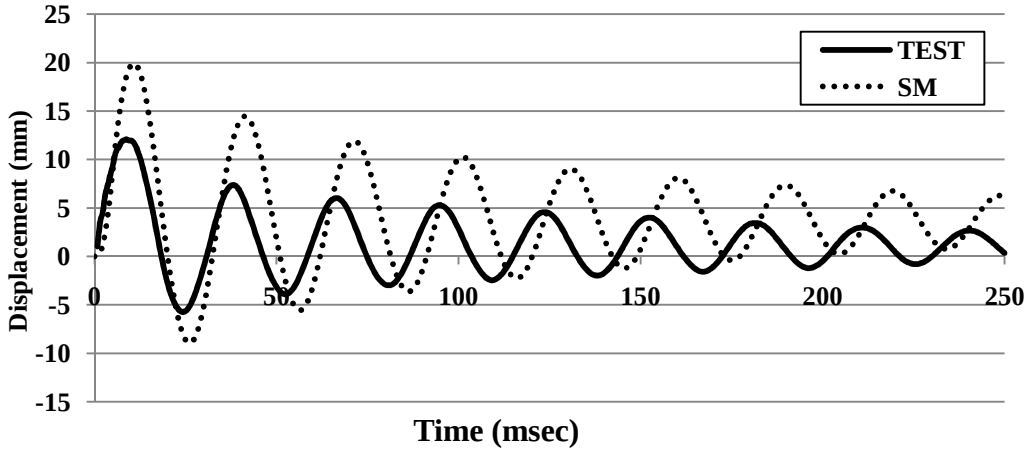

Figure 4.10. Comparison of observed and computed responses, SS1a

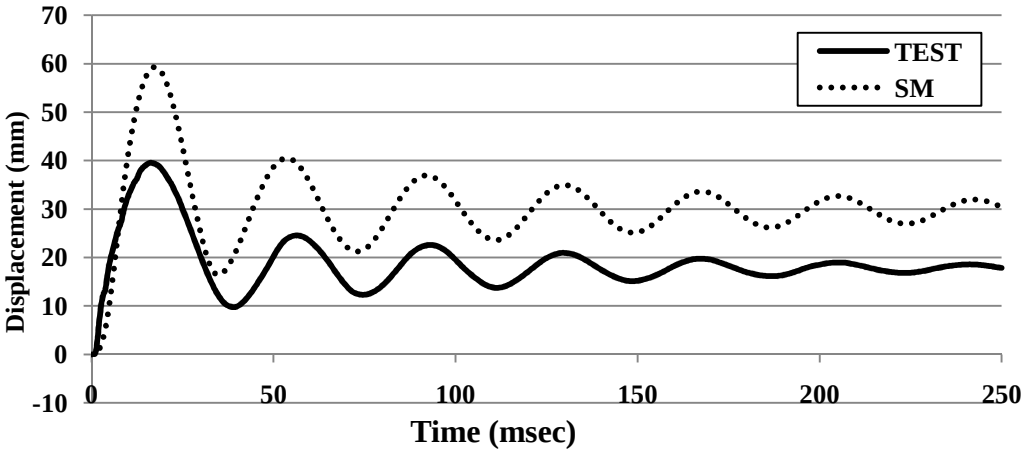

Figure 4.11. Comparison of observed and computed responses, SS1b

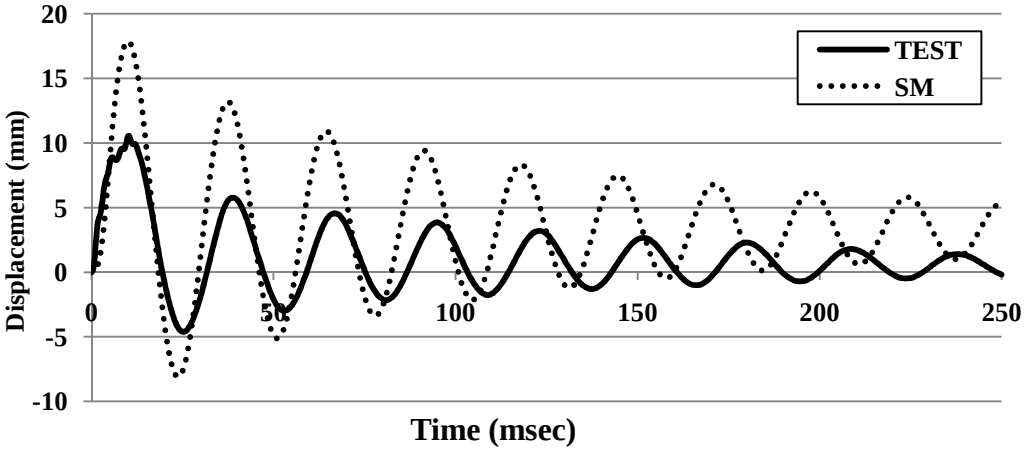

Figure 4.12. Comparison of observed and computed responses, SS2a

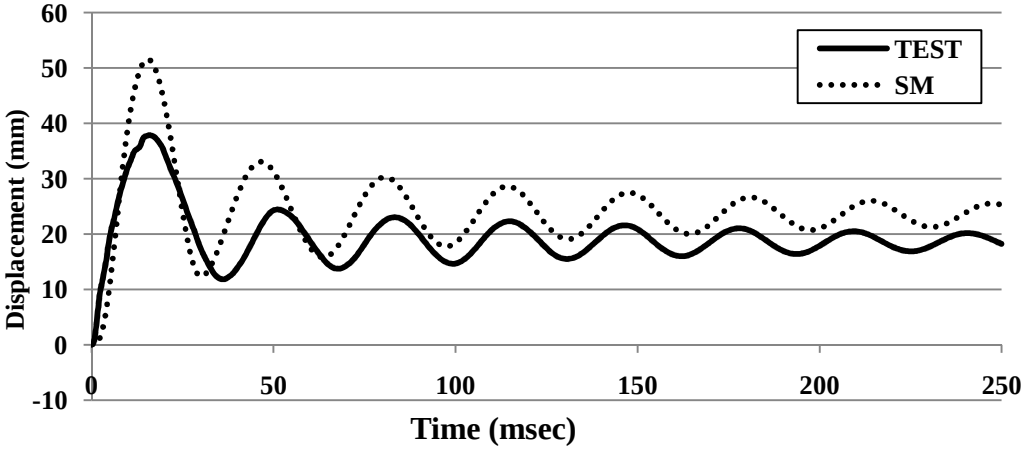

Figure 4.13. Comparison of observed and computed responses, SS2b

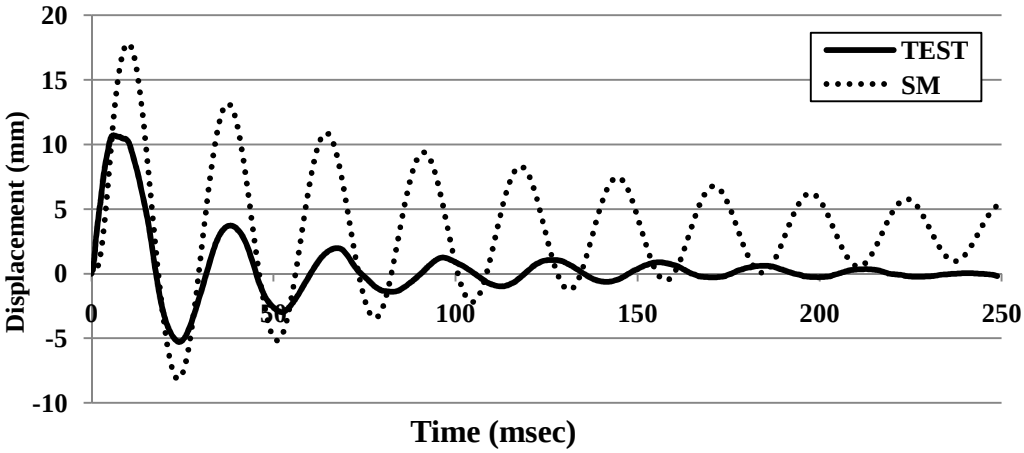

Figure 4.14. Comparison of observed and computed responses, SS3a

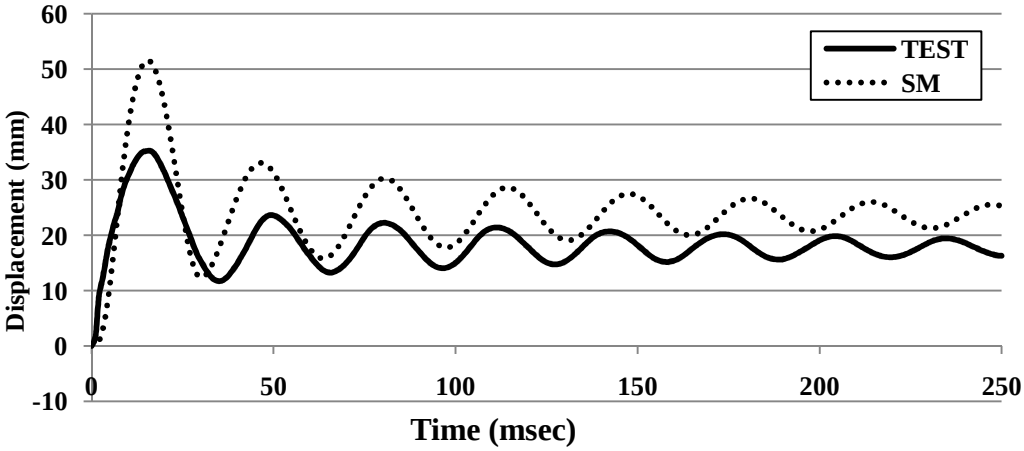

Figure 4.15. Comparison of observed and computed responses, SS3b

Table 4.2. Peak values as obtained from the tests and SM analyses

Test	TEST RESULTS		SM RESULTS		
	Max. Displacement (mm)	Time at Max. Displacement (ms)	Max. Displacement (mm)	Time at Max. Displacement (ms)	Error in Max. Displ. (%)
SS0a	9.32	10.83	23.90	13.14	-156.49
SS1a	12.08	8.75	19.93	10.76	-65.00
SS1b	39.55	16.25	59.30	17.39	-49.95
SS2a	10.54	10.42	17.88	9.89	-69.60
SS2b	37.86	16.25	51.59	15.39	-36.26
SS3a	10.70	6.25	17.83	10.03	-66.60
SS3b	35.29	15.83	51.59	15.39	-46.17

As shown in figures, the results of SM are shape wise very similar to the actual response observed in the test for moment critical beams (SS1a, SS1b, SS2a, SS2b, SS3a, and SS3b). However, in general, SM model highly overestimated the response. This can be attributed to two facts: First, the rules defined by Takeda et al. are based on ductile members which have a definite yield plateau as shown in Figure 4.7a. However, these beams, even if they were expected to be ductile under static loads, mostly exhibited shear dominant behavior under impact loading before undergoing large deformations. This is observed more clearly in SS0a. Secondly, the factors applied to the static properties to consider the strain rate effects were chosen through rough assumptions based on the expected strain rates. However, the actual strain rates may vary during the response and well exceed the assumed values, causing a stiffer response compared to the expected one.

Thus, it can be said that, although it is much simpler and quick to apply, SM models failed to predict the impact response of reinforced concrete beams accurately. This method has been further developed for better predictions (Fujikake et al. 2009). However, use of complicated methodologies to better define the structural response and the effect of strain rates costs the attractiveness of the method as a simple tool. Hence, nonlinear finite element methods seem to be more suitable for accurate predictions.

CHAPTER 5

CONCLUSION

The study presented in this thesis had several focus points. The main objective was to evaluate the numerical methods available for predicting the behavior of reinforced concrete (RC) structures subjected to impact loads. For this purpose, a two-dimensional nonlinear finite element reinforced concrete analysis program called VecTor2, a three-dimensional nonlinear finite element reinforced concrete analysis program called VecTor3 and a three-dimensional finite element program called ANSYS were used for analyses. A separate program employing simple mass-spring models were also developed in FORTRAN.

Shear-critical beams were selected for testing the methods, since modeling the shear behavior of RC structures presents a challenge. Moreover, shear mechanisms are known to dominate the impact behavior of reinforced concrete structures. Hence, if a method was found to be successful in modeling the shear dominant impact behavior, it is safe to claim that such a method would be successful in modeling the impact behavior of ductile members as well. Results of the experimental impact studies found in the literature were modeled with the mentioned methods and results were compared to evaluate the methodologies. In general, programs VecTor2 and VecTor3 performed well in estimating the impact response. The modeling methodology for RC employed in these programs, the Modified Compression Field Theory (MCFT), was known as one of the more successful methods in predicting the static shear behavior of RC structures, and it performed well in modeling the shear dominant impact behavior as well. Damage profiles, peak displacements and displacement characteristics were captured with good accuracy. Both two- and three-dimensional finite element applications performed alike, with limited dissimilarities due to their different way of handling the impact load. Thus, it can be said that the methodology would perform successfully in the structures where a two-dimensional analysis is not possible. Static analyses were also carried out with another well-known program ANSYS. Such analyses were also intended to be used to determine the static properties of the structures to be used in mass-spring models. However, ANSYS did not perform well in ductile members and severely

underestimated the deformation capacity of the members. Hence, the results of these analyses could not be further used.

Simple mass-spring models were also tried for modeling the shear-critical beams. However, they performed rather poorly with the material models chosen. Although possible enhancements to such models were reported in the literature, they were not applied in this study due to their complicated nature and still questionable accuracy.

REFERENCES

ANSYS Academic Research. *Help System,Coupled Field Analysis Guide*. 2009.

Belytschko, T., Liu, W. K., and Moran B., *Nonlinear Finite Elements for Continua and Structures.* John Wiley&Sons, 2000.

Bentz, E. C. *Augustus: Finite Element Post-Processor fot VecTor2 and TRIX*. Toronto: University of Toronto, 2003.

CEB Comite Euro-International Du Beton. *Concrete Structures Under Impact and Impulsive Loading.* Dubrovnik: Comite Euro-International Du Beton, 1988.

Chen, W. *Plasticity in Reinforced Concrete.* New York: McGraw-Hill, Inc., 1982.

Fanning, P. *Nonlinear Models of Reinforced and Post-tensioned Concrete Beams*. Electronic Journal of Structural Engineering, 2001: 111-119.

Fujikake, K., Bing L., and Soeun S. *Impact Response of Reinforced Concrete Beam and Its Analytical Evaluation*. Journal of Structural Engineering Vol. 135 No. 8, Aug. 2009: 938-950.

JSCE. *Japan Concrete Standard* . (in Japanese), 1996.

Kishi, N., Mikami, H., Matsuoka K. G., and Ando T. *Impact Behavior of Shear-Failure-Type RC Beams without Shear Rebar*. International Journal of Impact Engineering (Elsevier Science Ltd.), 2002: 955-968.

Palermo, D., and Vecchio F. J. *Behavior of Three-Dimensional Reinforced Concrete Shear Walls.* ACI Structural Journal 99, No. 1, Jan-Feb. 2002: 81-89.

Saatci, S. *Behaviour and Modelling of Reinforced Concrete Structures Subjected to Impact Loads.* Toronto: Univercity of Toronto PhD Thesis, 2007.

Saatci, S., and Vecchio F. J. *Nonlinear Finite Element Modeling of Reinforced Concrete Structures under Impact Loads.* ACI Structural Journal (American Concrete Institute) 106, No. 5, Sep.-Oct. 2009: 717-725.

Selby, R. G. *Three Dimensional Constitutive Relations for Reinforced Concrete*. Toronto: University of Toronto PhD Thesis, 1993.

Takeda, T., Sozen M. A., and Nielsen N. N. *Reinforced Concrete Responce to Simulated Earthquakes*. Journal of the Structural Division, Proceeding of the American Society of Civil Engineers Vol.96, Dec. 1970: 2757-2773.

Vecchio, F. J. *Disturbed Stress Field Model for Reinforced Concrete:Formulations*. Journal of Structural Engineering 126, No. 9, 2000: 1070-1077.

Vecchio, F. J., and Collins M. P. *The Modified Compression-Field Theory of Reinforced Concrete Elements Subjected to Shear*. ACI Journal 83, No. 2, Mar.-Apr. 1986: 219-231.

Vecchio, F. J., and Wong P. S. *VecTor2 & FormWorks User's Manual.* 2002.

Willam, K. J., and Warnke E. D.. *Constitutive Model for the Triaxial Behavior of Concrete.* Italy: International Association for Bridge and Structural Engineering. Vol. 19, 1975.

APPENDIX A

THE PROGRAM CODE IN FORTRAN

The program code in FORTRAN written by the supervisor Assist. Prof. Selçuk Saatci used in Chapter 4.

```
C PROGRAM SPRING
C
C This program calculates the response of a two-mass spring system
C simulating a hard impact
C The hysteresis rules for RC member are taken from
C Takeda, Sozen and Nielsen (1970), "Reinforced Concrete Response to
Simulated Earthquakes", ASCE Journal of the Structural Division
C
C v2.0
C June 17, 2010
C
      IMPLICIT NONE
C
C      COMMON /SPRING1/ R1,CRKLD, CRKDISP, YLDLD, YLDISP,
C    *                  ULTLD, ULTDISP, MASS1,TRNDISP, MAXDISP, STAT
      REAL*8 PI,DI,PS,DS,VI,VS, S,HRLN,A,B,RF,
     * PC,DC,PY,DY,PU,DU,OC,CY,YU,CPY,CSE,UM1,UM2,UM3,UM4,
     * S1,X0, X0UM,X0Y,U0D,U0,X1UM,U11,UlD X2U0,U22,X3UI,U3,QY,
     * ACHNG,SE,PSE,PSEOLD
      INTEGER IDRO,RNRL,IDR,IDRV,IDRVO,ISIGN,NRL,JI,IREVSL
      REAL*8 UM(2,2),UPOS(3),UNEG(3),EXCR(6),ESE (3),BOTT,S2,U1D,X2U0
      LOGICAL PRINT1, BTEST
C
      ALLOCATABLE U1(:), U2(:), V1(:), V2(:)
C
      CHARACTER*10 STAT
      INTEGER*4 TSNO, RECNO
      REAL*8 DUR, TSTEP
      REAL*8 CRKLD, CRKDISP, YLDLD, YLDISP, ULTLD, ULTDISP, MASS1
      REAL*8 MASS2, CNCTVEL, CNCTSTF
      REAL*8 U1, U2, V1, V2
```

```
      REAL*8 R1, R2, TRNDISP, MAXDISP, R1I, R1S
      INTEGER I, COUNT, MAXFLG
C
C
      OPEN(5,FILE='SpringInput.txt', STATUS='OLD', ERR=900)
      READ(5,'(/////////)')
      READ(5,801, ERR=901) DUR
      READ(5,802, ERR=901) TSNO
      READ(5,802, ERR=901) RECNO
      READ(5,'(//)')
      READ(5,801, ERR=902) CRKLD
      READ(5,801, ERR=902) CRKDISP
      READ(5,801, ERR=902) YLDLD
      READ(5,801, ERR=902) YLDISP
      READ(5,801, ERR=902) ULTLD
      READ(5,801, ERR=902) ULTDISP
      READ(5,801, ERR=902) MASS1
      READ(5,'(//)')
      READ(5,801, ERR=903) MASS2
      READ(5,801, ERR=903) CNCTVEL
      READ(5,801, ERR=903) CNCTSTF
C
      ALLOCATE (U1(TSNO),U2(TSNO),V1(TSNO),V2(TSNO))
      OPEN(6,FILE='SpringOutput.txt')
      WRITE(6,803) 'TIME', 'U1','U2','V1','V2','R1','R2','STAT'
      U1=0.
      U2=0.
      V1=0.
      V2=0.
      R1I=0.
      R1S=0.
      S=0.
      STAT='LOADING'
      TRNDISP=0.
      COUNT=0
C
      TSTEP=DUR/TSNO
      MASS1=MASS1/(10**6)
      MASS2=MASS2/(10**6)
      CNCTVEL=CNCTVEL*1000
C
```

```
      OC=CRKLD/CRKDISP
      CY=(YLDLD-CRKLD)/(YLDISP-CRKDISP)
      YU=(ULTLD-YLDLD)/(ULTDISP-YLDISP)
      CPY=(YLDLD+CRKLD)/(YLDISP+CRKDISP)
C
C
      V2(2)=CNCTVEL
C
      DO 10 I=2,TSNO-1
      COUNT=COUNT+1
C
C     IF (I.EQ.1) THEN
C           CALL SPR1(0.,U1(I),0.,V1(I))
C      ELSE
C         CALL SPR1(U1(I-1),U1(I),V1(I-1),V1(I))
C      ENDIF
      CALL                  HYST06(R1I,U1(I),R1S,U1(I-1),V1(I),V1(I-1),
S,HRLN,A,B,IDRO,
     * RF,CRKLD,CRKDISP,YLDLD,YLDISP,ULTLD,ULTDISP,OC,CY,YU,
     * CPY,CSE,RNRL,UM1,UM2,UM3,UM4,
     * S1,X0, X0UM,X0Y,U0D,U0,X1UM,U11,UlD X2U0,U22,X3UI,U3,QY,MAXFLG,
     * ACHNG,PRINT1,SE,ESE,PSE,PSEOLD,UPOS,UNEG,EXCR)
C
      R2=CNCTSTF*(U2(I)-U1(I))
      IF (R2.LT.0.) R2=0.
      V2(I+1)=V2(I)-TSTEP/MASS2*R2
      U2(I+1)=U2(I)+V2(I+1)*TSTEP
C     V1(I+1)=V1(I)+TSTEP/MASS1*(R2-R1)
      V1(I+1)=V1(I)+TSTEP/MASS1*(R2-R1I)
      U1(I+1)=U1(I)+V1(I+1)*TSTEP
      R1S=R1I
      R1I=R1I+(U1(I+1)-U1(I))*S
C
      IF (COUNT.EQ.RECNO) THEN
      WRITE (6,804) I*TSTEP, U1(I),U2(I),V1(I),V2(I),R1S,S
      COUNT=0
      ENDIF
C
   10 CONTINUE
  801 FORMAT (28X,E10.0)
  802 FORMAT (28X, I6)
```

```
  803 FORMAT (8(3X,A8))
  804 FORMAT (7(2X, E10.4), 3X, A10)
      STOP
  900 STOP 'ERROR: Error opening SpringInput.txt file'
  901 STOP 'ERROR: Error reading Analysis Parameters'
  902 STOP 'ERROR: Error reading Structural Parameters'
  903 STOP 'ERROR: Error reading Impacting Mass Parameters'
      END
C
C
C      SUBROUTINE SPR1(UU0,UU1,VV0,VV1)
C      IMPLICIT NONE
C      COMMON /SPRING1/ R1,CRKLD, CRKDISP, YLDLD, YLDISP,
C     *                 ULTLD, ULTDISP, MASS1,TRNDISP, MAXDISP, STAT
C      REAL*8 R1, TRNDISP, MAXDISP
C     CHARACTER*10 STAT
C     REAL*8 CRKLD, CRKDISP, YLDLD, YLDISP, ULTLD, ULTDISP, MASS1
C     REAL*8 UU0, UU1, VV0, VV1
C
C      IF((VV0*VV1).GT.0.) THEN
C       IF((VV1.GT.0.).AND.(UU1.GT.TRNDISP)) STAT='LOADING'
C       IF((VV1.GT.0.).AND.(UU1.LT.TRNDISP)) STAT='RELOADING'
C        IF((VV1.LE.0.).AND.(UU1.LT.TRNDISP)) STAT='UNLOADING'
C      ELSE
C       IF((VV0.GT.0.).AND.(VV1.LE.0.)) THEN
C         STAT='UNLOADING'
C         TRNDISP=UU1
C       ENDIF
C        IF((VV0.LT.0.).AND.(VV1.GE.0.)) THEN
C         STAT='RELOADING'
C       ENDIF
C     ENDIF
C
C      IF (STAT.EQ.'LOADING') THEN
C         IF (UU1.LT.CRKDISP) THEN
C           R1=CRKLD/CRKDISP*UU1
C           RETURN
C         ELSEIF (UU1.LT.YLDISP) THEN
C           R1=(YLDLD-CRKLD)/(YLDISP-CRKDISP)*(UU1-CRKDISP)+CRKLD
C             RETURN
C          ELSEIF (UU1.LT.ULTDISP) THEN
```

```
C           R1=(ULTLD-YLDLD)/(ULTDISP-YLDISP)*(UU1-YLDISP)+YLDLD
C           RETURN
C          ELSE
C           R1=0.
C           RETURN
C         ENDIF
C      ELSEIF ((STAT.EQ.'UNLOADING').OR.(STAT.EQ.'RELOADING')) THEN
C             R1=(YLDLD/YLDISP)*(UU1-(TRNDISP-YLDISP))
C           RETURN
C      ENDIF
C      RETURN
C     END SUBROUTINE
```